Author:
Young, Harry

Title:
Investigation into the Effect of Protein Disulphide Isomerase A3 on the Prom-Metastatic Phenotype of Breast Cancer Cells

Investigation into the Effects of Protein Disulphide Isomerase A3 on the Pro-Metastatic Phenotype of Breast Cancer Cells

Henry Young

BSc Cancer biology and immunology

M.Sc by Research in Biochemistry 2017-2018

Supervisor: Professor Jo Adams.

A dissertation submitted to the University of Bristol in accordance with the requirements for award of the degree of MSc by Research in the Faculty of Life Sciences.

School of Biochemistry

26-10-2018

Word Count: 29858

Abstract

Breast cancer has the second highest incidence in women and has high mortality when metastasis occurs. Protein disulphide isomerase A3 (PDIA3) is an endoplasmic reticulum-resident protein that effects post-translational disulphide bond formation on substrates with cysteine-rich domains including extracellular matrix (ECM) proteins. PDIA3 protein is increased in invasive ductal carcinomas (IDC) of the breast, but little is known about its functions in breast cancer. The Objective of this M.Res. project was to investigate the role of PDIA3 in pro-metastatic activities of three human breast cancer cell lines *in vitro*.

In pilot immunohistochemical studies of IDC, PDIA3 was present in luminal and triple-negative IDC. PDIA3 was present in the breast cancer cell lines by immunoblot. Effects of pharmacological inhibition of PDIA3 were examined with regard to cell-substratum attachment, F-actin organization and migration by fluorescence microscopy or 2-dimensional directional cell migration. PDIA3 inhibition, compared to PDIA1 inhibition or solvent-control, resulted in reduced cell attachment and spreading of all the cell lines with time, and decreased migration. However, 5-fluorouracil or cyclophosphamide mediated cell killing was unaffected.

To explore if PDIA3-dependent secreted proteins contribute to the tumour microenvironment, ECM was isolated from control or PDIA3-inhibited breast cancer cells. PDIA3-inhibition did not affect attachment of 'naïve" cells, but resulted in decreased spreading and altered F-actin organization. To explore possible PDIA3-dependent fibroblast-cancer communications, cells were treated with conditioned media (CM) from wild-type or *Pdia3*$^{-/-}$ mouse embryo fibroblasts (MEF). CM from *Pdia3*$^{-/-}$ MEF resulted in reduced spreading and F-actin organisation of all cell lines, compared to cells incubated with CM from WT-MEF.

These results contribute knowledge that PDIA3 functions in support of adhesion and migratory capacity of breast cancer cells, by processes involving secreted proteins of cancer cells or fibroblasts. Targeting of PDIA3 could have potential for inhibition of breast cancer metastasis.

Dedication and Acknowledgments

I would like to thank the Wolfson Bioimaging Facility for their help in this project. In particular, I am grateful to Dr Katy Jepson who instructed and advised me when completing the 'scratch-wound' experiments including training me to use the software for analysis. Also, Dr Alan Leard kindly trained me on the confocal microscope that was a huge part of this project.

I extend my thanks to the UCRF for funding this project and to Professor Michalak for the *Pdia3*$^{-/-}$ mouse embryo fibroblasts. Without these, this project would not have been possible.

I thank Professor Peter Green for his assistance in deciding upon statistical analysis to use throughout this project.

I would also like to thank Wales Cancer Bank for the histological samples for the pilot assay which gave insight to PDIA3 in the context human breast cancer.

Finally, I extend my thanks to Professor Adams, Dr Rosini and Dr Hellewell who patiently and informatively trained me throughout this project.

Author’s Declaration

I declare that the work in this dissertation was carried out in accordance with the requirements of the University's Regulations and Code of Practice for Research Degree Programmes and that it has not been submitted for any other academic award. Except where indicated by specific reference in the text, the work is the candidate's own work. Work done in collaboration with, or with the assistance of, others, is indicated as such. Any views expressed in the dissertation are those of the author.

SIGNED:  DATE:. 26-10-2018

Table of Contents

List of Tables

List of Figures

Abbreviations

1α25(OH)$_2$D$_3$	1α,25-dihydroxyvitamin-D3
5-FU	5'-Fluorouracil
aECM	Artificial extracellular matrix
ALDH	Aldehyde dehydrogenase
APS	Ammonium persulfate
ATCC	American Type Culture Collection
ATRA	All-trans retinoic acid
BM	Basement membrane
BSA	Bovine serum albumin
CAF	Cancer-associated fibroblast
cAMP	Cyclic AMP
CNX	Calnexin
COX	Cyclooxygenase
CP	Cyclophosphamide
CRT	Calreticulin
CSC	Cancer stem cell
CSF-1	Colony-stimulating factor-1
DAG	Diacylglycerol
DAPI	4’,6-diamidino-2-phenylindole
DCIS	Ductal carcinoma in situ
DMEM	Dulbecco Modified Eagle Medium - high glucose
DMSO	Dimethyl sulfoxide
DTT	DL-dithiothreitol
ECM	Extracellular matrix
EGF	Epidermal growth factor
EMT	Epithelial-mesenchymal transition
ER	Endoplasmic reticulum
ERAD	ER-associated degradation
ERBB2/HER2	Human epidermal growth factor receptor 2
ERp57	Endoplasmic reticular protein 57
EsR	Oestrogen receptor
FAK	Focal adhesion kinase
FBS	Foetal bovine serum
FEA	Flat epithelial atypia
FGM	Fibroblast growth medium
FITC	Fluorescein isothiocyanate
FN	Fibronectin
HIF	Hypoxia-induced factor
HPC	Haematopoietic progenitor cell
IDC	Invasive ductal carcinoma
IHC	Immunohistochemistry
IL	Interleukin
ILC	Invasive lobular carcinoma
LOX	Lysyl oxidase

MaSC	Mammary stem cell
MDSC	Myeloid-derived suppressor cell
MEF	Mouse embryonic fibroblasts
MET	Mesenchymal-epithelial transition
MHC	Major histocompatibility complex
MMC	Mitomycin-C
MMP	Matrix metalloproteinase
mTOR	Mammalian target of rapamycin
NF-κB	Nuclear factor-κB
PBS	Phosphate-buffered saline
PDGF	Platelet-derived growth factor
PDI	Protein disulphide isomerase
PDIA3	Protein disulphide isomerase A3
PERK	Protein kinase R-like endoplasmic reticulum kinase
PFA	Paraformaldehyde
PgR	Progesterone receptor
PLA2	Phospholipase A2
PLAA	PLA2-activating protein
PLC	Peptide-loading complex
RARA	Retinoic acid receptor-α
SDS	Sodium dodecyl sulphate
SHH	Sonic hedgehog
STAT	Signal transducer and activator of transcription
STIM1	Stromal interaction molecule 1
TAM	Tumour-associated macrophage
TEMED	N,N,N′,N′-Tetramethylethylenediamine
Th	T-helper cell
TME	Tumour microenvironment
TNF	Tumour necrosis factor
TRITC	Tetramethylrhodamine
UPR	Unfolded protein response

Chapter 1

Introduction

1.1 THE NORMAL HUMAN BREAST AND BREAST CANCER

This thesis focusses on breast cancer, so first, the normal breast is introduced for context. The human breast is a highly specialised tissue that facilitates the production and secretion of milk. The fully mature adult mammary gland consists of 3 distinct layers, epithelium; basement membrane (BM) and basal myoepithelial cells and is often surrounded by adipose tissue (**Figure 1.1**). Adult breast tissue is plastic in nature and can undergo rounds of remodelling to form lactating mammary glands and reform the resting, mature mammary glands in line with the need to breast-feed (Hassiotou and Geddes, 2012). It is this plasticity that is hypothesised to be part of the reason that breast tissue is highly susceptible to the formation of tumours during adult life (Radisky and Hartmann, 2009).

The normal, adult, pre-pregnancy breast consists of terminal duct lobular units surrounded by dense stroma and adipose tissue of variable thickness (**Figure 1.1**). During pregnancy these units differentiate into mature milk-producing alveoli due to stimulation by oestrogen- and progesterone-mediated signalling. Part of this remodelling also involves the activation of myoepithelial cells to highly express smooth muscle actin and heavy-chain myosin. This allows them to contract in response to oxytocin and eject milk produced by the luminal cells into the ducts (Hale and Hartmann, 2007). Myoepithelial cells are critical to maintenance of the BM through production of fibronectin (FN), collagen-IV, laminins and nidogen as well as possessing α1- and β4-integrins as part of a repertoire of BM-binding receptors (Gudjonsson et al., 2005).

Cancer originating in epithelial tissues (carcinoma) is the most common form, making up 85% of cancers in the UK (CancerResearchUK). Breast cancer is an example of carcinoma. It has the highest incidence rate of any cancer in the UK, accounting for 15% of new cancer cases every year; and is second only to lung cancer worldwide (CancerResearchUK). Moreover, breast cancer is the 4th most common cause of cancer mortality in the UK, accounting for 7% of UK cancer deaths in 2016 (CancerResearchUK). In general, cancers of epithelial cells, especially breast cancer, are least life threatening whilst the tumour is restrained within in its tissue of origin and has not invaded through the underlying BM. The process of tumour cells invading, resisting anoikis and travelling in the blood or lymphatic systems to secondary sites is termed metastasis and is predicted to cause up to 90% of cancer mortality (Chaffer and Weinberg, 2011).

There is still much debate on how tumour cells, of epithelial origin, undergo 'transformation' to migrate around the body. The prevailing hypothesis is that some cancer cells reactivate a pathway similar to developmental epithelial-mesenchymal transition (EMT) and mesenchymal-epithelial transition (MET) which represent a plastic spectrum of cellular phenotypes that allow each stage of metastasis (**section 1.2.3**).

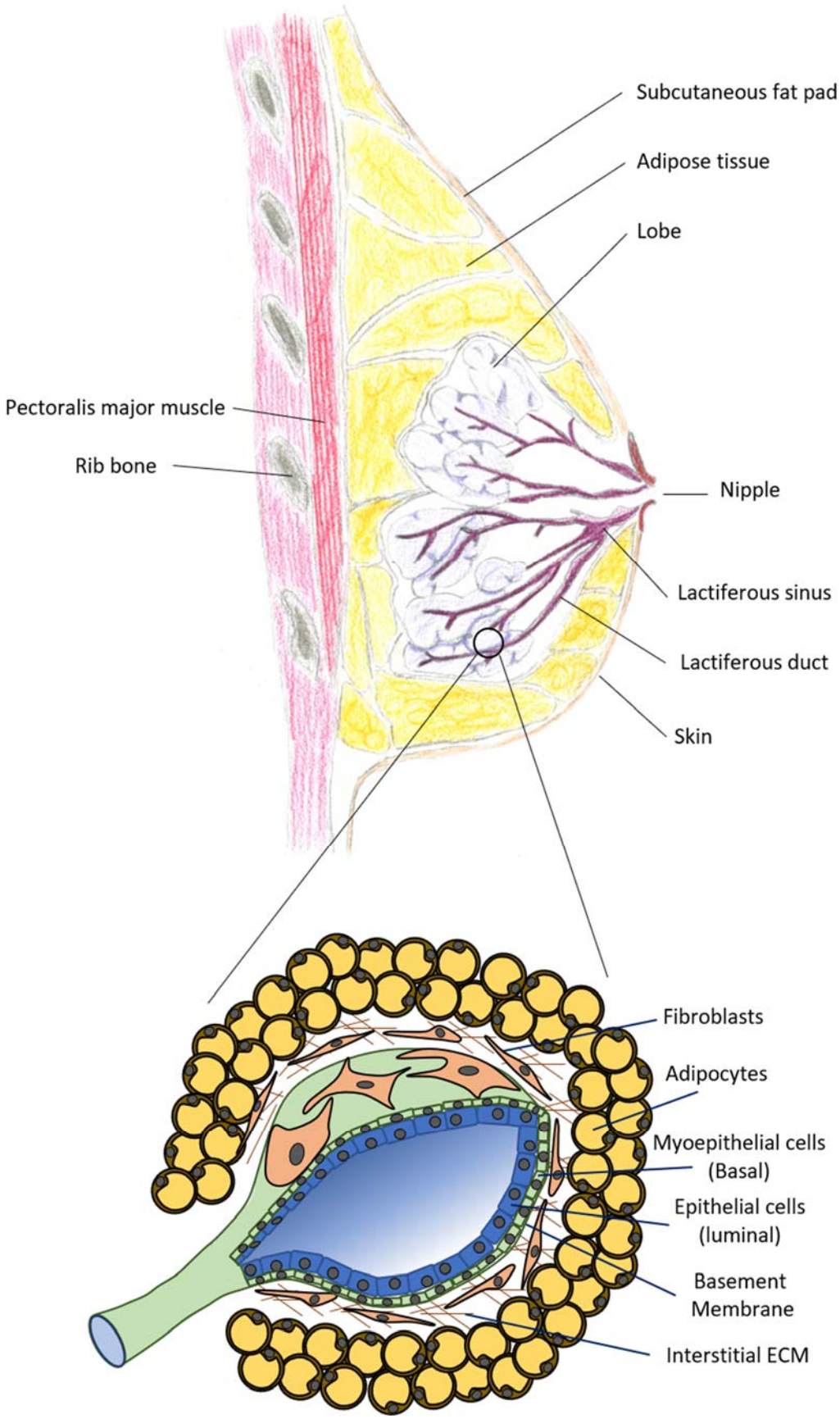

Figure 1.1 ***Anatomy of the Human Breast.*** *Schematic of the normal human breast with expansion of a single adult mammary gland.*

1.1.1 Clinical Staging of Breast Cancer

40-75% of breast cancers worldwide fall into so-called lobular and ductal subtypes that are clinically graded as follows.

Ductal: Normal tissue progressing through potential grades of flat epithelial atypia; atypical ductal hyperplasia; and ductal carcinoma in situ (DCIS) to finally form invasive ductal carcinoma (IDC) (Bombonati and Sgroi, 2011) (**Figure 1.2A**).

Lobular: Progresses from normal tissue through potential grades of atypical lobular hyperplasia and lobular carcinoma in situ into the final histological stage, invasive lobular carcinoma (ILC) (Bombonati and Sgroi, 2011) (**Figure 1.2B**).

For both ILC and IDC the distinguishing feature of their histology in comparison with less advanced cancer stages is the partial or complete loss of BM and myoepithelial layer (Kaushik et al., 2016).

1.1.2 Molecular Subtypes

There are several hypotheses on how breast cancer should be characterised. One widely accepted current hypothesis is that there are four molecular subtypes of breast cancer: luminal (A and B), basal, normal-like, and human epidermal growth factor receptor 2 (HER2 or ERBB2) expressing ($HER2^+$) (Bertucci et al., 2012). These subtypes have been defined by DNA microarrays over the last 2 decades and named according to the pattern of genes expressed with specific attention to key hormone receptors: oestrogen receptor (EsR); progesterone receptor (PgR) and HER2 (Bertucci et al., 2005; Perou et al., 2000). These subgroups are now almost 20 years old but remain as valuable prognostic tools. However, they are under review to be further divided for more specific and accurate prognosis and treatment (Prat et al., 2015; Vuong et al., 2014). The use of integrated genetic, transcriptomic, proteomic and metabolic data analysis will certainly aid these goals and has already been used to further divide the luminal A subtype (Aure et al., 2017).

1.1.2.1 Luminal A and B

Both luminal subtypes are named 'luminal' because the cancerous cells have an expression profile similar to normal luminal epithelial cells in the mammary gland (Bertucci et al., 2012) (**Figure 1.1**). These two subtypes are both EsR^+ and/or PgR^+. Luminal B tumours sometimes express HER2 and proliferative marker Ki-67. Luminal A represents the subtype associated with fewest deaths and low metastatic potential as shown by a German study of 4102 breast cancer patients in which luminal A had relative overall survival (ROS) (at 55 months) of 100% (Hennigs et al., 2016). In this same study luminal B was associated with a slightly worse prognosis of 93.4% ROS (at 55 months). A large contributing factor for the good prognosis of luminal cancers is their dependency on oestrogen to drive cell growth which can be blocked by Tamoxifen (CancerResearchUK) (**section 1.1.3**).

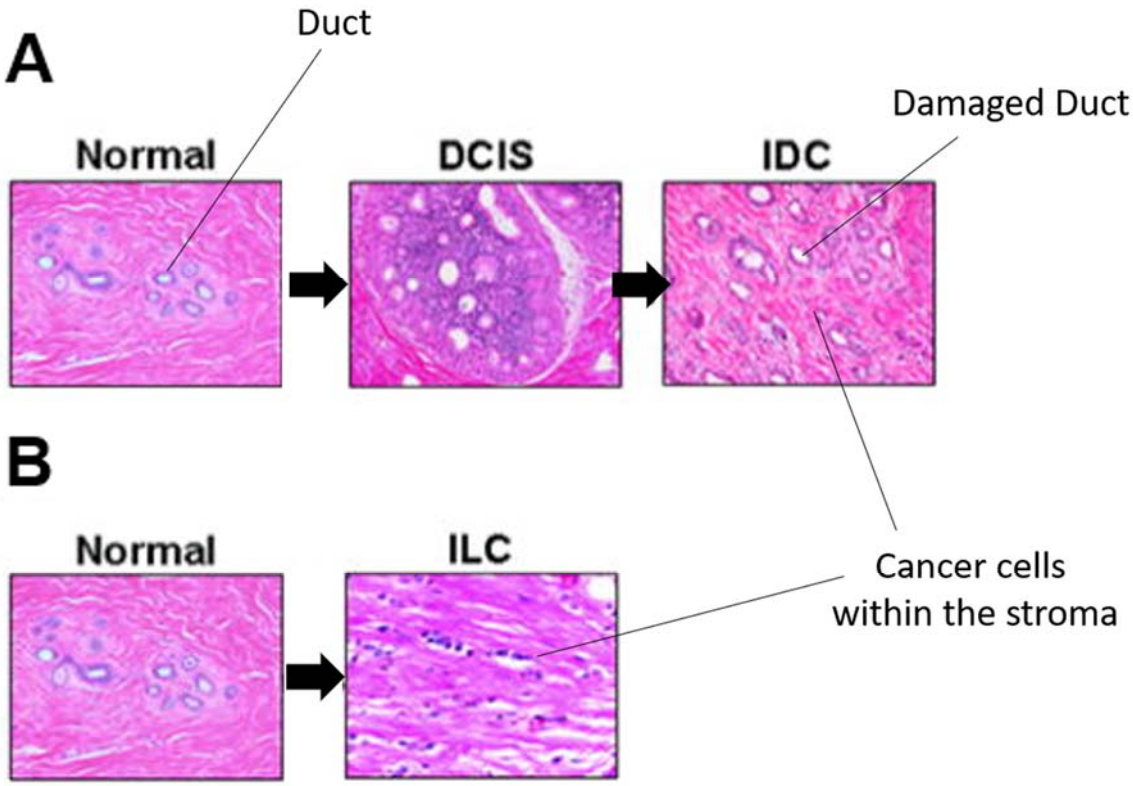

Figure 1.2 ***Current Models for the Progression of Ductal and Luminal Breast Cancers.*** *(**A**) Simplified model of ductal breast cancer progression. (**B**) Simplified model of lobular breast cancer progression. Each stained with Haematoxylin and eosin (H&E). Adapted from:* ***The molecular pathology of breast cancer progression, J. Pathol. Volume: 223, Issue: 2, Pages: 308-318, First published: 14 October 2010, DOI: (10.1002/path.2808) (Bombonati and Sgroi, 2011) Reproduction License Number: 4421221206193***

1.1.2.2 Basal

Basal breast cancer is named because the cancerous cells have a gene expression profile similar to normal myoepithelial cells that contact the BM and so reside on the basal side of the mammary epithelium (Gudjonsson et al., 2005) (**Figure 1.1**). This subtype represents the worst prognosis with a ROS of 80.1% (at 55 months) and is EsR^-, PgR^- and $HER2^-$ (Goldhirsch et al., 2013; Hennigs et al., 2016).

1.1.2.3 Normal-like

These tumours are identical to luminal A in terms of molecular profile (EsR^+ and/or PgR^+, $HER2^-$ and $Ki67^-$) but the pattern of expression resembles normal breast profile as opposed to specifically luminal and has worse prognosis (Dai et al., 2015).

1.1.2.4 Human Epidermal Growth Factor Receptor 2 Over-Expressing

$HER2^+$ tumours are clinically similar to luminal but are distinct in that they rely heavily upon epidermal growth factor (EGF) to drive oncogenic growth through HER2 (Dai et al., 2015). This allows the $HER2^+$ subtype to have good prognosis due to a highly effective specialised treatment, Trastuzumab, that blocks the action of HER2 (CancerResearchUK) (**section 1.1.3**).

1.1.3 Current Treatments and Strategies

This section is based on information on the Cancer Research UK website (CancerResearchUK). The main treatments include following four options, often in combination.

- Surgery
- Chemotherapy
- Radiotherapy
- Targeted cancer drugs (i.e. Specifically targeting the molecular markers driving the cancer) which include Hormonal (endocrine) therapies.

In most cases, the first stage of treatment is the removal of the main tumour bulk by surgery. If the tumour is particularly large, then chemotherapy or hormone therapy are used prior to surgery to shrink the tumour. Common chemotherapeutic combinations for breast cancer include:

- FEC (F – 5-fluorouracil (5FU), E – epirubicin and C – cyclophosphamide (CP))
- E-CMF or CMF (E – epirubicin, C – CP, M – methotrexate and F – (5FU))
- MM or MMM (mitoxantrone, (mitomycin-C) and methotrexate)
- EC (epirubicin and CP)

Targeted Therapies

Hormone therapies work by specifically targeting EsR-mediated growth of breast cancer cells. Commonly used hormone therapies include:

- Tamoxifen
- Anastrozole
- Exemestane
- Letrozole

- Goserelin

Tamoxifen, the first targeted cancer therapy, competitively inhibits EsR directly and via its metabolic products. It outcompetes oestrogen for binding which prevents the EsR-oestrogen complex from activating transcription of growth-related genes in EsR^+ breast cancer (Osborne, 1998). Anastrozole, Exemestane and Letrozole all reduce the amount of oestrogen in the body through interfering with the aromatisation reaction that converts androgens into oestrogen and so can only be used by post-menopausal women where they are more effective than tamoxifen (Poole and Paridaens, 2007). Goserelin can only be used by pre-menopausal women because it is a drug that inhibits the production of oestrogen from the ovaries (Nicholson et al., 1985).

If the tumour is $HER2^+$ then it will be susceptible to a monoclonal antibody therapy, Trastuzumab (Herceptin) that inhibits proliferation of $HER2^+$ cancer cells by competitively inhibiting HER2 (Drebin et al., 1985; Slamon et al., 2001). This can be used in isolation or in combination with common chemotherapeutics or hormone therapies.

Aside from the targeted therapies, the current strategy for treating breast cancer is similar to how we treat all cancer, flood the system with drugs that kill rapidly dividing cells to destroy the cancer. These treatments come with severe side effects and are not sensitive enough to eradicate the more resistant cancer cells such as cancer stem cells (CSCs) or senescent early metastatic cells (Fan et al., 2015; Gordon and Nelson, 2012; Ojo et al., 2015).

1.2 Cellular Development of Breast Cancer

Over the last 20 years there has been a substantial shift in the models of carcinoma development. Until recently, the most widely accepted model was that successive genetic alterations in somatic cells led to the accumulation of the 'hallmarks of cancer' (Hanahan and Weinberg, 2011) and that in turn led to a selective advantage allowing a cell to proliferate excessively and form a tumour. Then, as more genetic mutations are acquired at random, the most successful sub-clone becomes the predominant cell type that is driving tumour progression. Despite its merits, it is now appreciated that this is not the whole picture. More recently, cancer has been hypothesised to also be driven by CSCs and the milieu of cancer-associated cells in the tumour. It is also recognised that both cancer and cancer-associated cells are controlled by metabolic and stromal cues as well as their genetic makeup (Coller, 2014; Crabtree and Miele, 2018; Mitrus et al., 2012). Moreover, it is becoming increasingly apparent that even in the early stages of tumour growth there is dissemination of tumour cells known as 'early metastasis'. This concept is fundamentally opposed to the classical model of cancer development (Lambert et al., 2017).

1.2.1 The Cancer Stem Cell Model and Breast Cancer

A prevailing model of how cancer develops is the cancer stem cell hypothesis. This was first described over 40 years ago and states that cancer cells regenerate and expand the tumour using the same mechanisms as a normal epithelial tissue. In the latter, a hierarchy of cells is produced by a few dedicated stem cells residing in specific stem cell niches (Batlle and Clevers, 2017). The small population of CSCs has been shown to be associated with poor prognosis through the ability to initiate tumour formation, drive metastasis and resist chemotherapeutics, leading to tumour recurrence (Abdullah and Chow, 2013; Geng et al., 2014; Zhao, 2016).

In the normal mammary gland, mammary stem cells (MaSCs) drive expansion of the alveolar epithelium (to produce milk) and are also essential in the degeneration of this epithelium post-pregnancy (Lloyd-Lewis et al., 2017; Visvader and Stingl, 2014). The exact hierarchy surrounding these MaSCs is under debate with contradicting evidence from transplantation and lineage tracing studies in mice (Fu et al., 2014; Inman et al., 2015; Lloyd-Lewis et al., 2017). The model described by Lloyd-Lewis et al., 2017 suggests that multipotent stem cells exist during embryonic development and potentially as a pool of quiescent MaSCs that become activated under certain physiological conditions such as wound healing (**Figure 1.3**). Then, the majority of adult tissue homeostasis is carried out by unipotent luminal and basal stem cells (Lloyd-Lewis et al., 2017). In the context of breast cancer, this means that the cellular origin could be a MaSC of basal or luminal restriction or as a result of induction of a stem-like phenotype by EMT of transformed cells (Crabtree and Miele, 2018).

The balance between MaSC self-renewal and differentiation is poorly understood but developmental pathways have been shown to be regulated by NOTCH (Raafat et al., 2011), WNT (Yu et al., 2016), Hedgehog (SHH) (Hui et al., 2013), and Transforming growth factor-β/Bone-morphogenic protein (TGFβ/BMP) signalling pathways (Moses and Barcellos-Hoff, 2011). In breast cancer, one or more of these are often deregulated leading to acquisition of a stem-like phenotype through EMT (Czerwinska and Kaminska, 2015). The full extent of mechanisms that deregulate these pathways are not known but are of importance to consider when investigating cancer (Czerwinska and Kaminska, 2015; Lamouille et al., 2014).

In breast cancer, specific and consistent CSC markers have yet to be fully elucidated (Visvader and Stingl, 2014). $CD44^{hi}/CD24^{lo}$ (Al-Hajj et al., 2003) or high expression of ALDH1 (Ginestier et al., 2007) represent two major markers of breast CSCs. Other, more generic markers, include EMT-related (e.g. reduced epithelial-cadherin (E-cad) and increased neural-cadherin (N-cad), SNAIL1/2, and vimentin) and pluripotency related

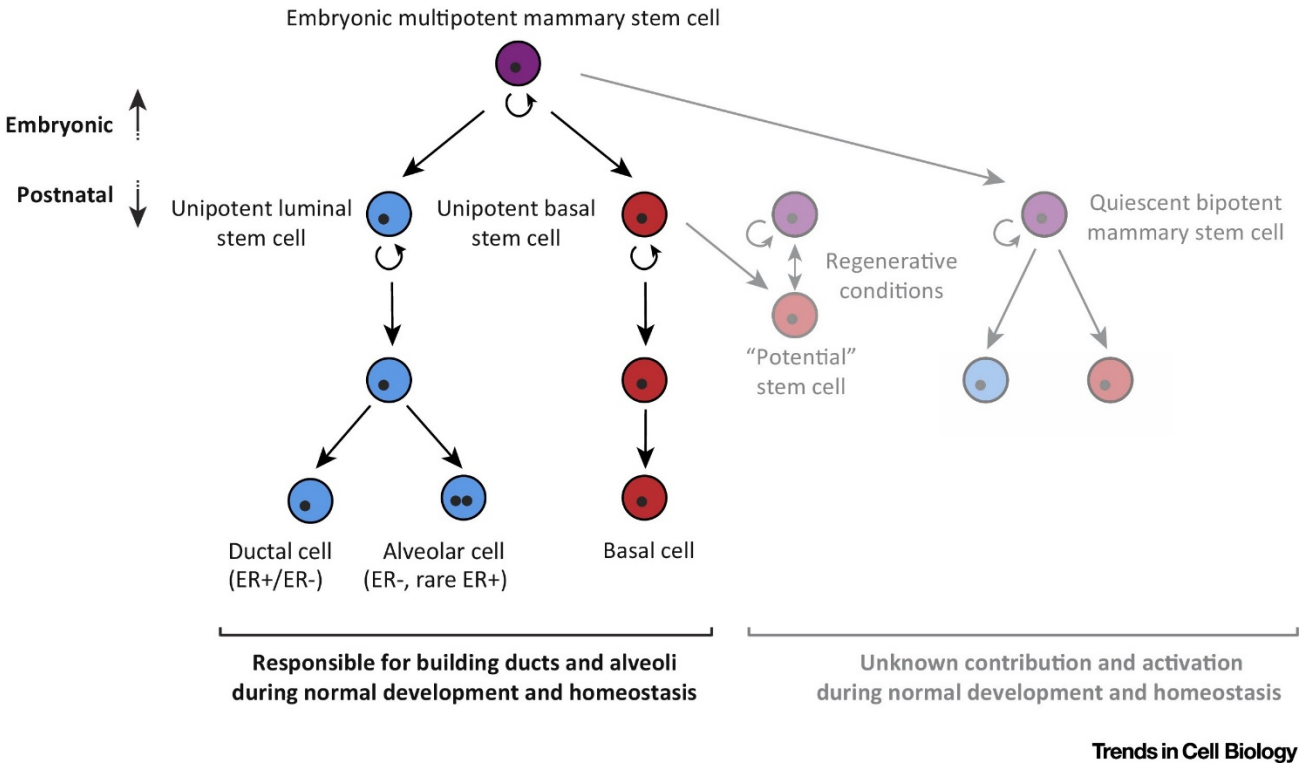

Figure 1.3 ***A Model for Mammary Stem Cell Hierarchy.*** *The model put forward by Lloyd-Lewis et al., 2017, describes an embryonic population of multipotent MaSCs that differentiate postnatally into unclear subpopulations. The left panel describes cells responsible for physiological regulation of the tissue. The unipotent luminal stem cell is responsible for production of Ductal and Alveolar cells that can be EsR+ or EsR-. Whether the basal cells that differentiate from the unipotent basal stem cells are also separated into Ductal- or Alveolar-associated is not known.*

The right panel shows the predicted pool of quiescent bipotent MaSCs that were undetectable in single-cell and quantitative lineage tracing studies. Also shown is another pool of intermediate 'potential' stem cells that may retain plasticity to become more potent and drive regeneration. This is similar to de-differentiation seen in luminal and basal progenitors when transformed with an oncogene (Lloyd-Lewis et al., 2017).

(e.g. increased SOX2 and NANOG) have all been identified through transcriptomic profiles (Akrap et al., 2016; Czerwinska and Kaminska, 2015). Akrap et al., 2016 described clustered populations of highly proliferative and less proliferative cancer cells in both basal and luminal subtypes in human breast cancer-derived cell lines and primary samples using anchorage-independent growth assays and transcriptomic data. This is a good indication of multiple CSC populations, including a common quiescent-like CSC pool that produces a full hierarchy of cell subtypes (Akrap et al., 2016). This complexity of tumour cell hierarchy indicates that there is a need to consider the CSC pool as several distinct and plastic populations.

Plasticity of CSC populations may be regulated by EMT mechanisms controlled by epigenetics (Brooks et al., 2015). This model hypothesises that there is a central, transient CSC population ($CD44^{hi}/CD24^{lo}$, $ALDH^{+}$) that can give rise to either: a mesenchymal-like CSC ($CD44^{hi}/CD24^{lo}$, $Vimentin^{+}$) that is more quiescent but more invasive that gives rise to a tumour that is mainly mesenchymal; or, a fast cycling epithelial-like CSC ($E\text{-}Cadherin^{+}$, $ALDH^{+}$) that is more proliferative and less invasive, producing an epithelial bulk tumour (Brooks et al., 2015). Given that expression of SNAIL and TWIST (two well-characterised transcriptional factors associated with EMT) in human mammary epithelial cells results in $CD44^{hi}/CD24^{lo}$ cells, it is possible that EMT regulates these stem cell populations (Brooks et al., 2015; Lamouille et al., 2014).

The potential existence of multiple CSC pools is particularly interesting for the work in this thesis because the tumour microenvironment (TME) sculpts the CSC niche (Plaks et al., 2015; Ye et al., 2014). Therefore, the ability of cancer and cancer-associated cells to modify the ECM may directly drive the CSC populations to a more invasive and dangerous phenotype. This is predicted to be regulated by reactivated developmental pathways including WNT, NOTCH and SHH (Arendt et al., 2010; Izrailit and Reedijk, 2012; Nwabo Kamdje et al., 2017). The specific effects of the ECM are reviewed in **1.3**.

1.2.2 The Effect of Non-Cancer Cells on Tumour Progression

In breast cancer, cancer cells often make up less than 20% of the tumour mass. The majority consists of remodelled ECM containing fibroblasts, immune cells, adipocytes and others (Arendt et al., 2010; Polyak and Kalluri, 2010). These are summarised in **Figure 1.4**.

1.2.2.1 Fibroblasts

In every tissue, the ECM is synthesised and remodelled by fibroblasts. Fibroblasts are professional ECM-secreting cells that have important roles in tumour initiation and progression and are the most abundant cells in the TME (Buchsbaum and Oh, 2016). Fibroblast phenotype is altered in the TME and so cells in this environment are referred to as cancer-associated fibroblasts (CAFs).

CAFs are being increasingly studied and their role in cancer progression is proving to be extensive. They are associated with the generation of highly aligned ECM that correlates with increased cell motility (Luo et al.,

2015). For example, CAFs are important in the deposition of aligned FN fibres, whereas normal fibroblasts secrete FN into a mesh-like structure. If FN is knocked down in CAFs then synthesis and alignment of ECM is lost and so FN is crucial for this specific organisation of ECM to aid cancer cell migration (Erdogan et al., 2017). The fact that CAFs are professional ECM remodelling cells is further evidence for the importance of alterations to ECM in carcinoma progression.

Currently, there is no exact genetic or epigenetic definition of the CAF, but several proteins are associated with the conversion of fibroblasts into CAFs and with tumour progression (Buchsbaum and Oh, 2016; Soysal et al., 2015). These include α-smooth muscle actin, Calveolin-1, Fibroblast activation protein, Tenascin-C, podoplanin and platelet-derived growth factor (PDGF) receptor (Buchsbaum and Oh, 2016), All of which have roles in the secretion and modification of ECM proteins. It is likely that CAF secretion and remodelling of the ECM contributes to the characteristic stiffening and linearization of breast cancer ECM that drives metastasis (Erdogan et al., 2017; Kaushik et al., 2016).

1.2.2.2 Immune Cells and Regulation

Cancer cells are detected by our immune system due to unique, modified antigens or altered spatial density of antigens that outweigh the self-antigen pro-tolerogenic response (Zitvogel et al., 2008). How the immune system targets cancerous tissue and how cancer subverts this process is an area of active and extensive research (Janssen et al., 2017). Most pertinent to this thesis is the action of the innate immune cells that make up a large percentage of the tumour bulk and have roles in ECM remodelling, fibroblast and endothelial cell activation, and immune suppression (Janssen et al., 2017).

Macrophages are key regulators of the TME. Tumour-associated macrophages (TAMs) infiltrate into the tumour mass. Macrophages exist on a phenotypic spectrum between pro-inflammatory, anti-tumorigenic M1 and anti-inflammatory, pro-tumorigenic M2 macrophages (Martinez and Gordon, 2014). In general TAMs are closer to the M2 phenotype (Genard et al., 2017). In mouse studies, breast cancer cells have been shown to secrete vascular endothelial growth factor A (VEGFA), colony-stimulating factor-1 (CSF-1), CXCL2 and CXLCL12 that chemotactically attract macrophages (Janssen et al., 2017; Noy and Pollard, 2014). Also, CSF-1 was highly expressed at the leading edge of breast tumours in mice (Noy and Pollard, 2014). Under hypoxia, cancer cells secrete eotaxin and oncostatin that chemotactically attract TAMs and polarise to the TAM2 phenotype. This was shown in mouse models, human breast cancer cell lines and human histological samples (Tripathi et al., 2014). This effect on TAMs is also produced through CAF secretion of CCL2, CCL12, interleukin-6 (IL-6) and CSF-1 (Buchsbaum and Oh, 2016; Ziani et al., 2018). It is highly likely that CAF alterations to the ECM will also affect TAM infiltration and polarisation and that there is a reciprocal

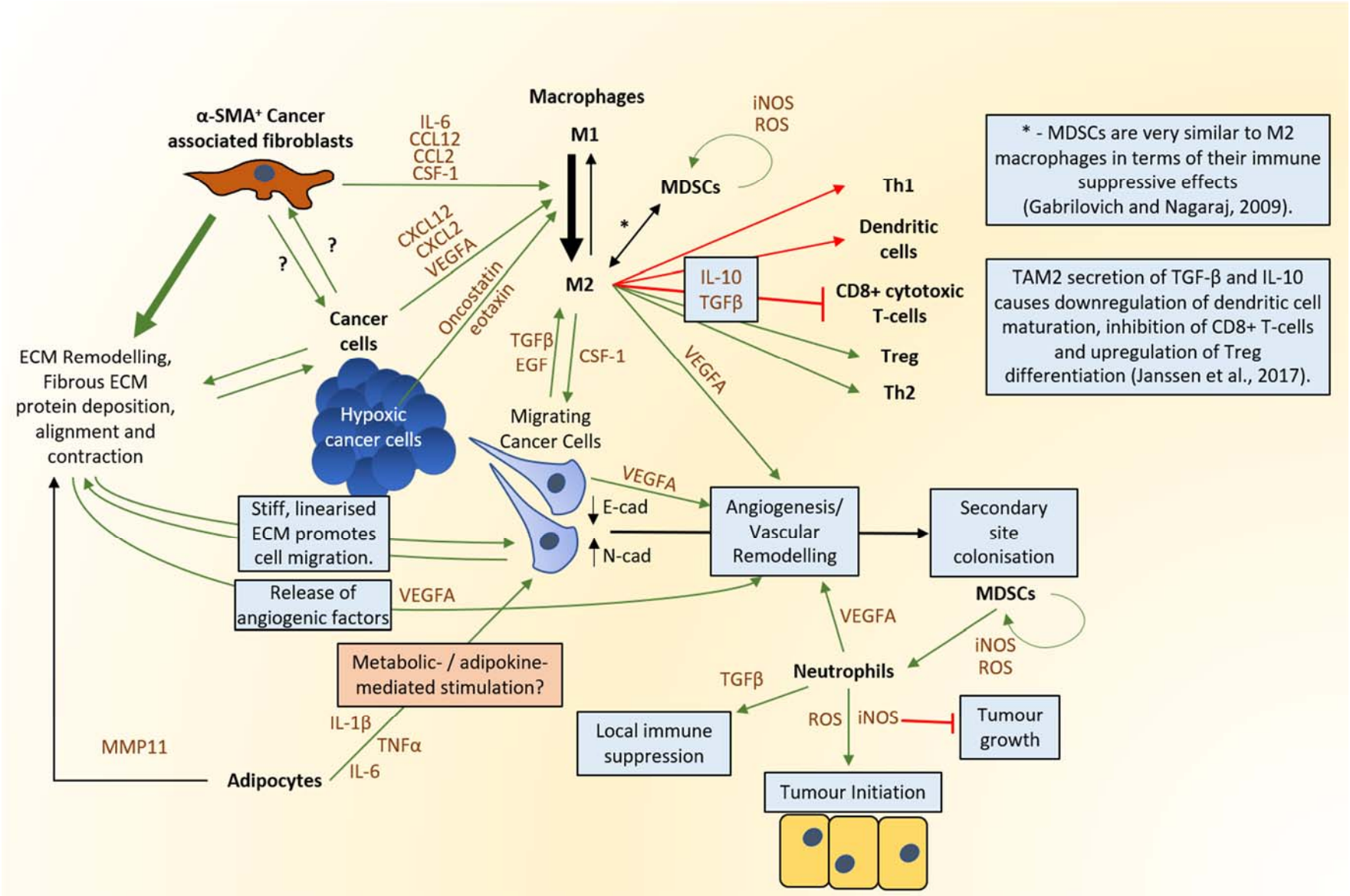

Figure 1.4 ***Cancer-Associated Cells.*** *The diagram shows various interactions between cancer and the tumour microenvironment explained in text.* ***Key:*** *ROS- reactive oxygen species, iNOS- inducible nitric oxide synthase.*

effect between TAMs and CAFs which will influence the ECM (Ziani et al., 2018). Once recruited by these signals, TAMs have a wide array of effects within the tumour that are summarised in **Figure 1.4** (Bonde et al., 2012; Janssen et al., 2017; Linde et al., 2018; Tripathi et al., 2014; Wyckoff et al., 2004).

Myeloid derived suppressor cells (MDSCs) are also recruited into tumours by the same mechanisms as macrophages. They suppress immune activity in the tumour through secretion of reactive oxygen species and cytokines. MDSCs suppress T-helper 1 cells (Th1), CD8+ and natural killer (NK) cells whilst stimulating regulatory T-cells, Th2 and M2 macrophages (Gabrilovich and Nagaraj, 2009). Heightened levels of MDSCs correlate with poor prognosis, highly metastatic breast cancer (Markowitz et al., 2013).

Neutrophils represent the first response to injury and are activated by, and cause, inflammation. They are derived from myeloid precursors and are attracted to chemokine ligands such as CXCL2 (which can be produced by cancer cells – above) and CXCL1 that binds to CXCR2 displayed on neutrophils (Coffelt et al., 2016). Although less studied than the macrophage, a wide, multifactorial role for neutrophils in tumour initiation and progression has been described by Coffelt et al., 2016 and is summarised in **Figure 1.4** (Coffelt et al., 2016; Ocana et al., 2017).

1.2.2.3 Adipocytes

Although less studied than other cancer-associated cell types, adipose tissue represents another important player in the TME. There is an epidemiological correlation between obesity and cancer incidence that is currently not understood. One hypothesis is that the differences between obese and lean adipocyte signalling is important to development of a pro-tumorigenic TME (Duong et al., 2017). As shown in **Figure 1.1**, the mammary ducts are surrounded by adipose tissue. This means that, upon breast tumour formation, there will be interactions between cancer cells and adipocytes. It has been shown that murine adipocytes co-cultured with human or murine breast cancer cells de-differentiate into fibroblast-like cells that have delipidated, display reduced adipose markers, and secrete matrix metalloproteinase-11 (MMP-11), Tumour Necrosis Factor α (TNFα), IL-6 and IL-1β (Bochet et al., 2013; Dirat et al., 2011). The loss of lipid filled adipocytes and increased fibroblast-like cells have been verified at the leading edge of human breast cancer samples (Dirat et al., 2011). Importantly, these alterations result in increased breast cancer cell invasiveness *in vitro* and in *in vivo* mouse studies (Dirat et al., 2011).

1.2.3 Metastatic Progression

In breast cancer, the most invasive forms of cancer are associated with high mortality and this is most often (90%) caused by metastatic disease (Lambert et al., 2017; Redig and McAllister, 2013). Metastasis is the process by which cancer, that is restricted to the tissue of origin, (1) undergoes a series of changes that allows invasion into the local tissue (2); entry into the blood or lymphatic system (3); anoikis resistance to allow transport to a distant site (4); and finally invasion and growth at this secondary site to form a

metastatic colony (5) (**Figure 1.5**). The most widely accepted hypothesis explaining how these processes occur is the EMT-MET model.

1.2.3.1 Epithelial-Mesenchymal Transition

EMT is an array of gene expression programs that are activated within epithelial cells during development, wound healing or fibrosis and is often reactivated by cancer (Lamouille et al., 2014). It is characterised by several molecular markers, most consistently, the reduction of epithelial-cadherin (E-cad) expression and upregulation of neural-cadherin (N-cad) and vimentin. These changes represent the loss of cell-cell-adhesions and gain of mesenchymal characteristics (Lamouille et al., 2014). Key properties of EMT associated with metastatic progression include increased cell motility, resistance to apoptosis and senescence, and the ability to remodel the ECM to enhance invasion (Lambert et al., 2017; Son and Moon, 2010). All these properties are controlled by EMT master transcriptional factors SNAIL, SLUG, TWIST and ZEB 1 (Lamouille et al., 2014).

EMT is a plastic process with several intermediate steps between epithelial or mesenchymal extremes. It is this dynamic phenotype switching that allows cancer cells to shift between proliferative tumour cells, migrating cells and circulating tumour cells to survive each step of metastasis (Chaffer et al., 2016; Lambert et al., 2017).

1.2.4 Angiogenesis

As a tumour grows, its core becomes physically further from the vasculature leading to hypoxic conditions. This means that cancer cells undergo hypoxia signalling, primarily controlled by hypoxia-induced factors (HIFs), causing transcriptional changes to drive a wide array of processes including production and secretion of angiogenic factors such as the VEGF family (of which VEGFA is most studied and the major effector of angiogenesis) (Chung and Ferrara, 2011). Angiogenic factors are also produced by TAMs, CAFs and platelets in response to cancer cell and TME signalling (Chung and Ferrara, 2011; Tripathi et al., 2014). These cumulative angiogenic signals drives the migration of endothelial tip cells and endothelial cell proliferation and elongation to produce new vasculature (Chung and Ferrara, 2011; Draoui et al., 2017). The vessels produced through cancer signalling are heterogenous (at least 6 different types) and chaotic in comparison to normal vasculature (Nagy et al., 2009). These abnormal blood vessels are the product of continuous, unregulated VEGFA expression by cancer cells and the TME and are described as ‘leaky’ (Bielenberg and Zetter, 2015). In general, the larger the tumour, the greater the extent of angiogenesis and the greater the chance of metastasis due to the many vessels for cancer cells to intravasate into (Bielenberg and Zetter, 2015).

Another key aspect of angiogenic regulation is the role of the ECM. Thrombospondin-1 and -2 inhibit angiogenesis by blocking migratory and proliferative capacity of endothelial cells and induce apoptosis

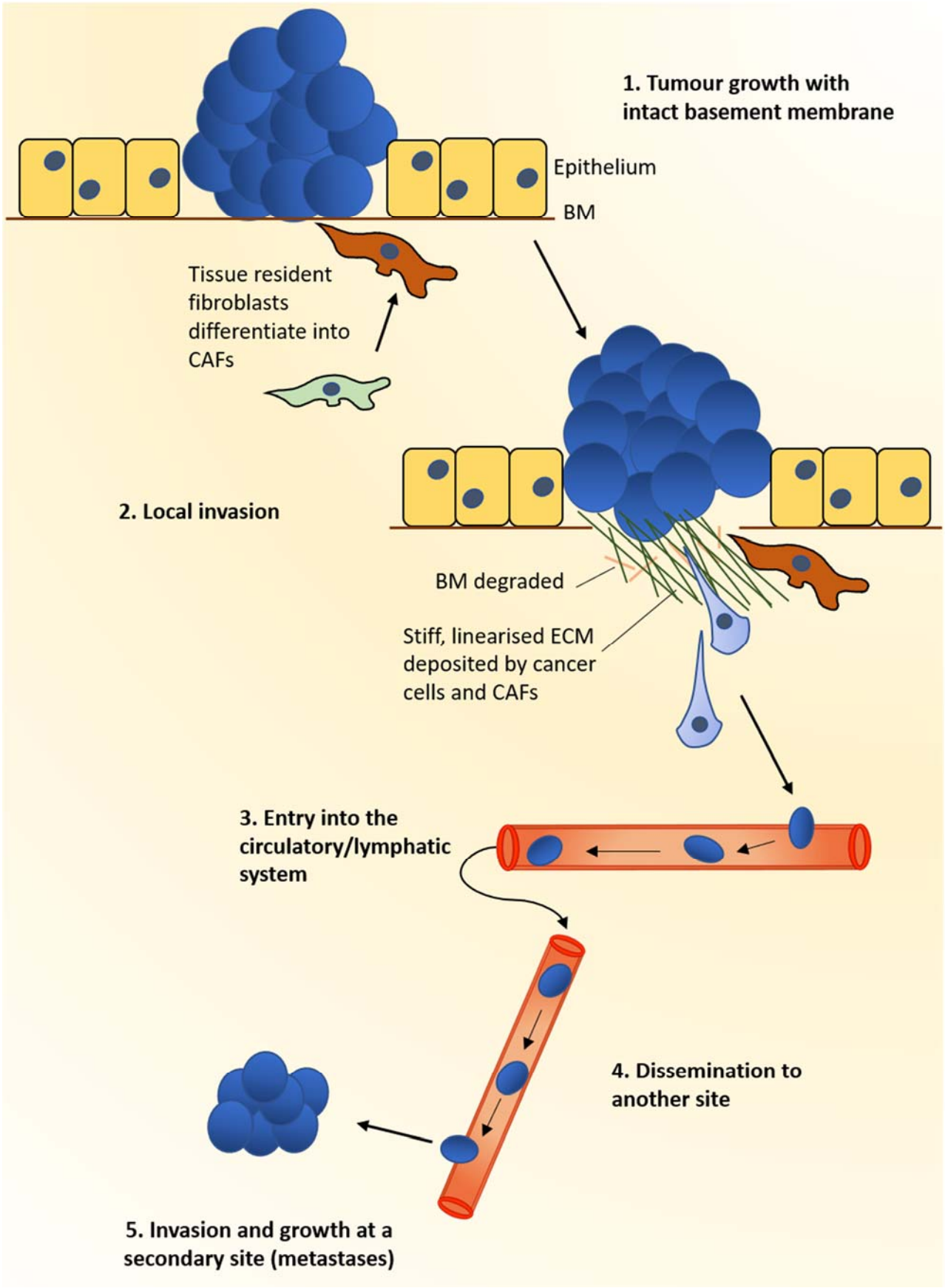

Figure 1.5 ***The Process of Metastasis.*** *A schematic showing an overview of metastasis.*

across many human and mouse *in vivo* and *in vitro* experiments (Ren et al., 2006). FN is essential in formation of healthy 3D ECM essential for angiogenesis and directly binds $\alpha_5\beta_1$ integrin to aid endothelial cell survival (Mongiat et al., 2016). Collagen-I and -IV promote angiogenesis through mechanotransduction by binding integrins whereas, collagen-XVIII contains the anti-angiogenic factor endostatin, which is released upon proteolytic degradation by MMPs (Mongiat et al., 2016). Proteoglycans, including Perlecan and decorin, bind and immobilise VEGF, PDGF and fibroblast growth factor that are released to stimulate angiogenesis upon MMP-mediated degradation of the ECM (Mongiat et al., 2016). This non-exhaustive list of ECM-mediated angiogenic control (based on a review by Mongiat et al., 2016) illustrates the extensive and integrated control of angiogenesis by ECM and partly explains why ECM remodelling is so important to cancer progression.

1.2.5 Cancer as a Metabolic Disease

A significant proportion of the ever-expanding repertoire of mutations associated with cancer have direct effects on cellular metabolism through aerobic glycolysis; glutaminolysis; and one-carbon metabolism (Wishart, 2015). These pathways represent the shift from ATP production to synthesis of intermediates associated with growth and proliferation, including fatty acids, amino acids and nucleotides (Wishart, 2015). Cancer cells uptake vastly more glucose than normal cells through upregulation of key metabolic enzymes under the control of common oncogenes or tumour suppressor genes (protein kinase B (Akt), MYC, HIF and p53) (Coller, 2014). The ability of cancer cells to sense metabolic changes is often perturbed by alterations to the phosphoinositide 3-kinase (PI3K)/Akt and mammalian target of rapamycin (mTOR) pathway (**Figure 1.6**). PI3K is often constitutively activated in cancer either by mutation (Sheen et al., 2016) or via growth factor receptor mutations leading to chronic activation. This results in constant Akt and so mTORC1 signalling (see **Figure 1.6**), driving cell cycling and protein production, resulting in loss of sensing of changes in growth factors and nutrients in the environment (Porta et al., 2014).

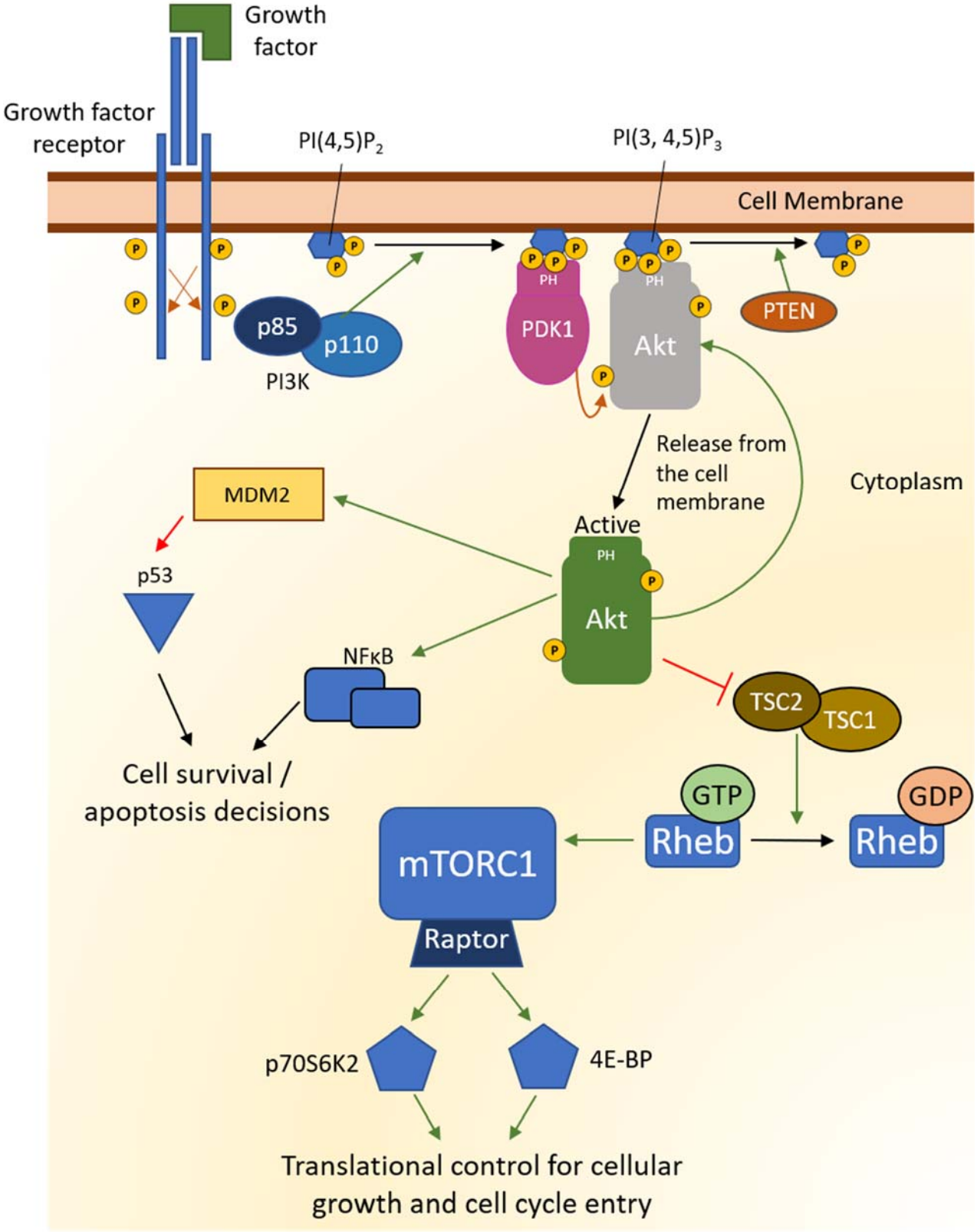

Figure 1.6 ***The PI3k/Akt/mTORC1 Signalling Pathway.*** *Adapted from Alberts et al. Molecular Biology of the Cell and (Porta et al., 2014).*

1.3 EXTRACELLULAR MATRIX

Throughout metastatic progression of breast cancer, there are substantial modifications to the ECM that both characterise and drive the process (Insua-Rodríguez and Oskarsson, 2016; Pickup et al., 2014). These modifications, although significant, are much less well studied than intracellular signalling pathways (Nwabo Kamdje et al., 2014).

The ECM is defined as the network of extracellular molecules that form a 3D structure associated with mechanical and biochemical support of cells. This includes the BM, that functions to separate epithelial or endothelial cells from stromal cells; and interstitial ECM, that is produced by stromal cell populations and makes up the connective tissue. The ECM consists of proteins, proteoglycans, water and polysaccharides. The collagens, FN, elastins and laminins are the core structural element, and proteoglycans (a protein core with multiple glycosaminoglycan chains), make up most of the ECM volume as a hydrated gel (Frantz et al., 2010). The composition of ECM determines tissue stiffness and alters intracellular signalling. The role of ECM in tumour progression is under research (Insua-Rodríguez and Oskarsson, 2016; Oskarsson, 2013; Pickup et al., 2014).

1.3.1 The ECM in Breast Cancer

The remodelled ECM compared to the normal ECM of the breast is summarised in **Figure 1.7** (Insua-Rodríguez and Oskarsson, 2016).

An essential early step in metastatic progression is the degradation of the sub-epithelial BM to facilitate tumour cell invasion of the stroma (Cox and Erler, 2011). The BM is a dense, 50-100nm sheet of highly cross-linked protein and proteoglycan. In cancer, the composition of BM is altered and resembles amniotic BM which is much less rigid and vulnerable to degradation and invasion of cells (Kalluri, 2003). The exact nature of these changes is different based on the location of the tumour but includes reduced collagen-IV and laminin (Albrechtsen et al., 1981; Morrissey et al., 2016; Tanjore and Kalluri, 2006). This facilitates cell invasion and could be the result of changes in secretome of BM-producing cells, perhaps caused by paracrine signalling from the cancer, or enhanced proteolysis by increased production of MMPs by cancer or cancer-associated cells (Gudjonsson et al., 2002). However, recently it has been shown that, in C. elegans, the proteolytic aspect of invasion is only a small and potentially superfluous part of the process that makes the process of physically breaching the BM easier but, with time, invasion still occurs (Morrissey et al., 2013). Upregulation of collagen-IV has been associated with progression of breast cancer through a signalling role (Burnier et al., 2011; Kehlet et al., 2016; Xiong et al., 2014). Although ECM remodelling does occur in non-invasive carcinoma *in situ* (Emery et al., 2009), entry of tumour cells into the connective tissue is associated with more extensive ECM remodelling (Kaushik et al., 2016; Lu et al., 2012; Pickup et al., 2014).

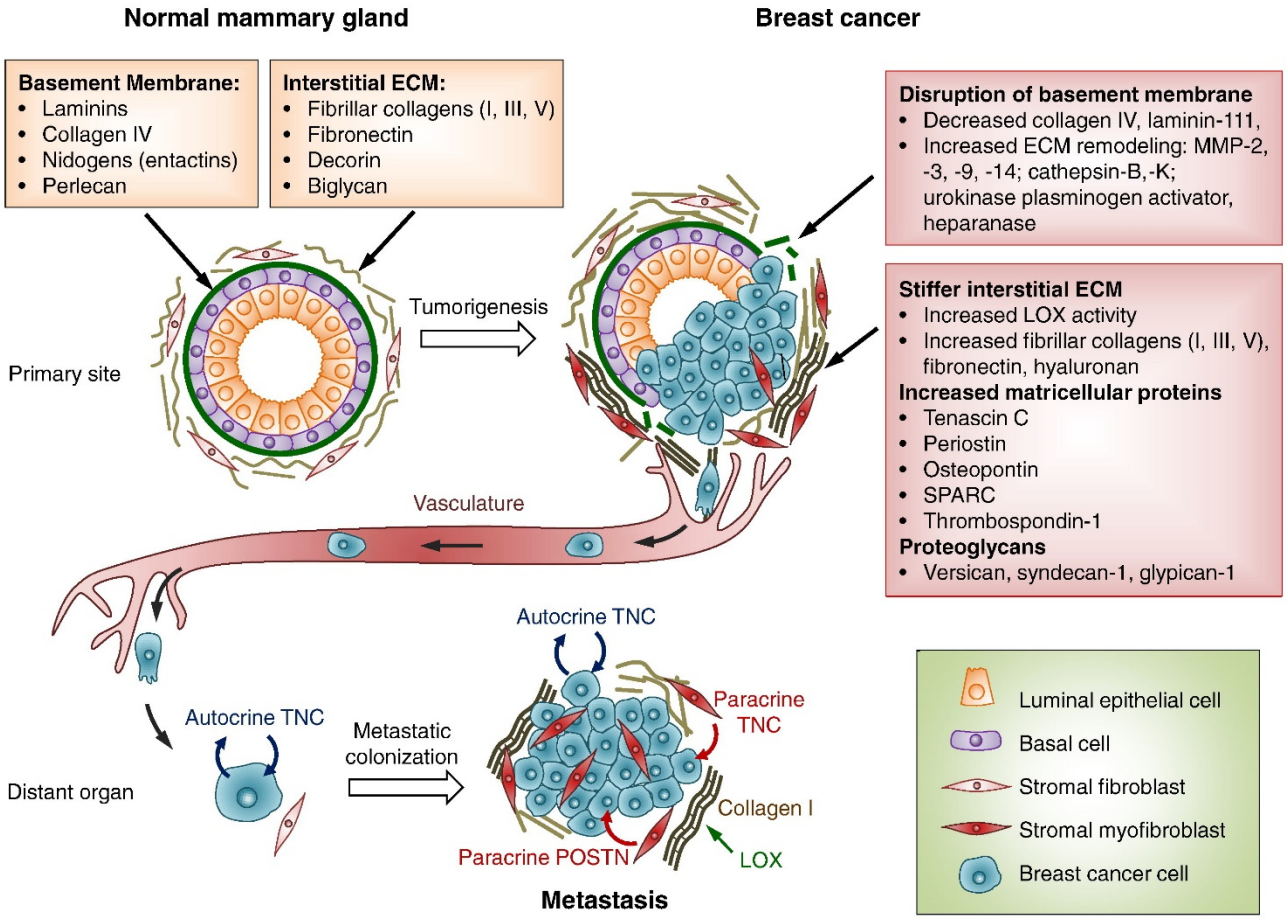

Figure 1.7 ***Changes in ECM with Carcinoma Progression.*** *(Insua-Rodríguez and Oskarsson, 2016)* ***Reprinted from Adv Drug Deliv, Vol 97, Insua-Rodríguez and Oskarsson, The extracellular matrix in breast cancer, Pages 41-55., Copyright (2016), with permission from Elsevier Reproduction Licence Number: 4395871485173.***

1.3.2 Physical Mechanisms Involved in Stiffening the ECM

Recently, the role of the physical properties of the ECM, especially stiffness, have been shown to be important in the mechanisms surrounding formation and progression of cancer. Stiffening of the ECM is defined as the increased ability to resist deformation by pressure and is caused by enhanced deposition of fibrillar proteins and cross-linking between them. For example, proteins significantly altered in the stiffened ECM associated with breast cancer include:

Collagens and lysyl oxidase - There is a significant shift in collagen production in breast cancer resulting in an increase of fibrillar collagens I, III and V and substantial reduction in the major BM component, collagen-IV (Insua-Rodríguez and Oskarsson, 2016). Reduced collagen-IV is caused by the destruction of the BM and is also associated with the menopausal process of involution (Oskarsson, 2013). This is a good example of the overlap between metastasis and developmental pathways.

The collagen crosslinking enzyme, lysyl oxidase (LOX), is expressed in response to HIF-1 and TGFβ. In breast cancer, LOX activity is increased and contributes to the stiffening of the surrounding stroma and resistance to proteolytic degradation or pH changes (Friedl and Alexander, 2011; Hu et al., 2017; Lu et al., 2012).

Fibronectin – FN is a glycoprotein that forms fibrils important to the structure of the ECM both directly and through retaining collagen-I and thrombospondin-1 in the ECM (Sottile et al., 2002). FN content is an important aspect of stiffening. Upregulation of FN is well documented in breast cancer cells, CAFs and as part of the wound healing response (Insua-Rodríguez and Oskarsson, 2016).

1.3.3 Biochemical Effects of the ECM on Cancer

The ECM has a major role in biochemical signalling involving integrins, growth factors and signalling intermediates. In addition to activating intracellular signalling by integrin binding (**section 1.3.5**), an array of growth factors such as TGF-β1, VEGF, SHH, BMPs and fibroblast growth factor-2 are bound and immobilised by heparan sulphate side chains of ECM glycoproteins. It is thought that growth factors are sequestered in the ECM so that there is a pool of pre-synthesised growth factors that release upon ECM remodelling to speed wound healing (Schultz and Wysocki, 2009). Cancer is often described as 'a wound that does not heal' and so it is unsurprising that these biochemical signals are used to promote cancer (Dvorak, 2015; Schultz and Wysocki, 2009). During tumour progression, cancer cells and cancer-associated cells secrete MMPs that partially digest the ECM to allow for remodelling and, in doing so, release various immobilised signalling molecules (Gialeli et al., 2011). TGF-β is a well-known inducer of mesenchymal cell migration and stem-like properties in cancer and VEGF enhances angiogenesis (Caja et al., 2018; Vempati et al., 2014). Also, fragments of ECM proteins can cause cell signalling events. For example, collagen-IV proteolytic fragments have been associated with immune infiltration and both angiogenic and anti-angiogenic

pathways (Fang et al., 2014) (**section 1.2.4**). It is likely that tumour progression drives production of ECM associated with growth and repair in both a biochemical and mechanical capacity to stimulate proliferation and allow formation of new vasculature (Dvorak, 2015).

1.3.4 The Effect of ECM Stiffness on Migratory Capacity

The stiffened and linearised ECM associated with breast cancer has a profound effect on the ability of cells to migrate. In artificial ECM (aECM) hydrogels, an increase in cross-linking density (and so high stiffness) **reduced** MC3T3-E1 mouse pre-osteoblastic cell spreading and migration in 3D (Ehrbar et al., 2011). (These cells have been shown to promote the formation of secondary tumours by breast cancer cells in mouse models and are used here as a model for cell migration in a common breast cancer metastasis site (Bodenstine et al., 2011)). This is contrary to what is seen in breast cancer *in vivo* (Schedin and Keely, 2011). It is hypothesised that reduced migration in response to heightened stromal stiffness is overcome in natural ECM by alignment of collagen fibres providing 'tracks' for cells to move along as opposed to a random mesh. Also, that the surrounding milieu of glycoproteins and proteoglycans are very pliable to protease-dependent and independent modifications by cancer and cancer-associated cells, whereas aECM is not (Ehrbar et al., 2011; Ilina and Friedl, 2009). The collagen tracks enhance motility by allowing an increase in focal adhesion formation required for cell migration, similar to how the follicular conduits in the lymph node enhance lymphocyte motility (Lu et al., 2012). In breast cancer, alignment of collagen fibres is perpendicular to the leading edge of the tumour and so increase motility away from the tumour mass, enhancing outward invasion (Kaushik et al., 2016).

Another interesting property shown in aECM is that migration of MC3T3-E1 cells through aECM resulted in formation of micro-tunnels that enhanced migration of other cells (Ehrbar et al., 2011). This is conserved in natural ECM which is not a homogenous scaffold but a complex network of channels and tracks including 3D collagen tubes (Friedl and Alexander, 2011). These channels could act as a highway for the invasion of cancer cells and the movement of macrophages or CAFs (Friedl and Alexander, 2011). This hypothesis is supported by the fact that human squamous cell carcinoma-derived CAFs deform collagen-I matrices *in vitro* in a force-dependent manner to form tracks that promote squamous cell carcinoma cell migration (Gaggioli et al., 2007).

1.3.5 Mechanotransduction

The stiffening of the stroma is sensed and translated into biochemical changes within a cell through mechanosensory adhesions such as integrin heterodimers. This process is termed 'mechanotransduction' (Schedin and Keely, 2011). β1-integrin clusters in response to stiffened ECM due to the increased ECM protein binding partners including collagen, FN and laminins (Friedl and Alexander, 2011). Integrin-ECM binding causes the integrin C-terminal, cytoplasmic tail to engage adaptor proteins such as talin and paxillin, forming an initial adhesion (Friedl and Alexander, 2011; Kanchanawong et al., 2010). This adhesion

then recruits mechanosensing modulator proteins vinculin and p130Cas which bind the actin cytoskeleton and focal adhesion kinase (FAK) to form a mature focal adhesion. The focal adhesion acts as a mechanical anchor between the actin cytoskeleton and the ECM and signals through FAK (Zhao and Guan, 2009). When FAK is ablated in mice, mammary tumour proliferative capacity is reduced through reduced ERK, PI3K and Rho/ROCK signalling (Gehler et al., 2013). Also, Cre/LoxP-mediated FAK or β1-integrin knock-out mouse models have shown that mechanosensing by β1-integrin is required for breast cancer tumorigenesis and maintenance (White et al., 2004).

Mechanotransduction feeds into cell fate decisions in both stem cells and cancer (Broders-Bondon et al., 2018; Engler et al., 2006). For example, in mesenchymal stem cells, it has been observed that growth on matrices of varying stiffness defines cell fate (Engler et al., 2006). In cancer, *in vivo* mouse studies have shown that mechanotransduction drives PI3K-mediated tumour progression and invasion through integrin β1-mediated signalling (Levental et al., 2009). β1 signalling potentiates EGF-stimulated Akt signalling that drives cell proliferation and survival (Levental et al., 2009). Moreover, in mouse and human breast cancer cells, the YAP/TAZ signalling pathway (which is heavily involved in proliferation and EMT), is triggered by high ECM stiffness (Broders-Bondon et al., 2018). Integrin signalling due to a stiffened ECM also causes TWIST1 phosphorylation which releases TWIST1 from its cytoplasmic sequestering protein G3BP2, allowing nuclear translocation to trigger transcriptional changes associated with EMT in human breast cancer cells *in vitro* and in xenografts in mice (Wei et al., 2015).

1.3.6 The Extracellular Matrix and Cancer Stem Cell Maintenance

CSCs exist in specific niches that vary between cancers. In breast cancer, CSC markers are promoted by a hypoxic and stiff microenvironment via integrin-linked kinase (Pang et al., 2016). Also, TNC, that is a protein associated with stiffened ECM and produced by fibroblasts, regulates the stem-like phenotype through WNT and NOTCH signalling (Kaushik et al., 2016). There is increasing evidence for the mechanical control of CSCs and this concept being integrated into work on microenvironmental control of CSCs focussing on outside-in signalling driving stemness (Davies and Albeck, 2018; Ye et al., 2014). Due to the extensive list of factors affecting CSC regulation, it is unlikely that one system will be found to be the main regulator and instead an integrated approach of studying several pathways and where they converge will need to be taken to fully understand CSC regulation (Davies and Albeck, 2018).

1.3.7 The Pre-Metastatic Niche

The pre-metastatic niche is a distant site that supports cancer cell growth and survival due to modifications to the local environment. The composition of ECM is important to this. For example, LOX has been shown to be essential in mice for the formation of a pre-metastatic niche in the lungs (Erler et al., 2009). LOX is secreted by human breast cancer cell xenografts under hypoxic conditions and this LOX accumulates at pre-metastatic sites (Erler et al., 2009). LOX then cross-links BM collagen-IV at the pre-metastatic niche, which recruits MDSCs into the tissue, that then secrete MMPs and versican (Kaushik et al., 2016). The secreted

MMPs digest the BM, producing collagen-IV peptides which chemotactically attract more MDSCs in a positive feedback loop (Erler et al., 2009). Versican is an ECM proteoglycan that helps migrating breast cancer cells to undergo MET in the lung, driving proliferation and accelerating growth of the metastatic tumour (Gao et al., 2012). This study was performed using MDA-MB-231 xenografts and in MMTV-PyMT mice that spontaneously develop pulmonary metastasis of mammary tumours.

Similarly, fibronectin is regularly upregulated in fibroblasts at pre-metastatic sites where it is laid down and binds $\alpha_4\beta_1$ integrin displayed on the cell surface of bone-marrow-derived infiltrating $VEGFR1^+$ haematopoietic progenitor cells (Erler and Weaver, 2009). The FN-$\alpha_4\beta_1$ complex is essential for formation of haematopoietic progenitor cell clusters that are critical for metastasis through MMP secretion and other unknown pathways (Erler and Weaver, 2009). Formation of the pre-metastatic niche is an ongoing area of research that is still in its infancy but recent advances in exosome biology are adding exciting concepts to this aspect of metastasis (Erler and Weaver, 2009; Kaushik et al., 2016; Lobb et al., 2017).

A compelling model to explain the role of ECM and secreted products in relation to tumour progression is 'Plasticity and Reciprocity'. This models states that there are mechanisms that results in 'plasticity' of cell phenotype that are a result of processing environmental signals (termed 'reciprocity'). When a cancer cell acquires migratory capacity and changes its position within the tissue, it becomes exposed to different biochemical and biophysical stromal conditions, and so different mechanotransduction, which in turn alters cell phenotype causing increased or subverted migratory and proliferative capacity (Friedl and Alexander, 2011).

1.4 PROTEIN DISULPHIDE ISOMERASE A3

Protein Disulphide Isomerase A3 (PDIA3, also known as ERp57, GRP58 or 1,25-D3 Membrane-Associated Rapid Response Steroid Binding Receptor) is a member of the PDI family of enzymes which are a part of the thioredoxin superfamily of which every member contains either a catalytically active or inactive thioredoxin domain (Hettinghouse et al., 2018). The thioredoxin superfamily is one of the key cellular antioxidant systems and thioredoxin domains contain highly conserved Cys-X-X-Cys (ER where XX is often glycine-proline) motifs for reduction and so disulphide isomerisation of proteins containing cysteines (High et al., 2000). PDIA3 functions in the quality control of folding of certain glycoproteins in the endoplasmic reticulum (ER) and this is thought to be its primary function (Turano et al., 2011). In addition, PDIA3 is proving to be an important enzyme in several other cellular pathways and is becoming increasingly studied in a plethora of diseases. *Pdia3*$^{-/-}$ is embryo lethal in mice (Coe et al., 2010).

Given the focus of this project on PDIA3, this protein is discussed in detail.

1.4.1 Structure

PDIA3 protein is 505 amino acids long and structurally similar to the namesake enzyme PDI. It has four thioredoxin domains, **a**-**b**-**b'**-**a'**, arranged into a "U-like" structure (Kozlov et al., 2006) (**Figure 1.8 and 1.9**). Domains **a** and **a'** each contain a catalytically active CXXC thioredoxin motifs and linker domains, **b** and **b**', contain catalytically inactive thioredoxin motifs and act as spacers between the active sites (Kozlov et al., 2006). The inactive **b'** domain contains a run of positive amino acids that is essential for binding P-domains (proline-rich) of calreticulin (CRT) or calnexin (CNX), where CRT is the soluble paralog of CNX (**section 1.4.4.1**) (Tannous et al., 2015).

There is considerable flexibility between linker and catalytic domains (**b** + **a** and **b'** + **a'**) that lock when a substrate is bound (Kozlov et al., 2010). Thus, the 'characteristic U-shape' is only present in bound complexes. A 2.6 Å resolution crystal structure of PDIA3 in complex with tapasin as part of the major histocompatibility complex class I (MHC-I) peptide-loading complex (PLC) exists (Dong et al., 2009). PDIA3 contains an N-terminal amino acid sequence associated with initial ER localisation; a C-terminal QDEL ER retention motif; and a nuclear localisation signal (Guo et al., 2002).

1.4.2 Cellular Localisation

PDIA3 is principally an ER resident protein, like PDI, but it has also been shown to be present elsewhere. Coppari et al., 2002 demonstrated that PDIA3 can be localised in the nucleus of HeLa and 3T3 cells using DNA-protein cross-linking (UV and cis-DDP) with nuclear lysate experiments and by immunofluorescence (Coppari et al., 2002). PDIA3 was also shown to be nuclear in NB4 leukemia cells by co-immunoprecipitation of Nuclear factor-κB (NF-κB) and PDIA3 followed by subcellular fractionation and confocal microscopy (Wu et al., 2010). These results were brought into question by a later study showing no functional interaction between NF-κB subunit, p65, and PDIA3 (Grindel et al., 2011). However, Grindel et al., 2011 reported a small cytoplasmic pool of PDIA3 in HepG2 cells (by subcellular fractionation and confocal microscopy) which is translocated into the nucleus in response to TNF-α. In this case, nuclear PDIA3 was shown with a PDIA3-GFP fusion protein and live-cell confocal microscopy (Grindel et al., 2011).

Guo et al. 2002 also showed a cytoplasmic pool of PDIA3, as well as plasma membrane localisation, using cross-immunoprecipitation of gel-filtration chromatography filtrates and differential sedimentation respectively (Guo et al., 2002). Localisation of PDIA3 to the plasma membrane has also been shown using co-immunoprecipitation of PDIA3, the traditional vitamin D receptor (VDR) and caveolin-1 in MC3T3-E1 cells (Chen et al., 2013). Finally, PDIA3 was shown to function extracellularly in renal fibrosis (**section 1.4.5.1**) through two-dimensional electrophoresis of conditioned media (Dihazi et al., 2013). Therefore, PDIA3 localisation is not as simple as initially thought. Some models to explain PDIA3 export to unexpected locations include selective proteolysis and formation of complexes to block, expose or remove retention

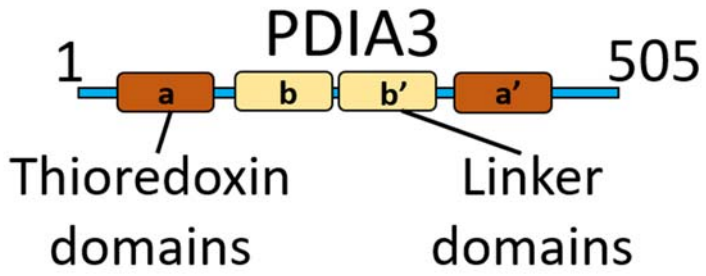

Figure 1.8 ***A Structural Schematic of PDIA3 Depicting the Four Domains.***

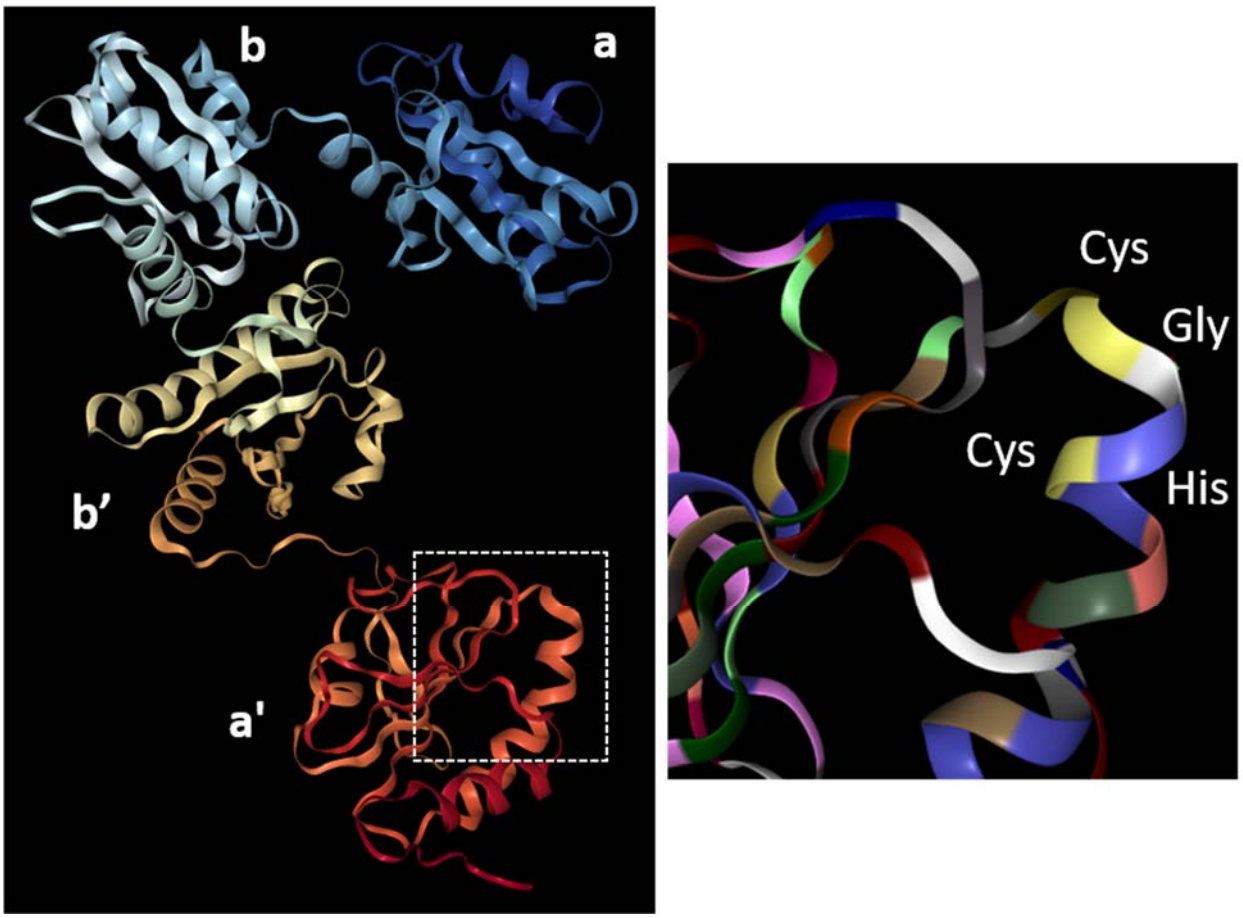

Figure 1.9 ***RSCB Protein Data Bank Structure of PDIA3.*** *The structure of human PDIA3-Tapasin complex (3F8U) expressed In Spodoptera frugiperda (Dong et al., 2009). 2.6 Å X-ray diffraction structure. The image displayed was modified to remove attached tapasin protein. The insert shows a magnified view of the CXXC active site in the* ***a'*** *domain using 'by residue' colouration. Images created with the PDB ID and associated publication, NGL Viewer (AS Rose et al. (2018) NGL viewer: web-based molecular graphics for large complexes. Bioinformatics dio:10.1093/bioinformatics/bty419), and RCSB PDB (Rose et al., 2018).*

sequences (Coe et al., 2010; Guo et al., 2002; Ramírez-Rangel et al., 2011). Grindel et al., 2011 state that PDIA3 contains a destabilising proline within its N-terminal signal sequence that may account for a weaker ER localisation allowing escape from the ER. Once cytoplasmic, the nuclear localisation signal is exposed and allows nuclear translocation (Grindel et al., 2011). Also, Dihazi et al., 2013, propose that escape from the oxidising ER environment could result in deformation and breaking of disulphide bonds to change the tertiary structure of PDIA3 allowing different localisations (Dihazi et al., 2013).

1.4.3 Inhibition

No completely specific pharmacological inhibitor of PDIA3 is currently commercially available. This is because the PDI family have highly conserved thioredoxin domains and so it has not yet proved possible to avoid off-target inhibition, or binding, of a PDIA3 inhibitor to other PDI family members. To address this issue, this project will use two inhibitors in parallel, PACMA-31 which is specific for PDIA1, and 16F16 that targets PDIA1 and PDIA3 (**Figure 1.10**) (Hoffstrom et al., 2010; Xu et al., 2012).

16F16

16F16 (**Figure 1.10A**) is a small molecule inhibitor of PDI family proteins PDIA1 and PDIA3. Its chloroacetyl moiety covalently binds and deactivates the CXXC active sites (Hoffstrom et al., 2010). This is the only commercially available PDIA3 inhibitor at present and was originally described as a PDIA1 inhibitor (Hoffstrom et al., 2010). The efficacy of 16F16 intracellularly along with its preferred PDI family protein target has been questioned but, so far, there have been no definite answers (Foster and Thorpe, 2017). For example, 16F16 has also been shown to bind PDIA6 using *in situ* proteome profiling of MCF-7 cells (Ge et al., 2013).

PACMA-31

PACMA-31 (**Figure 1.10B**) appears to act in the same way as 16F16 by covalently binding the active cysteines of the thioredoxin motif (Xu et al., 2012). However, PACMA-31 is very specific to PDIA1 with no reported off-target inhibition. It has been shown to modify the secondary structure of PDI and mirror the cellular effect of siRNA to PDI in ovarian cancer cell lines (Xu et al., 2012).

In this project, the effects produced by treatment with 16F16 that are distinct from those produced by treatment with PACMA-31 are deduced to depend on inhibition of PDIA3, not PDIA1.

1.4.4 Functions and Associations

1.4.4.1 Quality Control in the ER

PDIA3 was originally described as a protein of around 58kDa responsive to stress from glucose depletion in by Lee et al, 1981 and so originally named GRP58 (Lee, 1981). Since then its function as a key enzyme in correct protein folding of secreted or cell-surface proteins has been characterised. First, PDIA3 forms a complex with CNX or CRT which are ER chaperones that bind unfolded (non-native) and partially folded

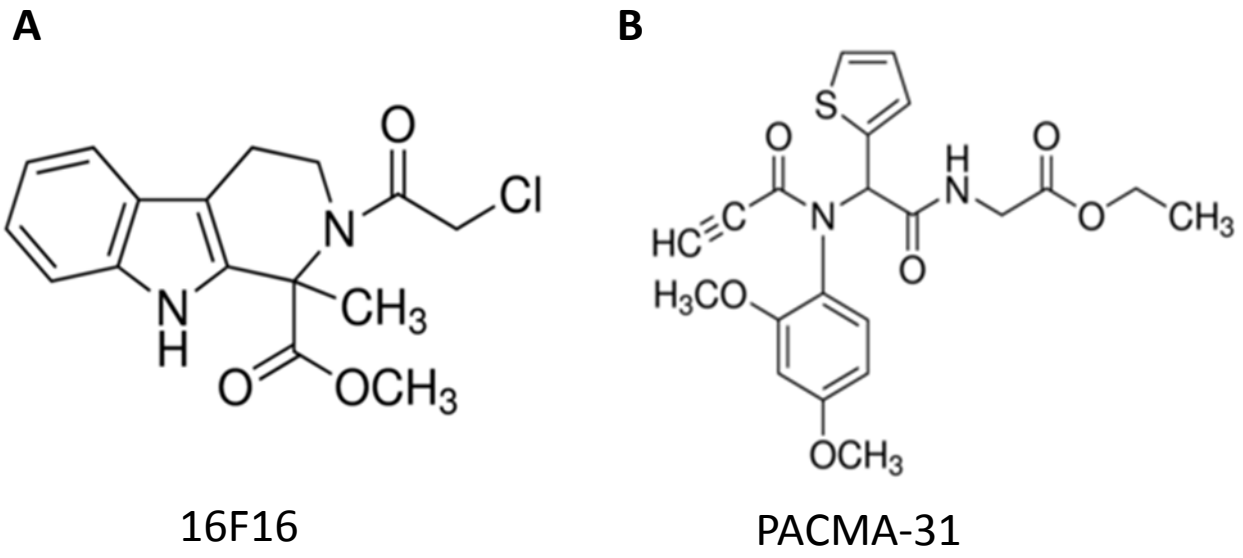

Figure 1.10 ***Structure of PACMA-31 and 16F16.*** *Skeleton diagrams acquired from the Sigma-Aldrich website. (**A**) 16F16, catalogue number-SML0021, PubChem-CID 4555562. (**B**) PACMA-31, catalogue number-SML0838 PubChem-CID 455556.*

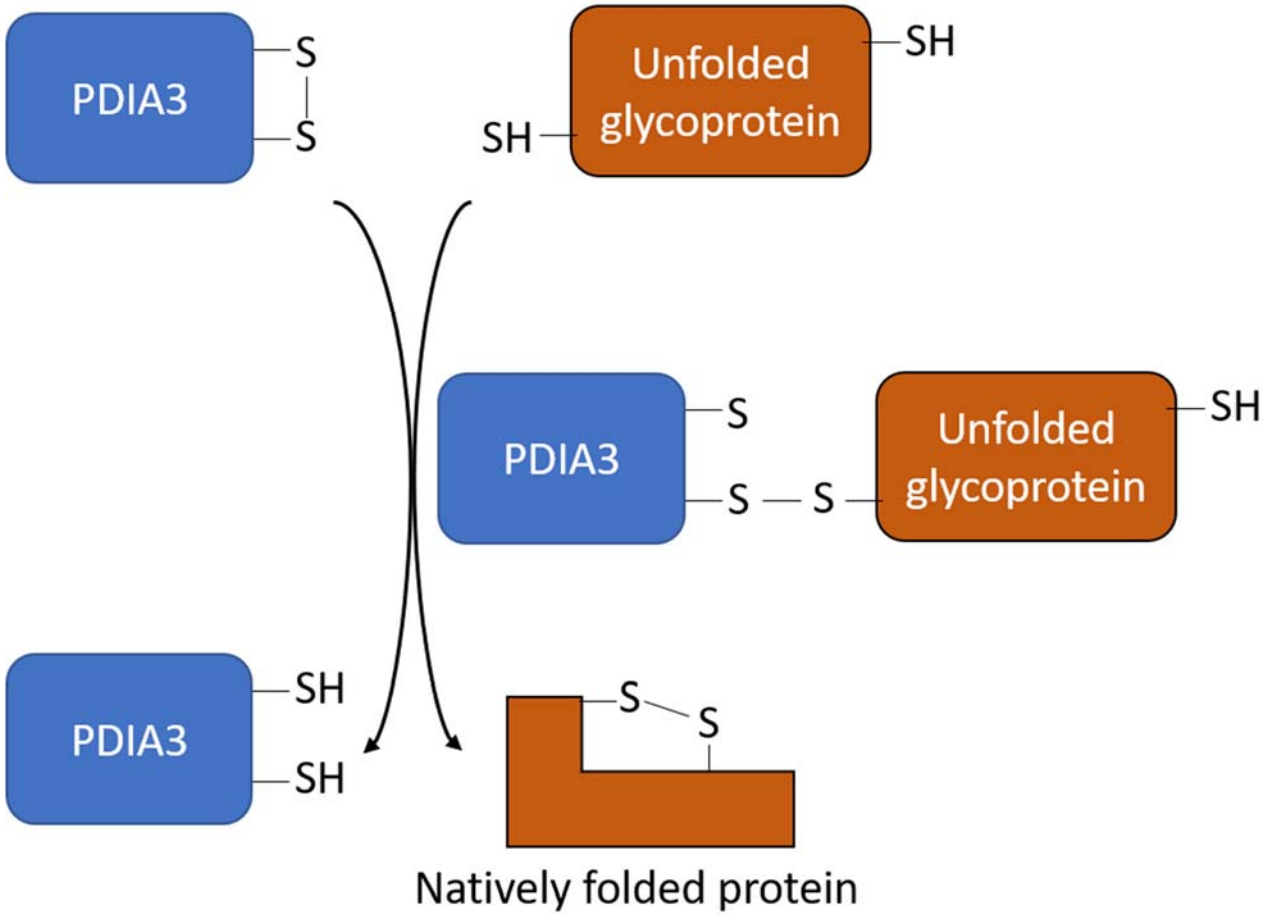

Figure 1.11 ***Schematic of Disulphide Bond Formation by PDIA3.***

$Glc_1Man_9GlcNAc_2$ glycoproteins via their lectin domains, and ATP, calcium and PDIA3 (Russell et al., 2004). $Glc_1Man_9GlcNAc_2$ glycoproteins that are the product of glucosidase-I and glucosidase-II trimming followed by addition of glucose by UDP-glucose-specific glycosyltransferase within the ER (Hebert and Molinari, 2007; van der Wal et al., 1998). PDIA3 functions as an oxidoreductase, using the CXXC motifs in the **a** and **a'** domains, to catalyse disulphide bond formation, which is important in folding and stabilisation of natively folded proteins (**Figure 1.11**) (Hebert and Molinari, 2007). CNX or CRT bound to PDIA3 cause slowing of the folding reaction for an overall increase in efficiency by reducing the release of incorrectly folded proteins (Hebert and Molinari, 2007).

Currently, there is no exhaustive list of PDIA3-specific substrates. To create this list, the interacting partners of the CRT-/CNX-PDIA3 complex must be considered as CRT and CNX are hugely influential in providing substrates for PDIA3 to react with (Jessop et al., 2007). This complex was found to preferentially target proteins that are heavily glycosylated with repeated structural domains dependent on disulphide bridges (Jessop et al., 2007). For example, secreted proteins such as laminin, collagen-VI α-chain and LOX homologue 2 along with cell surface ECM interacting molecules such as integrin (-α3, -α6, -β1, -β5) were identified as substrates for PDIA3 (Jessop et al., 2007). These substrates were identified using 2D-electropheresis separation on PDIA3-V5-protein complexes isolated from human fibroblast cell line lysates using agarose-V5 beads. Using the EMBL-EBI IntAct system (version 4.2.12), a total of 108 human PDIA3 protein binding partners have been described and a shortened list is displayed in **Table 1.1**.

If folding is incorrect, the polypeptide is shunted into the CNX/CRT cycle where the polypeptide is deglucosylated and re-glucosylated sequentially, allowing the CRT-/CNX-PDIA3 complex extra attempts at folding the polypeptide into the native conformation before committing to degradation (**Figure 1.12**) (Hebert and Molinari, 2007). Misfolded proteins within the ER are recognised by an ER transmembrane E3 ubiquitin ligase as part of the ER-associated degradation (ERAD) pathway (specifically the ERAD-L or ERAD-M pathway that recognise ER luminal and membrane protein misfolding). They are then retrotranslocated out of the ER into the cytoplasm where they are ubiquitinated and so degraded by the proteasome (Ruggiano et al., 2014). Accurate recognition of misfolded proteins is essential. The ERAD machinery recognises hydrophobic regions that are hidden in the native conformation. It also relies ER chaperone proteins such as BiP and 'late-acting' enzymes that mark proteins that have spent extensive time within the ER. However, the exact mechanisms of recognition are unknown (Ruggiano et al., 2014).

Interacting Protein	Species	UniProt reference
Antigen peptide transporter (TAP1)	Human	EBI-747259
Calnexin	Human	EBI-355947
Calreticulin	Human	EBI-1049597
Clusterin	Human	EBI-1104674
ERO1-like protein α (ERO1α)	Human	EBI-2564539
ERO1-like protein β (ERO1β)	Human	EBI-2806988
Insulin receptor	Mouse	EBI-6999015
Integrin α3	Human	EBI-2550768
Integrin-α2	Human	EBI-702960
Integrin-α5	Human	EBI-2550768
Integrin-β1	Human	EBI-703066
Integrin-β5	Human	EBI-1223434
Isocitrate dehydrogenase [NADP], mitochondrial	Human	EBI-3931130
Laminin subunit beta-1	Human	EBI-949174
Laminin subunit gamma-1	Human	EBI-714904
Low-density lipoprotein receptor	Human	EBI-988319
Lysyl oxidase homolog-2	Human	EBI-7172227
Procollagen-lysine,2-oxoglutarate,5-dioxygenase-1 (PLOD1)	Human	EBI-357174
Protein disulphide-isomerase A3	Human	EBI-979862
Protein disulphide-isomerase A4	Human	EBI-1054653
Stromal interaction molecule 1	Human	EBI-448878
Tapasin	Human	EBI-874801
Transcription factor AP-1	Human	EBI-852823

Table 1.1 ***PDIA3 Interacting Proteins.*** *From EMBL-EBI IntAct system (version 4.2.12). Access date (08-10-18).*

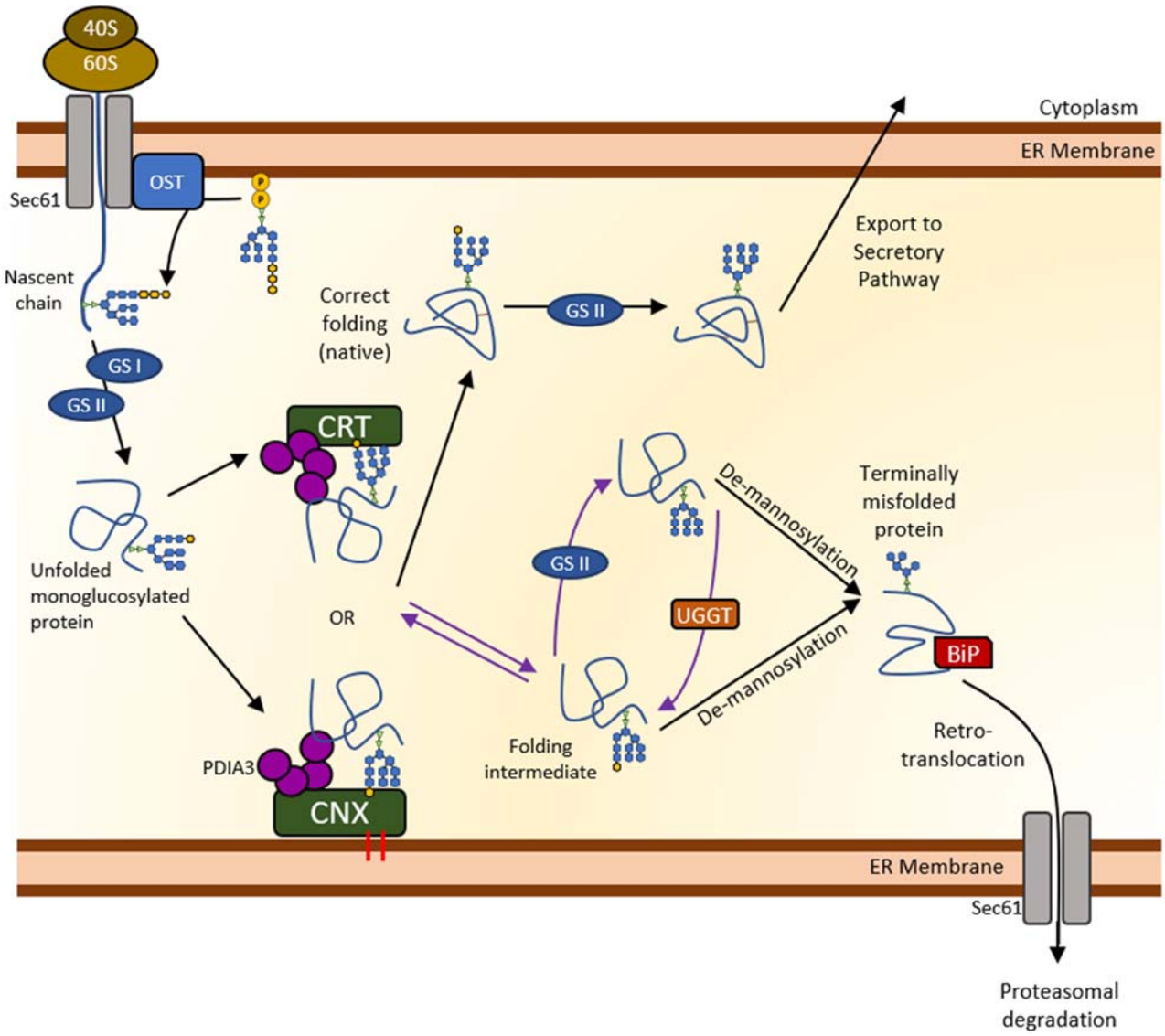

Figure 1.12 ***Protein Folding Quality Control in the ER.*** *Diagram of protein folding of freshly translated proteins with the CNX/CRT cycle shown with purple arrows. Adapted from reviews: (Hebert and Molinari, 2007; Tannous et al., 2015).* ***UGGT*** *- UDP-glucose-specific glycosyltransferase, GS – glucosidase, OST - Oligosaccharyltransferase*

1.4.4.2 The Involvement of PDIA3 in the Unfolded Protein Response and Apoptosis

Another pathway that is often perturbed in cancer is the unfolded protein response (UPR). A result of rapid tumour growth is activation of stress pathways, including the UPR, due to growth with insufficient nutrients or oxygen supply (Vandewynckel et al., 2013). The UPR acts to reversibly inhibit translation, promote expression of ER chaperones (such as CRT and CNX) to restore folding homeostasis, and, with prolonged stimulation of the UPR, trigger apoptosis through an overload of translation with downregulation of anti-apoptotic factors such as Bcl-2 (Chakrabarti et al., 2011). This role in both pro-survival and pro-apoptotic mechanisms is the basis of discussion around whether the UPR is pro-tumorigenic or anti-tumorigenic (Ojha and Amaravadi, 2017; Vandewynckel et al., 2013).

There are conflicting data on whether PDIA3 has a role in mediating the UPR. Work by Hussmann et al., 2015 in the HCT116 colon cancer cell line showed that, although critical to normal cellular function, perturbing PDIA3 using shRNA does not induce ER stress because compensatory mechanisms exist (Hussmann et al., 2015). The authors also showed that PDIA3 depletion in combination with etoposide or ionising radiation treatment acted to stimulate cytoplasmic, p53-dependent apoptosis via activation of the protein kinase R-like endoplasmic reticulum kinase (PERK) pathway of the UPR in HCT116 cells. This process was synergistic with the p53-independent inhibition of proliferation through loss of PDIA3-mediated mTORC1 assembly (Hussmann et al., 2015). PERK is a key kinase in the UPR that has a pro-survival effects, but also triggers apoptosis in response to prolonged UPR stimulation (Chakrabarti et al., 2011). An explanation for PDIA3 dependent PERK activation is that PDIA3 has been shown to hold PDIA1 in its reduced state, preventing oxidized (active) PDIA1 from activating PERK (Kranz et al., 2017).

In contrast, Xu et al., 2009 showed that PDIA3 is downregulated *in vivo* in neonatal rat lungs and *in vitro* in cultured human endothelial cells in response to hypoxia (Xu et al., 2009). They found that depletion of PDIA3 using siRNA in human endothelial cells increased protein levels of BiP and GRP78 (two ER chaperones associated with the UPR and pro-survival) which decreased apoptosis in response to tunicamycin and hypoxia. Moreover, overexpression of PDIA3 enhanced caspase-3-mediated apoptosis and reduced BiP/GRP78 protein levels (Xu et al., 2009). However, the association with PDIA3, the UPR and apoptosis is not always this simple. PDIA3 expression was associated with hepatocellular carcinoma cell proliferation and apoptosis resistance, as shown by Ki-67 and TUNEL immunohistochemistry staining in liver sections with high or low PDIA3 protein content (Takata et al., 2016). These correlations supported a previous study showing PDIA3 knockdown in L02 human hepatocyte cell line promoted apoptosis (Zhang et al., 2015). Contradicting this, PDIA3 (and PDIA1) caused apoptosis directly in mouse embryo fibroblasts (MEF) through oligomerisation of Bak in the mitochondrial outer membrane in response to various apoptotic signals (including thapsigargin and tunicamycin), whereas inhibition of PDIA3 subverted apoptosis (Zhao et al., 2015a). Also, miRNA-148a treatment of human ovarian cancer cell line (SKOV3) reduced PDIA3 protein

content which correlated with reduction of proliferation and promotion of paclitaxel-induced apoptosis (Zhao et al., 2015b).

Overall, high PDIA3 protein content is associated with enhanced hypoxia-induced endothelial cell apoptosis; apoptosis resistance and proliferation in HCC; and enhanced ER stress-induced apoptosis in MEF. Lowered PDIA3 protein content causes increased endothelial cell survival; increased HCC apoptosis; subverted ER stress-induced apoptosis in MEFs; and enhanced paclitaxel-induced apoptosis in ovarian cancer cells. This indicates that PDIA3 could have a differential effect on apoptosis based on the cell type, PDIA3 localisation and PDIA3 protein levels.

Endochondral ossification is where a template of cartilage ECM and chondrocytes mature into calcified bone tissue containing osteoblasts to form a functional bone. This requires extensive ECM deposition and extensive post-translational modification of these proteins takes place in the ER and so their production likely depends upon the action of PDIA3 (Bianco et al., 1998). A study of long-bone endochondral ossification used chondrocyte specific *Pdia3*$^{-/-}$ mice to show that loss of PDIA3 caused ER stress due to accumulation of unfolded/misfolded proteins in the ER (Linz et al., 2015). This contradicts the work by Hussmann et al., 2015 in colon cancer cells. ER stress can be induced in transgenic mouse models expressing a mutated form of matrillin-3 (Nundlall et al., 2010). Mutated matrillin-3 induces ER stress through failure to form its native conformation and so stimulates the UPR (Nundlall et al., 2010). During ER stress by matrillin-3, PDIA3, CNX and CRT protein are upregulated two-fold and this is perturbed in a chondrocyte-specific PDIA3 shRNA knockdown, and leads to compromised bone growth (Linz et al., 2015). This is good evidence for a role of PDIA3 in reducing ER stress. A final point regarding this study is that chondrocyte-specific *Pdia3*$^{-/-}$ resulted in reduced remodelling of the ECM, which in turn impaired differentiation of chondrocytes into osteocytes (Linz et al., 2015). This finding has potential significance to cancer, because, if PDIA3 can have a profound effect on ECM deposition and differentiation during development, then it could also play a role in stiffening of the ECM and EMT in breast cancer progression. This is particularly pertinent given the hypothesised role of PDIA3 in metastasis of breast cancer to bone (**1.4.5.2**) (Santana-Codina et al., 2013).

1.4.4.3 The Role of PDIA3 in MHC class I Antigen Presentation

Studied as ERp57, PDIA3 is well known to be essential in MHC-I antigen presentation (Zhang et al., 2006). Nascent MHC-I proteins undergo glycosylation and de-glucosylation to form a $Glc_1Man_9GlcNAc_2$ glycoprotein that is recognised by CNX (Leone et al., 2013). PDIA3 binds to CNX to facilitate correct folding and oxidation of MHC-I into the native conformation, allowing β2-microgobulin to bind MHC-I (Leone et al., 2013; Oliver et al., 1999). Upon β2-microglobulin binding, CNX is released and the remaining complex associates with CRT, and binds tapasin (a protein essential for MHC-I-peptide complex formation) to form

the PLC which localises to the peptide transporter involved in antigen processing (TAP) 1-TAP2 complex (Dong et al., 2009). The proteome degrades host proteins into small peptides that are transported into the ER by the TAP1-TAP2 complex. These peptides bind the MHC-I binding groove and if a peptide binds with high affinity, it cannot be displaced by the PLC and so triggers release of the mature MHC-I-peptide complex to the plasma membrane (Leone et al., 2013). PDIA3 binds tapasin through non-covalent stabilisation of a disulphide linkage between its active thioredoxin domains (**a** or **a'**) and cysteine 95 on tapasin (Santos et al., 2007). The crystal structure produced by (Dong et al., 2009) indicates that both active sites are engaged with tapasin, leading to the authors prediction that PDIA3 does not exhibit redox activity within the PLC. Instead, it is thought that the binding of PDIA3 to tapasin exposes the groove-binding surface of tapasin to hold the MHC-I binding groove in the open conformation until it is displaced by a high-affinity peptide (Dong et al., 2009).

1.4.4.4 The role of PDIA3 in Calcium Signalling

PDIA3 also functions as a molecular chaperone that binds stromal interaction molecule 1 (STIM1), an oligomer necessary for Ca^{2+} homeostasis (Prins et al., 2011). Ca^{2+} signalling is a versatile and universal second messenger system that is critical to normal cellular function and perturbed in many diseases (Petersen et al., 2005). STIM1 is an ER transmembrane protein, whose ER luminal domain binds Ca^{2+}. In resting conditions (high ER calcium), STIM1 has Ca^{2+} bound and remains as an inactive dimer. When Ca^{2+} is depleted from the ER in response to a signal, such as hormone or neurotransmitter signalling, STIM1 no longer binds Ca^{2+} and oligomerises. The process of oligomerisation extends and translocates the STIM1 complex to bind to the Orai1 pore of the calcium release-activated calcium channel at the plasma membrane, this allows an influx of Ca^{2+} from the extracellular space to replenishes Ca^{2+} stores (Hogan et al., 2010). STIM1 has been shown to be important for calcium homeostasis in Jurkat T-lymphocytes (Zhang et al., 2005), HEK293, SH-SY5Y (Roos et al., 2005) and HeLa cells (Liou et al., 2005). Prins et al., 2011 showed that, in MEF, PDIA3 binds to the ER luminal domain of STIM1 and forms a disulphide bond between the C^{49} and C^{56} conserved cysteine residues of STIM1. This is predicted to regulate STIM1-Ca^{2+} binding and is the first example of regulation of STIM1 via the ER lumen (Prins et al., 2011).

1.4.4.5 The Role of PDIA3 in Vitamin D Signalling

In cartilage, post-natal growth plate maturation and control of chondrocytes and osteoblasts is regulated by the 1α,25-dihydroxyvitamin-D3 (1α25$(OH)_2D_3$) pathways (Chen et al., 2013). 1α25$(OH)_2D_3$ signals via the classical VDR to cause transcriptional changes via a kinase cascade or by the calcium-dependent membrane-mediated pathway (Chen et al., 2013). The membrane-mediated pathway is initiated by a complex of VDR-1α,25$(OH)_2D_3$ at caveolin-coated caveolae, a specific type of lipid raft rich in glycosphingolipids and cholesterol (Doroudi et al., 2012). In studies using perfused chick duodenum to observe calcium (Larsson and Nemere, 2003) and phosphate transport (Nemere, 1996) in response to 1α,25$(OH)_2D_3$, cytoplasmic PDIA3 was shown to be an essential part of the VDR-1α,25$(OH)_2D_3$ complex and

resultant signalling. This was concluded because anti-PDIA3 N-terminal antibody treatment resulted in the abrogation of Ca^{2+} and phosphate transport across the membrane in response to 1α,25$(OH)_2D_3$. This explains the naming of PDIA3 as 1,25-D3 Membrane-Associated Rapid Response Steroid Binding Receptor (Nemere et al., 2004).

The VDR-1α,25$(OH)_2D_3$ complex at the caveolae interacts with phospholipase A_2 (PLA_2)-activating protein (PLAA) and calcium-dependent protein kinase II (Hii and Ferrante, 2016). PDIA3 binds to PLAA only in the presence of 1α,25$(OH)_2D_3$ and so its binding is predicted to depend on altered PLAA structure upon VDR-1α,25$(OH)_2D_3$ binding (Doroudi et al., 2012). The interaction of PDIA3 and PLAA drives PLA_2 activation to trigger this well-known pathway (Doroudi et al., 2012; Hii and Ferrante, 2016). The role of PDIA3 as an essential protein for PLAA mediated VDR–1α,25$(OH)_2D_3$ signalling was also shown by Boyan et al., 2012 *in vivo* and in the MC3T3-E1 cells (Boyan et al., 2012). Although the exact role of 1α,25$(OH)_2D_3$ signalling in bone formation is unknown, this pathway has been shown to regulate apoptosis, proliferation and growth in rat chondrocytes *in vivo* and in ATDC5 chondrocytes *in vitro* (Idelevich et al., 2011)

1.4.4.6 Association of PDIA3 with Mammalian Target of Rapamycin

mTOR associates with several proteins to form two key complexes: mTORC1 (mTOR, Raptor and mLST8) that regulates protein synthesis and cellular growth and mTORC2 (mTOR, Rictor, Sin1 and mLST8) which regulates survival, metabolism, growth and proliferation through its maximal activation of Akt by phosphorylation of Akt-S^{473} (Johnson et al., 2013) (mTORC1 pathway shown in **Figure 1.4**). Ramírez-Rangel et al., 2011 demonstrated that PDIA3 interacts with mTOR in the ER to aid assembly of mTORC1 specifically, but does not affect stability of this complex. PDIA3 knockdown resulted in reduced ability of mTORC1-associated kinase, Raptor, to phosphorylate downstream signalling targets such as p70S6K2 (a kinase involved in translational control) in response to an oxidising agent, phenylarsine oxide (Ramírez-Rangel et al., 2011). These findings suggest that PDIA3 is involved in mTORC1 activation through sensing of upstream signals such as insulin and redox-sensing signalling as well as direct involvement in assembly of mTORC1 (Hussmann et al., 2015; Ramírez-Rangel et al., 2011). This discovery is interesting as it implicates a role of PDIA3 in metabolic sensing by the mTORC1 pathway which is well known to be important in cancer cell biology.

1.4.4.7 The Interaction of PDIA3 with Signal Transducer and Activator of Transcription 3

PDIA3 interacts with signal transducer and activator of transcription 3 (STAT3) which is a member of the STAT family of cytoplasmic proteins associated with the Janus kinase-STAT pathway (Coe et al., 2010). This pathway is triggered by a range of growth factors and cytokines, such as PDGF and IL-2, and is widely known, through *in vitro* and *in vivo* models, for its association with cancer (Furqan et al., 2013; Yu et al., 2014). STAT3 plays a vital role in the TME through anti-tumour immune suppression, mediation of angiogenesis and tumour growth through interleukin signal transduction in mice (Avalle et al., 2017). Therefore, the implication of PDIA3 as an upstream regulator of this pathway is interesting and potentially

therapeutically important. Coe et al., 2010 showed that PDIA3 inhibits cytoplasmic STAT3 from inside the ER and that this inhibitory effect was enhanced by PDIA3 complexing with CRT. Although no exact mechanism has been elucidated, it is likely that PDIA3 is responsible for ER-mediated signalling that causes downstream inhibition of STAT3 (Coe et al., 2010). Given that PDIA3-mediated STAT3 activation was enhanced when CRT was also present, it is possible that PDIA3 affects STAT3 through its role in protein folding. Interestingly, PDIA3 was also reported to interact directly with STAT3 in a large scale 2D-immunofluorescence gel electrophoresis study of rat soleus muscle (Burniston et al., 2014). This finding was also reported by (Eufemi et al., 2004) who demonstrated that PDIA3 is present in the nuclear STAT3 complex and is essential for facilitating STAT3-DNA binding in the M14 human melanoma cell line. Burniston et al., 2014 went on to implicate mTOR in phosphorylation of serine^{727}of STAT3, by ERK family mitogen-activated protein kinases. This modification is important for STAT3-mediated mitochondrial control (Gough et al., 2014) and pluripotency (in mice) (Huang et al., 2014) as well as a key target of k-RAS oncogenic transformation in mouse models (Gough et al., 2014). Given that mTORC1 assembly is dependent upon PDIA3 (**section 1.4.4.6**) this could be another potential route by which PDIA3 activates STAT3. The data further implicate PDIA3 in cytokine-dependent signalling (Burniston et al., 2014).

It is unsurprising that PDIA3 is implicated in changing STAT3 transcriptional decision making due to likely involvement of PDIA3 in post-translational modification either directly or as an upstream regulator (Choe et al., 2015; Cocchiola et al., 2017; Coe et al., 2010).

1.4.4.8 The Role of PDIA3 in the Nucleus

PDIA3 has been reported to interact with proteins in the nucleus. Retinoic acid signals by binding to the retinoic acid receptor-α (RARA) which directly triggers its translocation from the cytoplasm to the nucleus where it binds DNA and acts a transcriptional factor (Cunningham and Duester, 2015). From a yeast two-hybrid screen, it was shown that PDIA3 binds to RARA (Zhu et al., 2010). This interaction was confirmed in COS-7 cells expressing histidine tagged RARA to capture RARA binding partners through nickel-nitrilotriacetic acid magnetic agarose beads (Zhu et al., 2010). In Sertoli cells (somatic cells essential to spermatogenesis), RARA and PDIA3 were co-translocated into the nucleus in response to all-trans retinoic acid (ATRA). PDIA3 siRNA knock-down resulted in subversion of nuclear translocation of RARA in response to ATRA as determined by immunofluorescence co-localisation studies (Zhu et al., 2010). They hypothesised that PDIA3 catalyses the refolding of RARA into a conformation that allows its nuclear translocation. Then, after RARA-ATRA has mediated transcriptional effects, the RARA-ATRA-PDIA3 complex is shuttled to the ER where it dissociates releasing ATRA and PDIA3 into the cytoplasm and RARA to be targeted for degradation (Zhu et al., 2010).

There is some evidence that PDIA3 and NF-κB interact and co-translocate the nucleus in response to $1\alpha25(OH)_2D_3$ signalling in promyelocytic leukemia cells (Wu et al., 2010). However, this is contradicted by

another study that showed that PDIA3 and NF-κB subunit p65 do not interact, and translocate independently in response to TNFα in hepatocellular carcinoma cells (Grindel et al., 2011). This discrepancy could be due to the difference in cell lines, but highlights that this interaction needs further research.

1.4.5 PDIA3 and Disease Associations

Changes in PDIA3 protein content has been correlated with several diseases as summarised in **Table 1.2**. Of interest to this project is the role of PDIA3 in fibrosis and cancer.

1.4.5.1 PDIA3 and Fibrosis

Fibrosis is the process of excessive deposition of fibrillar ECM such as collagens and fibronectin in response to chronic inflammation (Wynn, 2008). In normal wound healing, the epithelial/endothelial layer and fibroblasts secrete MMPs and cytokines to stimulate the migration of macrophages and neutrophils into the tissue and promote proliferation of these leukocytes. Now activated, phagocytes clear debris and secrete factors such as TGFβ, IL-13 and PDGF that promote fibroblast activation into myofibroblasts which then lay down new fibrillar ECM, especially collagen in a transient process. The combination of the secreted factors, new ECM and myofibroblast contractile ability allow epithelial/endothelial migration to seal the wound. In the case of chronic inflammation, wounds or other processes resulting in loss of tissue are sealed with highly fibrotic tissue, sacrificing normal functionality of the tissue through chronic activation of myofibroblasts (Wynn, 2008). This process has clear parallels to the stiffening of the ECM in cancer and is why cancer is often described as a 'wound that will not heal'.

PDIA3 was studied with regards to renal fibrosis in a proteomic study based on mouse and cell models (Dihazi et al., 2013). Renal fibrosis involves the extensive deposition of fibrous ECM in the kidney parenchyma (solid section of the kidney responsible for waste excretion). In this paper, TGF-β1, a known driver of fibrosis, was shown to stimulate the ER-stress and UPR pathways which upregulated PDIA3 (Dihazi et al., 2013). Also, TGF-β1 upregulated PDIA3 in a UPR independent manner which was associated with increased ECM protein abundance, that was reversed upon PDIA3 knock-down, PDIA3 inhibition or TGF-β1 antagonist, BMP-7, treatment (Dihazi et al., 2013).The study implicated TGF-β1 in causing secretion of PDIA3 into the extracellular space where it associated with fibronectin and collagen, with a predicted role of further post-translational modification and cross-linking of ECM proteins. Colocalization was assessed by immunoprecipitation. As well as implicating PDIA3 in the progression of renal fibrosis, Dihazi et al., 2013 showed that PDIA3 is stimulated by TGF-β1 to enhance fibrosis. This could be a very important aspect to consider in cancer progression. Also, given that PDIA3 was reported to function extracellularly in fibrotic disease, PDIA3 could potentially be targeted by antibodies for therapy.

Disease	Status of PDIA3	Association with Disease	Reference
Allergen-induced Asthma	Upregulation	Triggered by PRR responses	(Hoffman et al., 2016)
Alzheimer's disease	Pathway activation	Diosgenin activates PDIA3 pathways reducing Alzheimer's disease in mice	(Tohda et al., 2012)
Breast Cancer	Upregulation	Bone metastasis	(Santana-Codina et al., 2013)
Breast Cancer	Upregulation	Aggressive primary ductal breast cancer	(Ramos et al., 2015)
Cervical Cancer	Decreased	Poor prognosis cervical cancer	(Chung et al., 2013)
Gastric cancer	Decreased	Reduced abundance in gastric cancer compared to normal mucosa	(Leys et al., 2007).
Irritable bowel syndrome (Rats)	Upregulation	PDIA3 siRNA reduces Dendritic cell-mediated T-cell activation	(Zhuang et al., 2016)
Laryngeal cancer	Upregulation	Poor prognosis via STAT3 signalling	(Choe et al., 2015)
Non-alcoholic fatty liver disease	Upregulation	Correlated with heightened inflammation and fibrosis staging	(Wang et al., 2010)
Parkinson's disease	Upregulation	Overexpression of PDIA3 was neuroprotective in response to Parkinson's disease-inducing neurotoxin.	(Castillo et al., 2015)
Prion related disease	Upregulation	Prion protein biosynthesis and maturation.	(Sepulveda et al., 2016)
Prostate Cancer	Upregulation	Aggressive prostate cancers	(Basu et al., 2016)
Pulmonary Fibrosis	Upregulation	ATII to ATI trans-differentiation	(Mutze et al., 2015)
Renal Fibrosis	Upregulation	ECM deposition - progression	(Dihazi et al., 2013)

Table 1.2 ***Diseases Associated with Altered PDIA3 Protein Content.***

PDIA3 is also involved in pulmonary fibrosis. Mutze et al., 2015 demonstrated a role of PDIA3 and enolase-1 in driving the trans-differentiation of alveolar epithelial type II (ATII) cells into type I (ATI) cells. ATII cells are progenitor cells that are vital for self-renewal and replenishing the highly specialised ATI cells in response to lung injury. ATI cells are large squamous cells responsible for gas and ion transfer in the lung (Mutze et al., 2015). The exact mechanism of PDIA3 in ATII-to-ATI trans-differentiation was not discovered, but PDIA3 and enolase-1 expression were upregulated in response to WNT/β-catenin signalling and downregulated upon β-catenin inhibition. This indicates that PDIA3 might act downstream of WNT/β-catenin signalling (Mutze et al., 2015).

Proteomic analysis of human steatotic cells and human liver biopsies identified PDIA3 as an upregulated protein in non-alcoholic fatty liver disease, in correlation with both inflammation and fibrosis severity (Wang et al., 2010). Although the mechanisms of PDIA3-mediated pathogenic retention of fatty acids in the liver were not assessed, their data identify another fibrotic system involving PDIA3.

1.4.5.2 PDIA3 and Cancer

PDIA3 has been correlated with cancer in a several studies (**Table 1.2**) but its exact role remains unclear. This is unsurprising given the extensive and incomplete list of interactions (**1.4.4**) and disease associations. Only breast cancer will be discussed here.

Breast Cancer

Several comparative proteomic and transcriptomic analyses have identified alterations in PDIA3 abundance in cancerous versus normal breast tissue. One study of samples from Korean women assessed differentially expressed proteins between DCIS or IDC and matched normal tissue and quantified 244 of 298 proteins using IDEAL-Q software to produce distinct expression profiles for IDC, DCIS and normal tissue (Song et al., 2012). PDIA3 was highly upregulated, in comparison to the normal tissue, in both DCIS and IDC, and CRT was highly upregulated in IDC and marginally upregulated in DCIS (Song et al., 2012). Similarly, a study in rats analysed changes in the proteome of harvested mammary glands that correlated with the cancer preventative response of prepubertal consumption of genistein, the major isoflavone component of soy (Wang et al., 2011). PDIA3 was downregulated in 21-day old rats after genistein consumption, indicating a potential correlation with protection against development of breast cancer. Furthermore, Da Costa et al., 2015 showed that PDIA3 was highly upregulated in human IDC compared to normal breast tissue and correlated with lymph node metastasis. This was replicated by studies showing that PDIA3 and PDIA6 protein were more abundant in IDC than in ILC (Oliveira et al., 2016) or normal tissue (Ramos et al., 2015).

PDIA3 has been identified as a key mediator of bone metastasis-associated proteins and genes by differential transcriptome and proteome analysis of the bone-metastasis-prone breast cancer cell line

MDA-MB-231-BO2 and parental MDA-MB-231 line (Santana-Codina et al., 2013). This study demonstrated that ER stress downregulated HLA class I molecules (immune avoidance) and vimentin (mesenchymal cell marker) and that these effects could be regulated by increased levels of PDIA3 protein after low glucose, hypoxia and/or ER stress. There are two interesting points to be drawn from this work. 1. Knock-down of PDIA3 inhibited the ability of MDA-MB-231 cells to form bone metastasis in mice with no effect on lung metastasis, leading to the hypothesis that PDIA3 is specifically involved in bone metastasis. 2. The inverse correlation of PDIA3 and vimentin protein content suggests that PDIA3 drives MET to promote metastasis (Santana-Codina et al., 2013; Satelli and Li, 2011). A recent review on breast cancer EMT suggested that EMT was more important in allowing breast cancer cells to adapt to stressful environments such as hypoxia than metastasis (Bong and Monteith, 2017). By considering these data in combination with the roles of PDIA3 in calcium and vitamin D signalling (**1.4.4.5**), long-bone ossification (**1.4.4.2**), and the observation that PDIA3 is upregulated in response to hypoxia (Xu et al., 2009), there is good, indirect evidence for PDIA3 to be important in adapting disseminated tumour cells to the bone microenvironment through MET mechanisms.

The role of PDIA3 in breast cancer-derived cell lines has also been examined *in vitro*. PDIA3 is involved in growth signalling through facilitation of EGFR autophosphorylation and internalisation in triple negative MDA-MB-468 breast cancer cells (Gaucci et al., 2013). PDIA3 did not affect the levels of EGFR protein, EGF-EGFR binding or EGFR membrane localisation (Gaucci et al., 2013). Whether PDIA3-mediated facilitation of EGFR signalling was achieved through a direct PDIA3-EGFR interaction or through other PDIA3-protein interactions was not investigated in this study. Three members of the PDI family (PDIA3, PDIA1 and ERp44) promote growth of mammosphere [1] cultures of SUM159PT cells (Wise et al., 2016). As these cultures vastly increased mRNA for several ECM components (such as collagen-3-α1 and FN) than the equivalent adherent cells, the upregulation of PDIA3 could act to resolve the increased load in ER-folding (Wise et al., 2016). The ability of breast cancer cells to form mammospheres shows that they resist anoikis and is a strong *in vitro* indicator for metastatic potential *in vivo*.

Another hallmark of carcinoma progression is the ability of cells to resist chemotherapy and/or radiotherapy. Depletion of PDIA3 in MDA-MB-231 breast cancer cells has been associated with reduced proliferation in response to irradiation and etoposide treatment (Hussmann et al., 2015). Moreover, PDIA3 has been shown to enhance the DNA cross-linking capacity of mitomycin-C (MMC) in mice and Chinese hamster ovary cells (Celli and Jaiswal, 2003). This cross-linking capacity is what causes DNA breaks and kills proliferating cancer cells yet causes substantial side effects. Suppression of PDIA3-mediated MMC DNA-

[1] A mammosphere is defined as a three-dimensional sphere-like colony of mammary cells usually formed through growth in a gel or other 3D culture system.

crosslinking with curcumin in MCF-7 breast cancer xenografts in mice resulted in substantial tumour shrinking with reduced side effects such as weight loss and kidney failure (Zhou et al., 2009). This is clinically relevant because it shows that PDIA3 has been targeted in combination with MMC, a chemotherapeutic, to reduce off-target effects.

1.4.5.3 Unpublished Work from this Laboratory on PDIA3-Dependent Secreted Proteins.

PDIA3 is clearly important in protein folding and quality control yet its range of target proteins remain unclear. However, PDIA3 has been identified to associate with, and function in, folding of large proteins associated with the ECM and has even been shown to be secreted to function extracellularly (Dihazi et al., 2013; Halperin et al., 2014; Jessop et al., 2007). Unpublished research, carried out by Dr Andrew Hellewell in Professor Adams' laboratory under Medical Research Council (K018043), showed that *Pdia3*$^{-/-}$ MEF had reduced spreading in comparison to wild-type MEF, and that spreading of *Pdia3*$^{-/-}$ MEF could be normalised by WT-CM. Similarly, human fibroblasts treated with 16F16 had reduced spreading. Along with work to identify differences in secreted proteins between wild-type and *Pdia3*$^{-/-}$ MEF these data implicated PDIA3 in fibroblast adhesion and motility. This raised a new question, whether PDIA3 could have a role in promoting a migratory phenotype in breast cancer cells. This question is the basis of the experiments presented in this thesis.

1.5 AIMS

PDIA3 has been shown to be important in a wide array of cellular pathways and diseases. Despite this, little is known about the effects of PDIA3 on breast cancer cell behaviour. The central aim of this project is to further uncover the role of PDIA3 in the cellular context of breast carcinoma progression, as addressed by cell culture experiments with human breast cancer cell lines.

The specific goals are:

1. To characterise PDIA3 protein in a pilot Immunohistochemistry study of breast tumour samples.

2. To use human breast cancer cell lines (MDA-MB-231 (basal), HCC1937 (basal), MCF-7 (luminal) and BT-483 (luminal) to examine the effects of pharmacological inhibition of PDIA3 on cell morphology, attachment and 2D migration.

3. To examine effects of PDIA3 inhibition or loss-of-function on secreted proteins, by examining effects of inhibition on ECM production by breast cancer cell lines, and comparing effects of conditioned media from WT- or *Pdia3*$^{-/-}$-MEF on the F-actin structures and cell attachment.

4. To examine if PDIA3 inhibition would increase the sensitivity of breast cancer cell lines to chemotherapeutic inhibition.

Chapter 2

Materials and Methods

2.1 CELL CULTURE

2.1.1 Cell Culture Media

The following 3 media were used depending on cell type. Fibroblast Growth Medium (FGM) (Promocell - C-23110), Dulbecco Modified Eagle Medium high glucose (DMEM - D5671) (Sigma) and RPMI medium 1640 (Sigma - R8758), which contain 3.3μM, 44.5μM or 13.2μM phenol red, respectively.

2.1.2 MDA-MB-231 Cells

MDA-MB-231 cells (described originally by R. Cailleau et al. 1973) (Cailleau et al., 1974) were purchased from ATCC (American Type Culture Collection) and grown in DMEM supplemented with 10% foetal bovine serum (FBS) (Sigma) at 37°C in a sterile, humidified, copper-lined incubator gassed with 5% CO_2. Medium changes were performed every 2 days with cells being passaged or used in experiments at 80% confluence. Passaging was performed as follows, MDA-MB-231 cells were rinsed briefly with 0.05% trypsin/EDTA (1x) (Sigma - T3924) to remove any dead or dying cells and then incubated at 37°C in 0.05% trypsin/EDTA for 2-3 minutes. Trypsin was then inactivated by resuspending cells in DMEM containing 10% FBS to be re-plated according to requirements.

2.1.3 MCF-7 Cells

MCF-7 cells (Soule et al., 1973) were obtained from ATCC and treated identically to MDA-MB-231 cells for culture conditions.

2.1.4 HCC1937 Cells

HCC1937 cells(Tomlinson et al., 1998) were purchased from ATCC and grown in RPMI1640 containing 10% FBS and trypsinised for 3-5 minutes. Other than this, HCC1937 cells were treated identically to MDA-MB-231 cells.

2.1.5 Mouse Embryo Fibroblasts

Pdia3$^{-/-}$ MEF and WT MEF were the kind gift of Professor Marek Michalak, University of Alberta, Canada (Coe et al., 2010) and were grown in FGM (serum-free) at 37°C in a sterile humidified copper-lined incubator gassed with 5% CO_2. Medium changes were performed every 2 days with cells being passaged or used in experiments at 80% confluence. Passaging was performed as follows. MEF were rinsed briefly with 0.05% trypsin/EDTA(1x) and incubated in 0.05% trypsin/EDTA for 1-2 minutes. Trypsin was then removed by suspending in 5ml of FGM; centrifuging at 1000rpm for 5 minutes and the cell pellet resuspended in fresh FGM. Cells were then counted using a haematocytometer and plated according to requirements.

2.1.6 Long Term Storage of Cells

After trypsinisation and centrifugation of cell stocks, the supernatant was removed, and the cell pellet resuspended in fresh medium containing 10% FBS and 10% dimethyl sulfoxide (DMSO) (**Table 2.1**). 1ml of cell suspension was aliquoted per cryovial (Fisher Scientific) (≈10^6 cells). The cryovials were placed in a

polystyrene container at -80^{o}C for 24 hours allowing cells to freeze slowly to avoid formation of ice crystals. Cells were then moved into liquid nitrogen (-196^{o}C) for long-term storage.

2.2 CHEMICALS AND INHIBITORS

Table 2.1 and **Table 2.2** list all chemicals and inhibitors (respectively) that have been used in this project.

Table 2.1 ***The chemicals used in this project.***

Name	Supplier	Catalogue Number
40% Acrylamide	Bio-Rad	1610140
Affi-gel® heparin beads	Bio-Rad	153-6173
Ammonium hydroxide solution	Honeywell - FLUKA	221228
Ammonium Persulfate powder (APS)	BDH (now VWR life science)	BDH9214-500G
Bromophenol Blue	Sigma	B0126
Bacto™ Agar	Becton, Dickson + company	214010
2% Bis Solution	Bio-Rad	1610142
Cyclophosphamide (CP)	Sigma	C0768
DL-dithiothreitol (DTT)	Sigma	D0632
Dimethyl sulfoxide (DMSO)	Simga	D2650
Elite Universal ABC IHC Kit	VectorLabs	PK-6200
Enhanced Chemiluminescence (ECL)™ WB detection reagent	Amersham	RPN2209
Ethylenediaminetetraacetic acid (EDTA)	Sigma	ED2SS
5-Fluorouracil (5-FU)	Sigma	F6627
Gills Haematoxylin Sol. No.2	Sigma-Aldrich	GHS216
Glycerol	Sigma	G5516
Histo-Clear2	National Diagnostics	HS-202
Hydrochloric acid	Sigma	H1758
Hydrogen Peroxide 30%	Sigma	H1009
ImmPACT 3,3' Diaminobenzidine (DAB) reagent with diluent	VectorLabs	SK-4105
L-ascorbic acid	Sigma	A4403
Methanol	Sigma	322415
Paraformaldehyde (PFA) 16% (w/v)	ThermoFisher Scientific	28906
Ponceau S	Sigma	P7170
Phalloidin Fluorescein isothiocyanate (FITC)	Sigma	P5282
Phalloidin Tetramethylrhodamine (TRITC)	Sigma	P1951
Precision Plus Protein™ Dual Colour Standards	BIO-RAD	#1610374
Resazurin sodium salt (Alamar Blue)	Sigma	R7017 (Lot#MKBZ4934V)
Sodium Dodecyl Sulphate (SDS)	Fisher Scientific	28906
N,N,N′,N′-Tetramethylethylenediamine (TEMED)	Sigma	T9281
Trisodium citrate dehydrate	Fluka Analytical (Sigma-Aldrich)	71406
Triton-X100 (TX100)	Sigma	10789704001
Trizma Base (TRIS)	Sigma	T6066
VectaShield with 4′,6-diamidino-2-phenylindole (DAPI)	Vector	H1200
VectaMount	Vector	H5000
Xylene	Sigma-Aldrich	33817(bottle) OR 214736(website)

Table 2.2 ***The inhibitors used in this project.***

Inhibitor	Mechanism of action	Supplier	Catalogue Number	CAS
16F16	Irreversible inhibitor of PDIA3 and PDIA1	Sigma	SML-0021	922507-80-0
PACMA-31	Irreversible inhibitor of PDIA1	Sigma	SML-0838	1401089-31-3
Pierce™ Protease inhibitor tablets - mini	Broad spectrum inhibitors of cellular proteases	ThermoFisher Scientific	88665	30827-99-7

2.3 BUFFERS

The compositions of buffers and solutions prepared in the laboratory are listed in **Table 2.3**.

Table 2.3. ***The Solutions used in this project.*** *Key: WB: Western Blot.*

Buffer	Abbr.	Working Composition	Experiment
Immunoblot Blocking Buffer	BB	PBS containing 2 % (w/v) semi-skimmed dried milk and 0.2 % (v/v) Tween 20	WB
Phosphate buffered saline	PBS	NaCl 0.138 M; KCl - 0.0027 M; pH 7.4	Cell lysate; staining; fixing
Phosphate buffered saline, 0.2% Tween	PBS, 0.2% Tween	PBS containing 0.2 % (v/v) Tween 20	WB
Resazurin Salt Stock Solution		1g Resazurin salt powder in 100ml sterile PBS	Alamar Blue assay
Resolving Gel 10% acrylamide Final		5 ml of 40% Acrylamide, 1.5 ml of 2% Bis solution, 7.4 ml of 1M Tris base pH 8.7, 6.55 ml of H_2O, 190 µl of 10% APS (w/v in dH_2O), 90µl 20% SDS, 72 µl of TEMED	WB
Resolving Gel 7.5% acrylamide Final		3.42 ml of 40% Acrylamide; 1.71ml 2% Bis solution; 5.9ml dH_2O; 6.7ml Tris 8.7; 90µl 20% SDS; 190 µl of 10% APS; 72 µl of TEMED	WB
20% SDS stock solution	20% SDS	20% SDA (w/v)	WB
SDS-PAGE Running Buffer		24.9mM Trizma base; 191.8mM glycine; 5ml 20% SDS, made up to 1l in dH_2O	WB
SDS-PAGE Sample Buffer	SDS-SB	100 mM Tris pH 6.8, 4 % SDS, 0.2 % bromophenol blue, 20 % glycerol	WB
Stacking Gel 4% acrylamide Final		1.28 ml of 40% Acrylamide, 0.65 ml of 2% Bis solution, 1.25 ml of 1M Tris base pH 6.8, 6.77 ml of H_2O, 150 µl of 10% APS, 20 µl of TEMED	WB
Transfer Buffer	TB	24.9mM Trizma base; 191.8mM glycine; 200ml Methanol, made up to 1l in dH_2O	WB

2.4 BREAST TUMOUR SAMPLES (WALES CANCER BANK)

Table 2.4 ***Reference and receptor status of primary IDC samples obtained from Wales Cancer Bank.***

WCB reference number	Receptor Status
RR6BL0000290PT3AH	$ER^+/PR^+/HER2^-$
RR6BL0000987PT3AH	$ER^-/PR^-/HER2^-$

2.5 PLASTICWARE

Table 2.5 ***The plasticware used in this project.***

Supplier	Type	Abbreviation	Catalogue number
Falcon®	Cell scraper	-	35386
Falcon®	Falcon®100mm TC-treated cell culture dishes	P90	353003
Falcon®	Falcon®60mm TC-treated cell culture dishes	P60	353002
Falcon®	6-well plate	-	353934
Falcon®	24-well plate	-	353226
Nunc	96-well plate (clear)	-	167008
IncuCyte®	96-well image-lock plates	-	4379
SARSTEDT	15ml centrifuge tube	-	62.554.002

2.6 ANTIBODIES

The primary antibodies used in this project are listed in **Table 2.6** and secondary antibodies are listed in **Table 2.7.**

Antigen	Antibody	Supplier	Cat. Num.	Dilution			Incubation time (h) IF/IHC/WB	Incubation Temp IF/IHC/WB
				IF	IHC	WB		
Beta-catenin	Mouse monoclonal	Merck	MAB2081	1:600	-	-	1.5/-/-	RT/-/-
Collagen1α1	Rabbit polyclonal IgG	NovusBiotechnic	NB600408	1:400	-	-	1.5/-/-	RT/-/-
Fibronectin	Rabbit polyclonal IgG	Sigma	F3648	1:200	-	1:600	1.5/-/ O/N	RT/-/4°C
Glyceraldehyde-3-phosphate dehydrogenase (GAPDH)	Mouse monoclonal IgG2b	Abcam	ab9484	-	-	1:1000	-/-/2	-/-/RT
GAPDH (2)	Mouse monoclonal	Invitrogen	MA5-15738	-	-	1:600	-/-/O/N	-/-/4°C
PDIA1	Rabbit monoclonal (C81H6) IgG	Cell Signalling Technology	3501	-	-	1:2000	-/-/2	-/-/RT
PDIA3/ERp57	Mouse monoclonal (Map.ERp57) IgG1	Abcam	Ab13506	-	1:500	1:2000	-/0.5/2	-/RT/RT
PDIA3/ERp57 (C-terminal)	Rabbit polyclonal IgG	Abcam	Ab137456	-	1:500	1:2000	-/0.5/2	-/RT/RT
α-Tubulin	Mouse monoclonal	Sigma	T9026	-	-	1:1000	-/-/2	-/-/RT
Vinculin	Mouse monoclonal	Sigma	V4505	1:300	-	-	1.5/-/-	RT/-/-

Table 2.6 ***Primary antibodies.*** *Key: IF: Immunofluorescence; IHC: Immunohistochemistry, WB: Western blot, O/N: overnight, RT: Room temperature*

Antigen	Antibody	Supplier	Cat. Num.	Dilution		
				IF	IHC	WB
Mouse IgG	Alexafluor®488 conjugated polyclonal goat IgG	Life	A11001	1:200	-	-
Mouse IgG (Fab specific)	FITC-conjugated goat IgG	Sigma	F8771	1:500	-	-
Mouse IgG, IgA, IgM	HRP-conjugated goat IgG	LI-COR	926-80010	-	-	1:50000
Rabbit IgG	TRITC-conjugated sheep IgG	Novex	A16177	1:500	-	-
Rabbit IgG, IgA, IgM	HRP-conjugated goat IgG	LI-COR	926-80011	-	-	1:50000
Universal (mouse/rabbit)	Biotinylated horse IgG	Vector	PK-6200	-	1:50	-

Table 2.7 ***Secondary antibodies used in this project.*** *Key: IF: Immunofluorescence; IHC: Immunohistochemistry, WB: Western blot.*

2.7 CELL-BASED ASSAYS

2.7.1 Determining Inhibitor Concentration for Cell-Based Assays

Cancer lines grown under normal conditions were trypsinised, centrifuged and washed 3 times in FGM to remove serum. The cells were then plated into a 24 well plate (**Table 2.5**) at $2.6x10^4$cells/cm^2 ($5x10^4$cells/well) and grown for 24 hours in the presence of various concentrations of each inhibitor, PACMA-31 or 16F16. Two methods were used for determining the effect of each inhibitor:

1. 7-8 phase contrast images of each condition were taken using an inverted Leica microscope (Leica DMI4000B with Leica DFC310fx camera and controlled by Leica application Suite (LAS) 4.5 Software, UK) under a 20x lens. The number of cells with a flat or rounded morphology were counted.
2. 25 Images per well were taken once an hour for 24 hours on the IncuCyte ZOOM™ (Essen BioScience) 'in incubator' live-cell imaging system with 10x (0.3 NA) lens. Using the software's inbuilt 'confluence-mask' setting, the change in 'confluence' (essentially a measure of cell density) was calculated for each condition.

2.7.2 Inhibitor Pre-treatment of Breast Cancer Cells

Breast cancer lines grown under normal conditions were trypsinised, centrifuged and washed 3 times in FGM. They were then seeded into P60 dishes (**Table 2.5**) in FGM such that they would grow to 70-80% confluence over the next 24 hours (e.g. p90 1:3, minimum of $5x10^5$cells/p60). These P60 dishes were treated at 0h with 16F16, PACMA-31 or equivalent volume of DMSO (see **Table 3.2** for the final concentrations used) and grown for 24 hours. Cells were then trypsinised, centrifuged, counted and seeded in the continued presence of inhibitor according to the exact experimental design.

2.7.3 Breast Cancer Cell Attachment and Spreading on Glass

After inhibitor pre-treatment (**2.7.2**), breast cancer cells were seeded onto glass coverslips in 6-well plates (**Table 2.5**) at $1.3x10^5$ cells/cm^2 ($2.5x10^5$cells/well) and treated with the same concentration of inhibitor as in the pre-treatment. After a further 2h, 6h, 12h or 24h at 37^{o}C, the medium was gently removed from each well and the cells were washed three times in PBS and fixed in freshly-made 4% PFA (ThermoFisher Scientific) (**Table 2.1**) in PBS for 10 minutes. Fixed cells then stored in PBS for up to three days before staining (**2.8.2.2** and **2.8.2.3**) and imaged within 7 days.

2.7.4 'Scratch Wound' Closure Assay using the IncuCyte ZOOM™ Microscope

After inhibitor pre-treatment, (**2.7.2**) MDA-MB-231 or HCC1937 cells were seeded into an IncuCyte® ImageLock 96-well plate (**Table 2.5**) in FGM containing either inhibitor (at concentrations displayed in **Table 3.2**) or DMSO (the solvent) and incubated at 37^{o}C overnight to attach.

OR

MCF-7 cells were seeded into an IncuCyte® ImageLock 96-well plate (**Table 2.5**) at 1.25x10^{5} cells/cm^{2} (4x10^{4}cells/well) in DMEM with 10% FBS containing either inhibitor (**Table 3.2**) or DMSO solvent and pre-treated for 24h.

Then, all wells were 'scratched' using the WoundMaker™ (Essen) and MCF-7 cells had media replaced with fresh, DMEM 10% FBS treated with the same concentrations of inhibitor or DMSO. One image per well taken once an hour for 48h using the IncuCyte ZOOM™ 'in incubator' system and 10x (0.3 NA) lens. CellPlayer™ software was used to analyse the change in 'relative wound density' over a 48-hour period. These experiments were carried out with the help of Dr Katy Jepson, Wolfson Bioimaging Facility, Bristol.

2.7.5 Breast Cancer Cell Attachment and Spreading on Extracellular Matrix

Breast cancer cells were seeded onto glass coverslips in 6-well plates at 2.6x10^{5} cells/cm^{2} (5x10^{5}cells/well) and treated with the same concentration of inhibitor as for the pre-treatment (**2.7.2**). After 48h at 37^{o}C, the medium was gently removed. The cells were washed three times in PBS and lysed using ammonium hydroxide (Honeywell Fluka) for 5 minutes with rocking (Hellewell et al., 2017). The lysate was then removed by washing 5 times in a large excess of sterile dH_2O, and the coverslips with ECM left finally under PBS. Meanwhile, breast cancer cells (from the same cell line that made the ECM but grown under normal conditions without inhibitor) were trypsinised, washed twice in FGM and plated onto the ECM-coated coverslips at 1.3x10^{5}cells/cm^{2} (2.5x10^{5}cells/well) in FGM and incubated at 37^{o}C. After 1h, the medium was gently removed, the cells washed three times in PBS and fixed in freshly made 4% PFA for 10 minutes. Fixed cells were then stored in PBS for a maximum of three days before staining (**2.8.2.2**) and imaged (**2.8.2.3**) within 7 days.

2.7.6 Preparation of Extracellular Matrix from Breast Cancer Cells

The ECM was isolated from breast cancer cells as described above (**2.7.5**) but naïve cells were not seeded. Instead, the ECM coated glass coverslips were fixed in freshly made 4% PFA for 10 minutes. The fixed ECM was stored in PBS for up to three days before staining (**2.8.2.4**) and imaged within 7 days.

2.7.7 Preparation of Cellular Samples for Western Blotting

Two methods were used to prepare samples from cells for SDS-PAGE and Western blotting.

1. Breast cancer cell lines grown under normal conditions were trypsinised, centrifuged and washed 3 times in FGM. They were then seeded into P60 dishes at $4x10^4$cells/cm^2 ($8x10^5$cells/well) in 3ml FGM and treated with the appropriate concentrations of PACMA-31, 16F16 or DMSO. After 6h at 37°C the medium (3ml per P60) was taken out of the dish, placed in a 15ml tube (**Table 2.5**) and centrifuged at 400xg for 5 minutes to remove any cell debris. The supernatant was passed through a sterile 0.22µm filter (Millex-GP - SLGP033RS) and transferred to a new 15ml tube with 1x protease inhibitor cocktail (**Table 2.3**) and placed on ice. Heparin-binding proteins were isolated through incubation with rotation with 25µl Affi-gel® heparin-beads (Bio-Rad) (**Table 2.1**) at 4°C. The heparin-beads with bound proteins were washed 3 times in PBS (centrifuging at 1000xg each time) and then mixed in a 1:1 ratio with SDS-PAGE sample-buffer containing 100mM DTT (**Table 2.1**). Samples were stored at -20°C. Meanwhile, each cell layer was lysed separately in 150µl SDS-PAGE sample buffer (**Table 2.3**) containing 100mM DTT using a cell scraper (**Table 2.5**). Cell extract was stored at -20°C.
2. The same procedure was carried out on cells after 24 hours of inhibitor pre-treatment (**2.7.2**).

2.7.8 Breast Cancer Cell Attachment and Spreading on Glass in Response to Conditioned Medium from *Pdia3*$^{-/-}$ or Wild-type Mouse Embryo Fibroblasts

After trypsinisation and centrifugation, WT and *Pdia3*$^{-/-}$ MEF were resuspended and seeded into separate P90 dishes (**Table 2.5**) (1xP90 per cancer line) at $2x10^4$cells/cm^2 ($5x10^5$cells/P90) in 8ml of serum-free FGM treated with 300µM L-ascorbic acid (**Table 2.1**). These cells were grown for 48h at 37°C to allow ECM to be deposited. Conditioned medium (CM) was taken out of each dish and passed through a 0.22µm filter (filter-sterilisation and removal of cell fragments) into separate 15ml tubes. Meanwhile each of the breast cancer cell lines was trypsinised, washed 3 times in 5ml FGM and resuspended at a high cell density (approx. $6x10^6$cells/ml) in FGM. Each cancer cell suspension was then seeded into the CM or fresh FGM only (control) at the required concentration for seeding densities as stated in (**2.7.8.1** and **2.7.8.2 -** see below).

2.7.8.1 Studies of Breast Cancer Cells Exposed to Fibroblast-Conditioned Media by Immunofluorescence

Breast cancer cells in CM or FGM were seeded onto glass coverslips in 6-well plates at $2.8x10^4$cells/cm^2 ($2.5x10^5$cells/well). After 2h at 37°C the medium was drained. The cells were washed three times in PBS to remove non-adherent cells and fixed in freshly made 4% PFA for 10 minutes. Fixed cells were stored in PBS for a maximum of three days before permeabilization and staining (**2.8.2**).

2.7.8.2 Studies of Breast Cancer Cells Exposed to Fibroblast-Conditioned Media by SDS-PAGE and Western Blotting

Breast cancer cells in CM or FGM were seeded into p60 dishes at $4x10^4$cells/cm^2 ($8x10^5$cells/well). After 6h at 37°C the medium was taken out of the dish, pipetted into a 15ml tube (**Table 2.5**) and centrifuged at 400xg for 5 minutes to remove any cell debris. The supernatant was transferred to a new 15ml tube with 1x protease inhibitor cocktail (**Table 2.3**) and placed on ice. Heparin-binding proteins were isolated and stored as in **2.7.7**. Meanwhile, each cell layer was lysed separately in 150µl SDS-PAGE sample buffer containing 100mM DTT using a cell scraper. Cell extract was then stored at -20°C.

2.7.9 Sensitivity of Breast Cancer Cells to 5-Fluorouracil or Cyclophosphamide

Cells were seeded into a 96-well plate (**Table 2.5**) at $3x10^4$cells/cm^2 ($1x10^4$cells/well) and 5-fluorouracil (**Table 2.1**) added at 0, 0.5, 1, 5, 10, 50, 100, 500 or 1000µM concentrations or cyclophosphamide (**Table 2.1**) at 0, 5, 10, 50, 100, 500, 1000, 5000, 10000 or 20000µM in 100µl of FGM. There were 8 replicate wells per concentration of each compound. 5-FU-treated cells were grown for 48 hours whereas CP-treated cells were grown for 72h as minimal killing had occurred at 48h. After incubation, medium was drained from the wells and 100µl of Alamar blue working solution (180µl Resazurin salt stock solution (**Table 2.3**) in 50ml sterile PBS) was added for 2 hours. The fluorescence of each well was then measured using a SpectraMax M2 plate reader (MolecularDevices) at excitation: 544nm and emission: 590nm. The change in fluorescence is directly proportional to the number of viable cells and is caused by resazurin salt reduction by an unknown enzyme and the reducing environment of a healthy cell (Larson et al., 1997). Results were standardised by subtracting the background fluorescence (mean value of wells containing pure Alamar Blue working solution and no cells). The mean of the 'DMSO only' condition was then set as '100% survival' and all results divided by this value to convert the fluorescence value into % survival.

2.7.10 The Effect of 16F16 on Killing of Cancer Cells by 5-Fluorouracil or Cyclophosphamide

The method of **2.7.9** was repeated, with inclusion of 4 wells per 5-FU or CP concentration that were also treated with the desired concentration of 16F16 or equivalent volume of DMSO (**Table 3.2**).

2.8 MICROSCOPY

2.8.1 Phase Contrast Images

Breast cancer cell lines grown under normal growth conditions in a P90 dish were imaged by phase-contrast microscopy, at 60-70% confluence with an inverted Leica microscope (Leica DMI4000B) and

images captured with Leica DFC310fx camera controlled by Leica application Suite (LAS) 4.5 Software, UK under a 20x objective lens.

2.8.2 Fluorescence Microscopy

2.8.2.1 Beta-catenin and Vinculin Study

Breast cancer cell lines were seeded into a P60 dish containing 7-8 glass coverslips, at $1x10^5$ cells/P60. After 24h growth under normal conditions, cells were fixed in 4% PFA for 10 minutes. Coverslips were stored for a maximum of 3 days before permeabilisation by 0.5% Triton-X100 in PBS for 10 minutes. Once permeabilised, the coverslips were blocked in 2% BSA in PBS for 30 minutes in a humidified chamber; washed 3 times in PBS. The blocked coverslips were then incubated for 90 minutes at RT in a humidified chamber with anti-β-catenin or anti-vinculin primary antibody (**Table 2.6**) in 2% BSA in PBS. Next, the coverslips were washed 3 times in PBS and incubated with appropriate secondary antibody (**Table 2.7**) in 2% BSA for 45 minutes at RT in a humidified chamber in the dark. Finally, the coverslips were washed 3 times in PBS and 3 times in dH_2O and mounted using VectaShield® with DAPI (**Table 2.1**). Slides were examined using a Leica SP5-AOBS confocal laser scanning microscope attached to a Leica DM I6000 inverted epifluorescence microscope with an HCX PL APO lambda blue 63x 1.4NA oil objective. Using Leica Application Suite AF software 2.7.3.9723, Z-stack images were taken at approx. 0.25µm Z slice thickness with an overall z volume of 5µm. A 100mW 488nm Argon laser was used to detect the Alexafluor®488 secondary antibody and 50mW 405nm diode laser for DAPI. Images were saved as tif files and displayed as single channel 'Maxintensity' z-stack merges and Maxintensity merged red-green-blue (RGB) images.

2.8.2.2 Quantification of Cell Areas of Breast Cancer Cells

After growing and fixing breast cancer cells as described in **2.7.3, 2.7.5** and **2.7.7.1** the coverslips were placed in 0.5% Triton-X100 in PBS for 10 minutes to permeabilise cells, washed in PBS and placed into a humidified chamber at RT. Coverslips were then stained with Phalloidin-TRITC or Phalloidin-FITC fluorescent compound (**Table 2.1**) diluted to 1/100 ratio, in PBS for 50 minutes, before washing 3 times in PBS, then dH_2O, and mounting onto glass microscope slides using VectaShield® with DAPI. For all cell area studies except 'Breast Cancer Cell Attachment and Spreading on Extracellular Matrix' (**2.7.5**), slides were examined using Leica SP5-AOBS confocal laser scanning microscope attached to a Leica DM I6000 inverted epifluorescence microscope with an HCX PL APO lambda blue 63x 1.4NA oil objective. Using Leica Application Suite AF software 2.7.3.9723, z-stack images were taken at approx. 0.50µm z-slice thickness, 2-2.5µm total z-stack thickness (base of the cell). A 100mW 488nm Argon laser was used to detect the Phalloidin-FITC; a 10mW solid state yellow laser (561nm) was used to detect phalloidin-TRITC and a 50mW 405nm diode laser for DAPI. Three independent experiments were performed, and 2 coverslips were imaged per condition per

experiment. 6-8 z-stack images were taken over these two coverslips such that approx. 50 cells could be scored (NOTE: Experiment 1 had much fewer than 50 cells in MCF-7 cells under 16F16 due to low attachment and limited microscope time). Images were saved as tif files. Cell outlines were defined from Maxintensity merges of the z-stack from tif files using ImageJ freehand outline tool or automated threshold->binary->measure particles where possible. The cell outlines were then measured by region-of-interest (ROI) analysis in ImageJ. For **2.7.5**, slides were examined using an inverted Leica microscope (Leica DMI4000B) and images were captured with a Leica DFC310fx camera controlled by Leica application Suite (LAS) 4.5 Software, UK with 20x objective. A 100mW 488nm Argon laser was used to detect the Phalloidin FITC and a 50mW 405nm diode laser for DAPI. Single images were taken from 3 or 4 random locations on the coverslip and saved as tif files. Cell outlines were defined using ImageJ threshold->binary->measure particles or freehand outline (to measure the few that could not be detected automatically). The cell outlines were then measured by region-of-interest (ROI) analysis in ImageJ as above. For each cell line a minimum of 150 cells were measured per condition per repeat for a total of approx. 400 cell area comparisons.

2.8.2.3 Cell Attachment of Breast Cancer Cell Lines

Coverslips from **2.7.3 (2h and 6h)** or **2.7.7.1** were observed using an inverted Leica microscope (Leica DMI4000B) and images were captured using a Leica DFC310fx camera controlled by Leica application Suite (LAS) 4.5 Software, UK) under a 63x 1.4NA objective lens. Nuclei were counted from 20 random fields per coverslip from 2-3 coverslips per condition per experiment. Coverslips from **2.7.5** and the 12h and 24h timepoints of **2.7.3** were observed using the same microscope but under a 20x objective lens. Nuclei were counted from 7 random fields per coverslip from 2 coverslips per condition per experiment. The Images taken were stored as high definition tif files.

2.8.2.4 Breast Cancer Cell ECM Deposition (Collagen and Fibronectin Staining)

The coverslips with fixed ECM (**2.7.6**) were blocked in 2% BSA in PBS for 30 minutes in a humidified chamber and washed 3 times in PBS. Next, they were incubated for 90 minutes at RT in a humidified chamber with collagen or fibronectin primary antibody (**Table 2.6**) in 2% BSA in PBS. The coverslips were then washed 3 times in PBS and incubated with anti-rabbit TRITC-conjugated sheep secondary antibody (**Table 2.7**) in 2% BSA for 45 minutes at RT in a humidified chamber in the dark. Finally, the coverslips were washed 3 times in PBS and 3 times in dH_2O and mounted using VectaShield® with DAPI. Slides were examined using an inverted Leica microscope (Leica DMI4000B) and images were captured using Leica DFC310fx camera controlled by Leica application Suite (LAS) 4.5 Software, UK with HCX PL APO lambda blue 63x 1.4NA oil objective. Single images were taken because a z-stack was not needed to visualise the thin layer of ECM.

2.9 SDS-PAGE AND IMMUNOBLOTTING

Proteins were separated by electrophoresis using freshly made 10% or 7.5% (for fibronectin blots only), SDS-polyacrylamide gels (**Table 2.3**) with Precision Plus Protein™ Dual color Standards markers (**Table 2.1**) for molecular weight references. All samples were boiled in SDS-PAGE SB (**Table 2.3**) that contained 100mM DTT prior to loading. If the sample contained heparin-beads, the samples were also centrifuged at 10000xg for 5 minutes to pellet the beads and the supernatant loaded. Samples were 'stacked' by running at 125V for 30-45 minutes (until marker was visibly into resolving gel) and then separated by running at 185V for up to 2h 30mins. For immunoblotting of proteins, the resolved proteins were transferred to a 0.2µm pore polyvinylidene difluoride (PVDF) membrane (Millipore) at 15V for 90 minutes using a Trans-Blot® SD Semi-Dry Transfer Cell (BioRad). All transferred proteins were visualised on the PVDF membrane using Ponceau S stain (**Table 2.1**), then washed in dH_2O and the membrane blocked using immunoblot blocking buffer (BB) (**Table 2.3**) for 1-2h at room temperature or overnight at 4^oC. Membranes were then probed with primary antibody to the required protein based on the experiment (**Table 2.6**). In all cases the primary antibody was diluted in BB according to **Table 2.6** and incubated with the membranes for at least 90 minutes at room temperature whilst under constant agitation or overnight at 4^oC. Non-specifically bound antibody was removed by three 10-minute washes in BB and membranes were then incubated with the appropriate secondary antibody (**Table 2.7**) in BB for 60 minutes. Following this incubation, the membranes were washed three times in BB (10 minutes per wash) and twice in PBS (five minutes for each wash). Membranes were then incubated in Amersham ECL Western blot detection reagent and locations where antibody was bound imaged in a Syngene G:BOX Chemi XRQ. Digital images were taken using partnered GeneSys software. Bands were quantified and normalised to the loading control using the GeneTools automated system.

2.10 IMMUNOHISTOCHEMISTRY

Paraffin-embedded tumour sections on glass slides from Wales Cancer Bank (**Table 2.4**) were deparaffinised in 2x 5-minute washes in Histo-Clear2; 2 x 5-minute washes in 100% ethanol; and 1 x 5-minute wash in 70% ethanol. The slides were then washed in tap water for 2 minutes before antigen retrieval by incubation in hot sodium citrate buffer (pH6.0) for 20 minutes. The samples were quenched in 0.6% H_2O_2 (**Table 2.1**) for 17 minutes followed by 2 x 2-minute washes in PBS. Using the VectaStain® Universal Elite® ABC immunohistochemistry kit (Vector Laboratories – PK-6200), the samples were blocked with normal horse serum for 30 minutes and then incubated with primary antibody to PDIA3 developed in rabbit or mouse (**Table 2.6**) for 45 minutes, then washed 2x in PBS. The slides were then incubated with universal secondary antibody (**Table 2.7**) for 30 minutes at room temperature and washed 2x in PBS. The sections were stained using ImmPACT DAB reagent

(**Table 2.1**) for up to 10 minutes based upon how quickly colour developed (time under DAB kept constant between slides within each experiment). The slides were washed for 5 minutes in running tap water to prevent excess staining and briefly counterstained in Gills Haematoxylin 2 II reagent (**Table 2.1**) for approx. 15 seconds.

The stained slides were dehydrated in 1x 5-minute wash in 70% ethanol; 2x 5-minute washes in 100% ethanol; and 2x 5-minute washes in xylene in a fume cabinet. Finally, a glass coverslip was sealed over the sample using VectaMount and left to dry overnight at RT.

Digital images were taken on an inverted Leica microscope (Leica DMI4000B) with a Leica DFC310fx camera and controlled by Leica application Suite (LAS) 4.5 Software, UK under a 5x or 40x objective lens in bright field and saved as tif files.

2.11 REPLICATION OF EXPERIMENTS

All cell-based experiments have been performed three times as biologically independent repeats, with technical replicates and controls in each experiment, unless stated otherwise in the figure legend.

2.12 STATISTICAL ANALYSIS

Data were first plotted as a frequency histogram using R with basic descriptives such as Shapiro-Wilk and Skewness/kurtosis to determine normality. Data were then analysed using two-way ANOVA with Tukey's multiple comparisons post-hoc test through GraphPad Prism and data were displayed as mean $\pm$ standard deviation (S.D).

As the majority of data were non-parametric these ANOVA/Tukey's p-values were verified using the inbuilt Kruskal-Wallis non-parametric multiple comparisons test with Dunn's multiple corrections in GraphPad Prism 7.0 and, where possible on normalised data (log transformed).

All analysis was performed after consultation with Professor Peter Green, a statistician at University of Bristol School of Mathematics.

Chapter 3

Results

3.1 IMMUNOHISTOCHEMISTRY OF BREAST TUMOUR SAMPLES

PDIA3 has been shown to be differentially expressed in several cancers including breast cancer (Da Costa et al., 2015; He et al., 2016; Oliveira et al., 2016; Zou et al., 2018) (**section 1.4.5**). To investigate PDIA3 protein in human breast IDC, a pilot immunohistochemical study was carried out on single specimens of luminal and basal molecular subtypes of breast IDC cancer. Images were taken under identical settings for anti-PDIA3 test and non-immune IgG control images. PDIA3 protein was detected in both specimens and the staining patterns were absent from the IgG controls (**Figure 3.1**). In the luminal IDC specimen, PDIA3 was mostly localised to epithelial-like, ductal cells (black arrows) with occasional staining within the stroma (white arrows) (**Figure 3.1 – left**). The basal IDC sample, as expected, exhibited greater loss of normal histological structures. Staining for PDIA3 was more ubiquitous and possibly included more stromal staining than in the basal sample (**Figure 3.1 – right**).

3.2 INTRODUCTION TO BREAST CANCER CELL LINES

In order to assess the role of PDIA3 in breast cancer using *in vitro* techniques, age-matched basal and luminal breast cancer cell lines were chosen from ATCC (Neve et al., 2006) (**Table 3.1**). HCC1937 and BT-483 cells were isolated from the primary tumours of young women (ages 21 and 24 respectively) whereas MDA-MB-231 and MCF-7 are from pleural effusions and are extensively studied cell lines that are not age-matched (40y and 64y respectively). HCC1937 and MDA-MB-231 represent the basal subtype and BT-483 and MCF-7 represent the luminal subtype. The original goal was to work with age-matched cell lines derived from primary tumours. Unfortunately, BT-483 cells failed to grow in multiple culture conditions and there was not time to obtain different cell lines, so experiments were continued with the three other cell lines.

Cell morphology and behaviour under normal growth conditions was first assessed using phase contrast microscopy (**Figure 3.2**). MDA-MB-231 cells were mesenchymal in morphology, forming long spindle-like cells, whereas HCC1937 (of the same molecular subtype) form more regular squarish shapes and grow in clusters, characteristic of epithelial cells (**Figure 3.2A, B**). MCF-7 cells were also epithelial-like in morphology and formed packed cell clusters but seemed to be more irregular in shape than HCC1937 cells (**Figure 3.2C**). All cell lines grew at a similar rate. For example, a seeding of $2.5x10^5$ cells into a P90 dish would grow to confluence in 4-5 days. HCC1937 cells were most resistant to trypsinisation and took 3-5 minutes to detach fully where the other cell lines took between 1 and 3 minutes (data not shown). MCF-7 cells readily grew into three-dimensional structures at high confluence whereas the other cell lines did not.

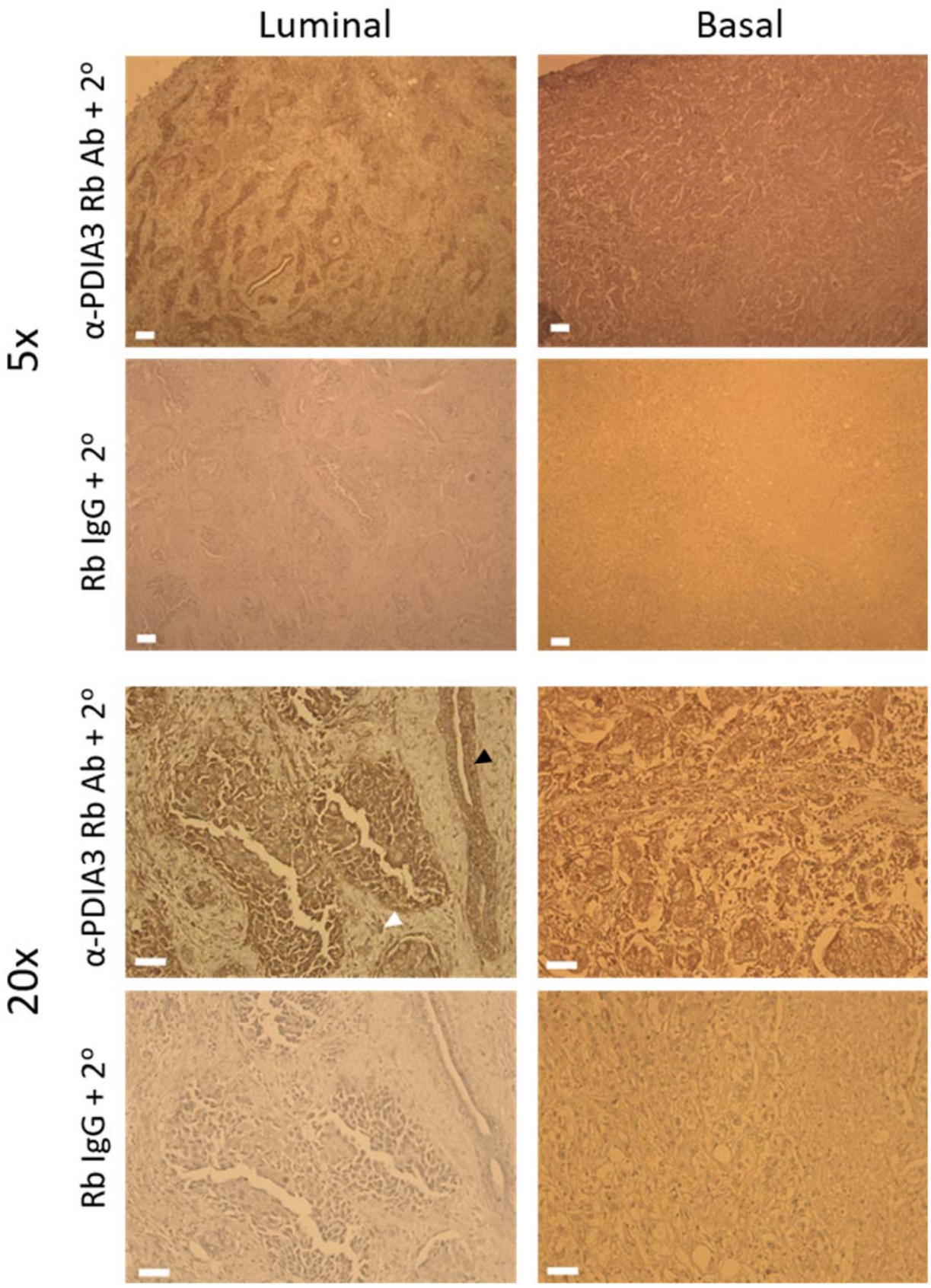

Figure 3.1 ***Immunohistochemistry of PDIA3 in Luminal and Basal IDC.*** *Images of IHC of IDC from basal (right) or luminal (left) tumour samples from Wales Cancer Bank, ref#: RR6BL0000987PT3AH-basal + RR6BL0000290PT3AH-luminal. Scale bar: 50µm*

Breast Cancer Cell Line	Tissue Source	Patient Age (y)	TP53	HER2	Basal/Luminal	ER/PgR status
MDA-MD-231	PE	40	M	Absent	Basal	ER^-/PgR^-
HCC1937	P	24	-	Absent	Basal	ER^-/PgR^-
MCF7	PE	69	wt	Absent	Luminal	ER^+/PgR^+
BT-483	P	23	-	Absent	Luminal	ER^+/PgR^+

Table 3.1 ***Properties of the Breast Cancer Cell Lines used in This Project.*** *Key: **M** – mutant, **PE** – Pleural effusion, **P** – Primary tumour, **wt** – wild-type, **ER –** Oestrogen receptor, **PgR** – Progesterone receptor.*

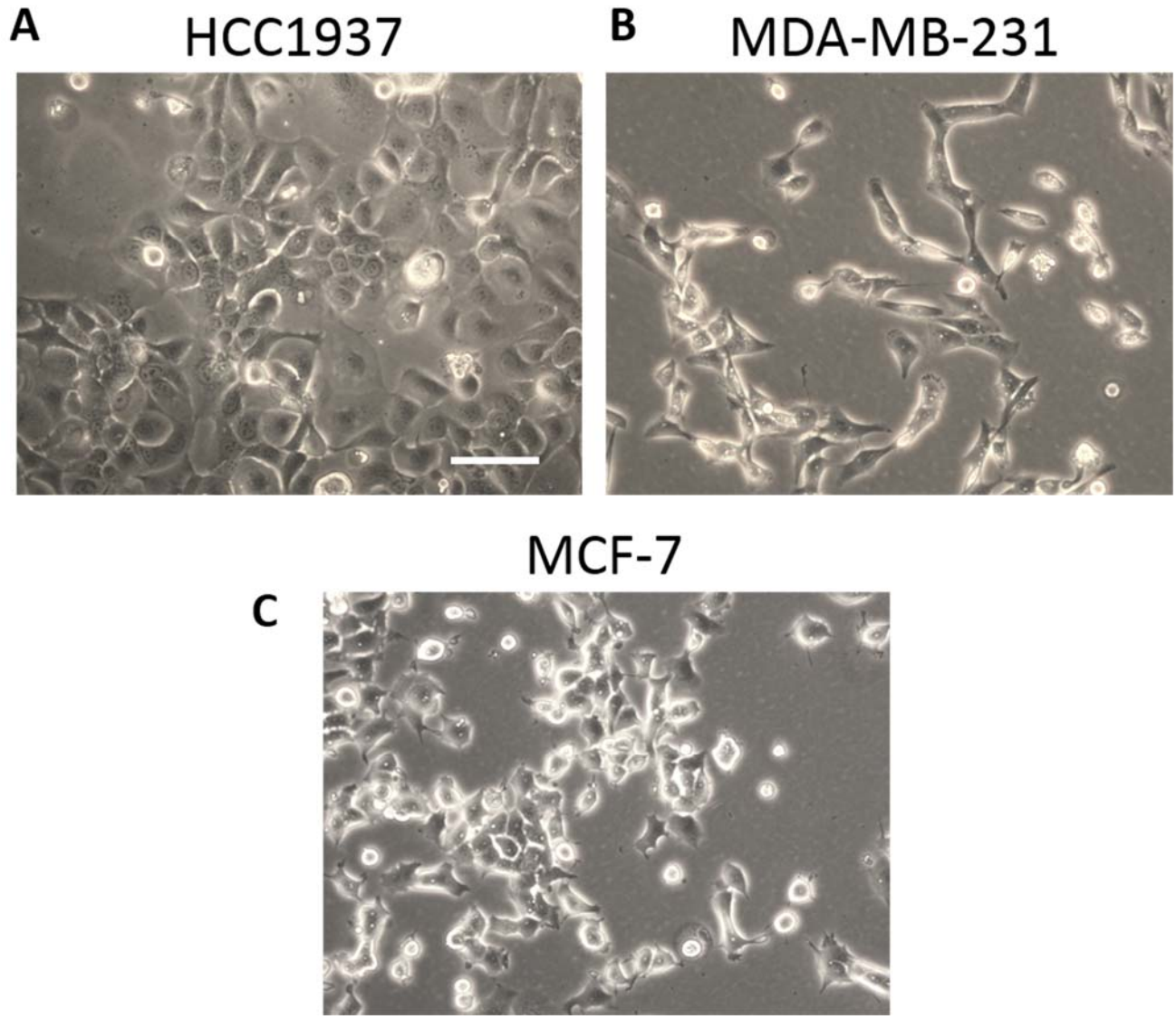

Figure 3.2 ***Phase Contrast Images of Breast Cancer Cell Lines.*** *(**A**) HCC1937 cells. (**B**) MDA-MB-231 cells. (**C**) MCF-7 cells. 20x Phase contrast images of each cell line. Scale bar: 100µm.*

Next, proteins relevant to the actin cytoskeleton and EMT were examined by immunofluorescence. Vinculin is vital to the formation of focal adhesions and sensing external forces by anchoring integrin cytoplasmic tails to the actin cytoskeleton and other mechanosensory linker proteins (Atherton et al., 2016). Therefore, it was relevant to determine vinculin localisation in each of the three breast cancer cell lines. Indirect immunofluorescence for vinculin after 24h of culture (**Figure 3.3A-C**) showed that only MDA-MB-231 cells produced clear leading edges containing focal adhesions (**Figure 3.3B**). HCC1937 and MCF-7 had minimal focal adhesions and did not appear to have a distinct leading edge (**Figure 3.3A, C**). These observations were made at a low seeding density as shown by the images in **Figure 3.3A-C** to encourage cell migration and avoid cell-cell overlap.

WNT/β-catenin signalling is often upregulated in cancer, causing nuclear translocation of β-catenin. This results in β-catenin-mediated transcriptional changes that are associated with de-differentiation and EMT which is characterised by loss of E-cadherin and gain of N-cadherin (Lamouille et al., 2014). To characterise the cell lines with regards to adherens junctions and status of WNT signalling, the localisation of β-catenin was visualised by indirect immunofluorescence after 24h of culture (**Figure 3.3 A-C**). In each cell line, there was a substantial nuclear immunofluorescence signal for β-catenin (**Figure 3.3 A-C**). Only HCC1937 cells contained clearly visible β-catenin at the cell-cell boundaries (**Figure 3.3 A**). It is possible that at higher seeding densities, cell-cell junctions might form, and peripheral β-catenin signal would increase.

For the purpose of this project, PDIA3 and PDIA1 were examined by immunoblotting. Single bands of the expected molecular weight (approx. 55kDa PDIA3 and PDIA1) were observed in all three cell lines (**Figure 3.4A**). The graph represents data from one experiment and so is not accurate but gives some insight into the potential relative abundance of PDIA1 and PDIA3 in breast cancer cell lines (**Figure 3.4B**). The basal cell lines, HCC1937 and MDA-MB-231, both had similar quantities of intracellular PDIA1 protein whereas MCF-7 cells had much higher levels (**Figure 3.4B**). Also, MDA-MB-231 cells had substantially less PDIA3 protein than the other two cell lines (**Figure 3.4B**).

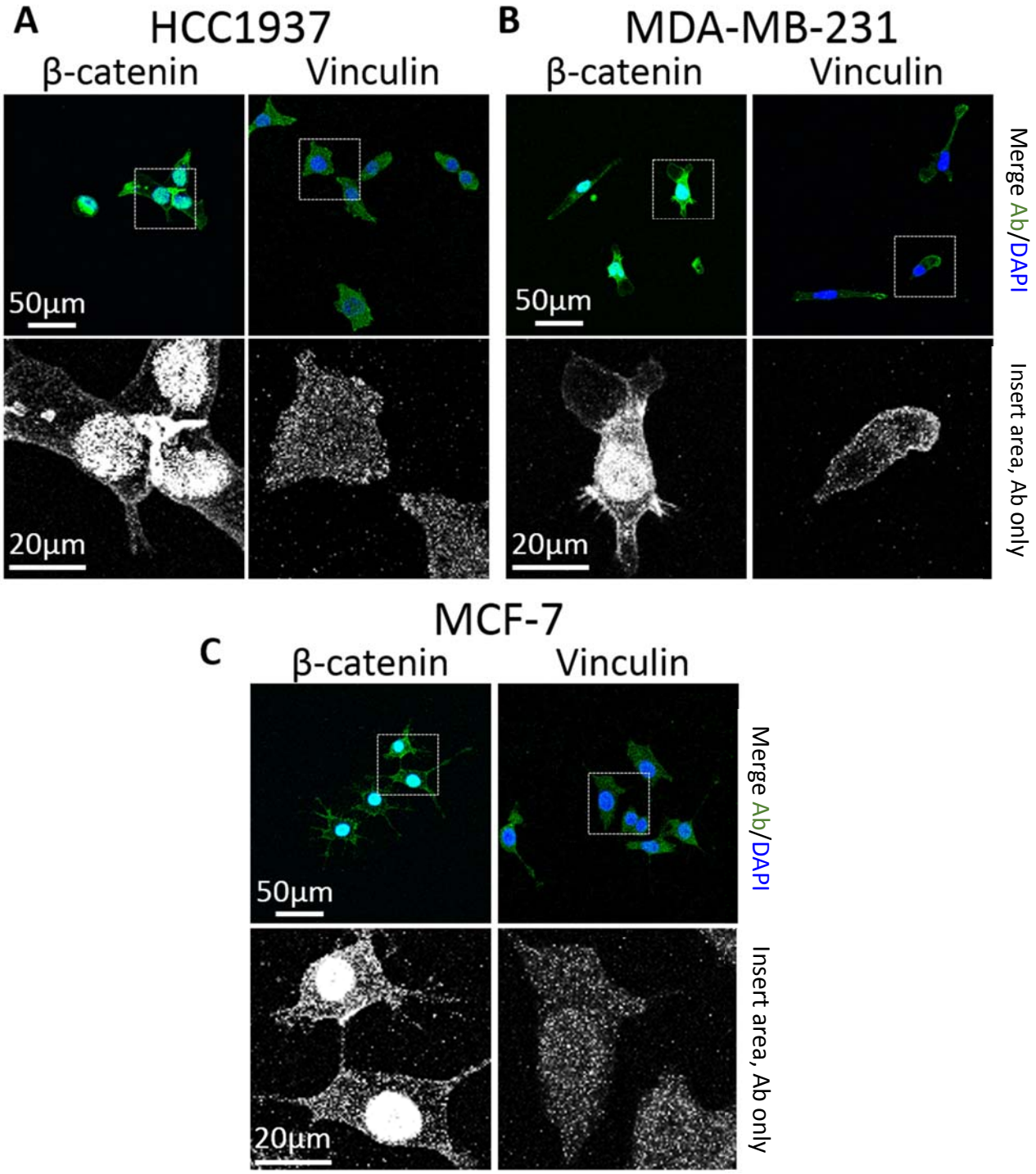

.

Figure 3.3 ***Immunofluorescence Images of HCC1937, MDA-MB-231 and MCF-7 Cells Stained for β-catenin or Vinculin.*** *(**A**) HCC1937 cells. (**B**) MDA-MB-231 cells. (**C**) MCF-7 cells. Each panel shows the 63x frames (top row) and enlargement of boxed areas (lower row) of each cell line stained for β-catenin or vinculin. DAPI also shown in upper rows.*

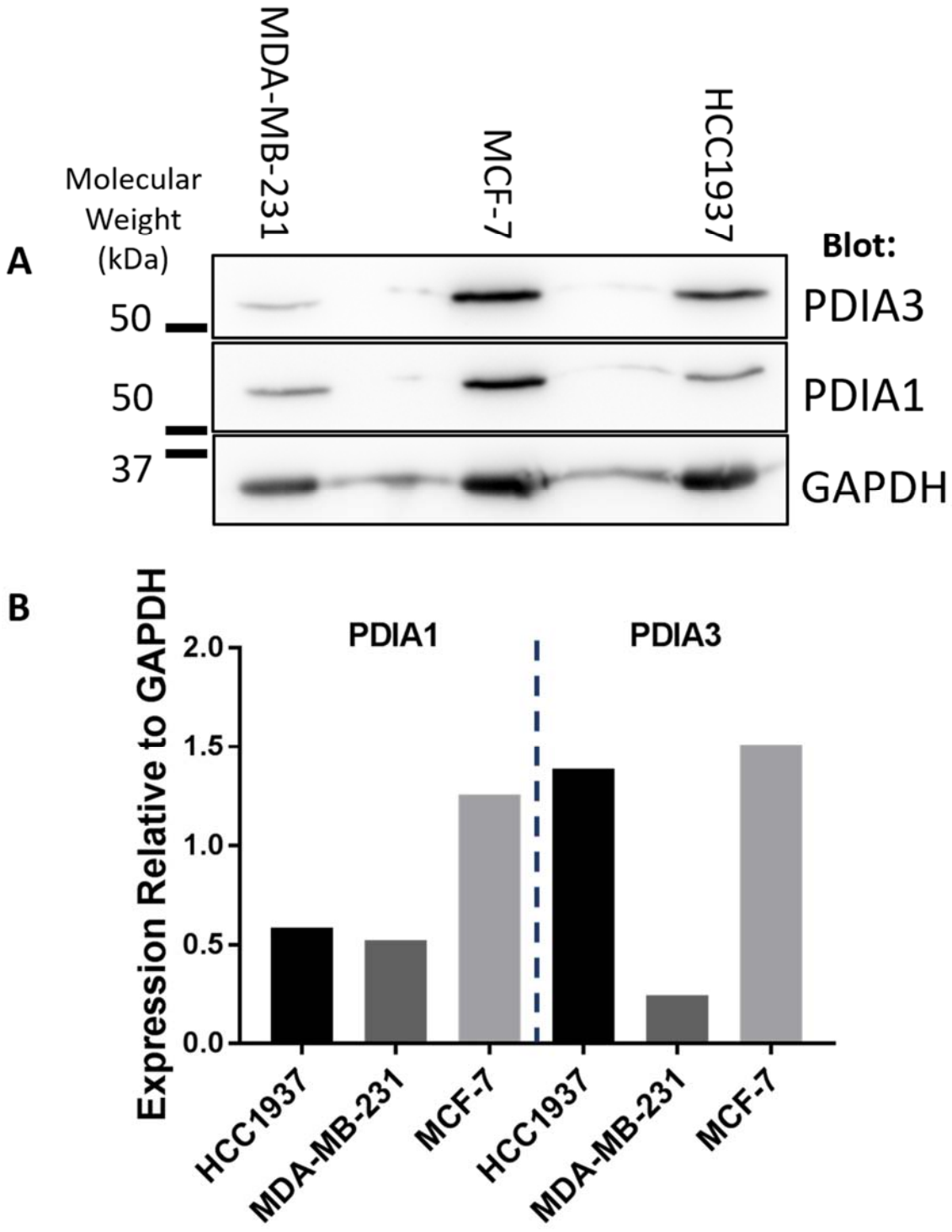

Figure 3.4 ***Western Blotting of Cell Lysates for PDIA1 or PDIA3 and GAPDH.*** *(**A**) Western Blot of cell lysates from each cell line run on 10% acrylamide gel under reducing conditions. (**B**) Automated quantification (Syngene GeneTools©) of the PDIA1 or PDIA3 band intensities normalised to the GAPDH loading control to give relative amounts of protein in each cell lysate. Plotted in GraphPad Prism with data from a single immunoblot.*

3.3 TESTING THE MORPHOLOGICAL RESPONSES OF BREAST CANCER CELLS TO PDIA3 INHIBITORS

Currently there is no PDIA3-specific inhibitor commercially available. To test the response of breast cancer cell lines to PDIA3 inhibition, a PDIA3 and PDIA1 inhibitor, 16F16, was used in parallel with a PDIA1-specific inhibitor, PACMA-31 (**Section 1.5.3**). Any effects observed could then be deduced as due to inhibition of PDIA3 from the cell response to PACMA-31 versus 16F16.

First, working concentrations of each inhibitor were established, with the requirement of causing a morphological change to the breast cancer cells without resulting in substantial cell death. An assay to examine the percentage of 'flat', healthy and attached cells in comparison to the 'round', unhealthy or detached cells after 24h treatment with either inhibitor was designed. After research into the literature and preliminary experiments (not shown) the 0.1-10µM concentration range was focussed on. Using 10x phase contrast images, the number of flat and round cells were counted and % of flat cells/field calculated. This design was then extended into examining the quantitative change in cell density using the IncuCyte® system to produce a similar metric. In both designs, these observations were compared against cells treated with the equivalent volume of the solvent the inhibitors were dissolved in, DMSO or untreated media (DMEM containing 10% FBS or serum-free FGM). Where possible FGM was used because it is serum-free and so better ethically as well as removing inaccuracies associated unknown serum components. However, the first experiments involving MDA-MB-231 and MCF-7 cells used DMEM containing 10% FBS because they were completed before we had established FGM as a viable condition to grow these cancer cells in.

HCC1937 cells were analysed in the flat versus round experiment in FGM over three separate experiments to produce quantified data (**Figure 3.5A-C**). **Figure 3.5C** is the accumulation of all data points shown in **A** and **B**, divided by the mean of the DMSO condition to standardise any variation between repeat experiments. Then, an 'inhibitor dose-response' curve was fitted using GraphPad Prism. This showed that HCC1937 cells were more sensitive to PACMA-31 than 16F16 (**Figure 3.5C**). For example, at 0.5µM PACMA-31 there was a 30-40% reduction in % flat cells compared to treatment with 0.5µM 16F16 (**Figure 3.5C**). From these data, and adjustment after initial experiments, a concentration of 0.75µM for PACMA-31 or 7.5µM for 16F16 was chosen for future experiments (**Table 3.2**). The difference in experiment type between HCC1937 and MCF-7 or MDA-MB-231 was because HCC1937 cells were too flat to be detected accurately by the IncuCyte ZOOM™ confluence-mask analysis.

After one preliminary flat versus round experiment using MCF-7 and MDA-MB-231 cells it was deduced that the IncuCyte® would be more accurate (data not shown). These cells were analysed using the IncuCyte®

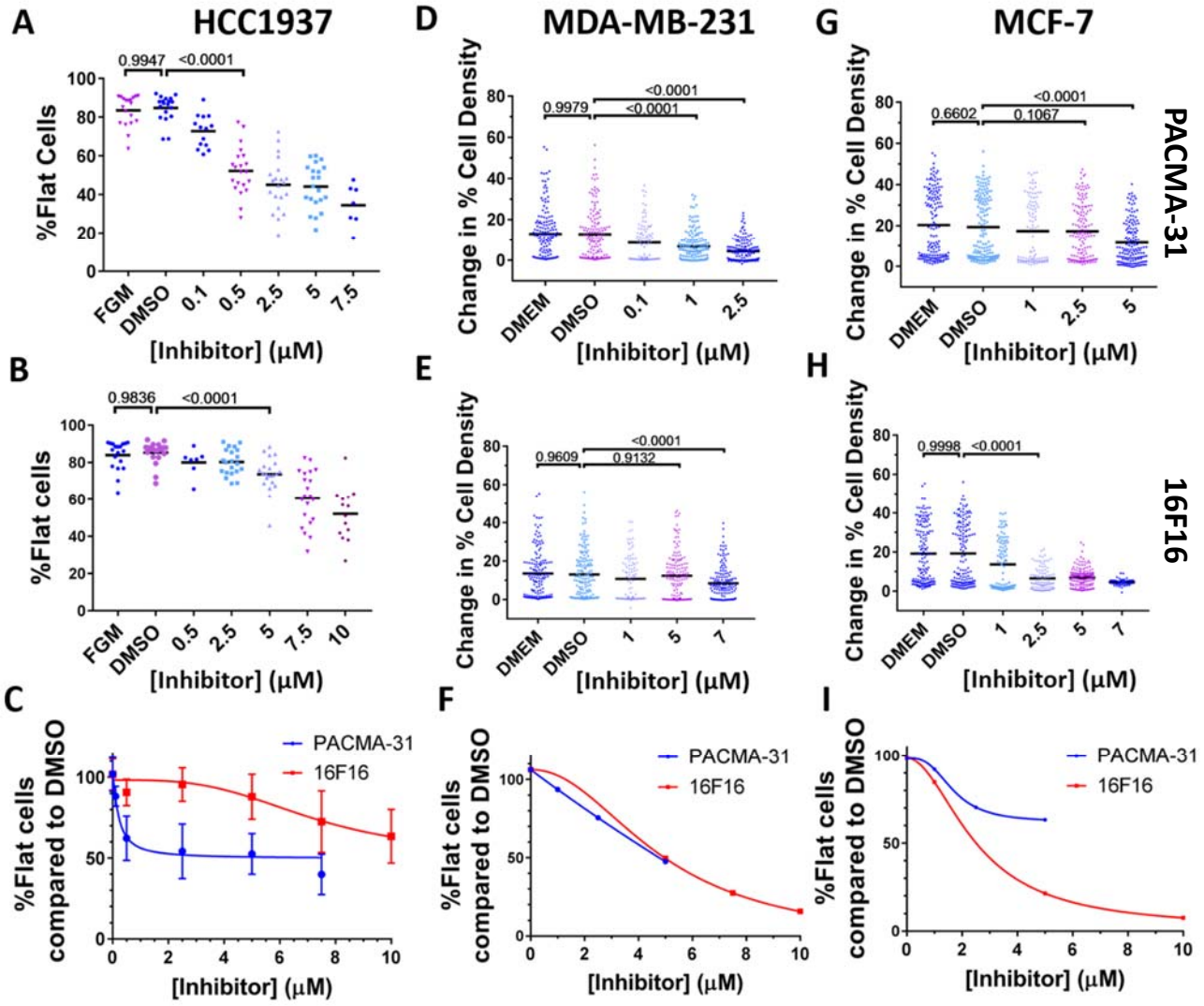

Figure 3.5 ***Testing the Morphological Responses of Breast Cancer Cells to 16F16 and PACMA-31.*** *(**A, B**) Change in % flat cells in HCC1937 cells in response to various concentrations of PACMA-31, 16F16 or equivalent volume of DMSO in FGM. (**C**) Pooled data from (**A**) and (**B**) divided by the mean % flat cells for the DMSO condition to standardise data. (**D-E, G-H**) Change in cell density, calculated using the IncuCyte ZOOM ™ 'confluence mask', in MDA-MB-231 (**D-E**) and MCF-7 (**G-H**) cells in response to PACMA-31, 16F16 or equivalent volume of DMSO in DMEM containing 10% FBS. n=2-4 experiments (exceptions **A-7.5μM, B-0.5μM, H-7μM,** all n=1 experiment) (**F, I**) Response of cells to various concentrations of PACMA-31, 16F16 or equivalent volume of DMSO in FGM. n=1 experiment using flat/round cell counts divided by mean % of flat cells for the DMSO condition to standardise data. All data compared with two-way ANOVA follwed by Tukey's multiple comparisons using GraphPad Prism. p values given in the panels.*

system over three separate experiments per cell line in DMEM containing 10% FBS (**Figure 3.5D, E, G, H**). It was also deduced that cells showed a similar response in FGM by the flat versus round cell count method (**Figure 3.5F, I**). MDA-MB-231, like HCC1937, were more sensitive to PACMA-31 than 16F16 (**Figure 3.5D-F**) whereas MCF-7 cells were more sensitive to 16F16 than PACMA-31 (**Figure 3.5G-I**). The concentrations displayed in **Table 3.2** were chosen based on these data. The key descriptive values of the curves fitted in **Figure 3.5 C, F, I** are summarised in **Table 3.3**. As **Figure 3.5 F and I** are based upon a single experiment, the corresponding IC_{50} values should not be taken as accurate. MDA-MB-231 failed to fit the model well for PACMA-31 (denoted by "ambiguous" output). So, initial experiments similar to those in **section 3.4** were carried out for the cell lines to ensure these concentrations were working as expected.

Finally, this experiment showed that the amount of DMSO equivalent to the volume used as solvent for each inhibitor resulted in very similar distributions to cells grown in untreated DMEM containing 10% FBS or FGM. So, effects of PDIA3 inhibition in all experiments can be assumed to be independent of the effect of DMSO.

		Inhibitor (μM)	
		PACMA-31	**16F16**
Cancer Cell Lines	**MDA-MB-231**	2.50	5.00
	MCF-7	5.00	2.00
	HCC1937	0.75	7.50

Table 3.2 ***Inhibitor Concentrations Selected for Future Experiments.*** *The concentrations of PACMA-31 or 16F16 that produced a significant change in cell morphology or cell density compared to the equivalent volume of DMSO in the three breast cancer cell lines. See text for details.*

		Inhibitor			
		PACMA-31		**16F16**	
		R^2	**IC_{50}**	**R^2**	**IC_{50}**
Cancer Cell Lines	**MDA-MB-231**	N/A	Ambiguous	0.9462	4.871
	MCF-7	0.8031	1.676	0.9749	2.512
	HCC1937	0.7109	0.215	0.4664	7.129

Table 3.3 ***Nonlinear Dose-Response Fit from Figure 3.5. (G-I)*** *GraphPad Prism [Inhibitor] versus. response - Variable slope (four parameters) equation was fitted to each dataset. The R^2 value is displayed, denoting fit of the model to the data. The IC_{50} denotes the concentration at which the maximal response is reduced by half.*

3.4 THE EFFECTS OF PDIA3 INHIBITION ON BREAST CANCER CELL SPREADING, ATTACHMENT AND ACTIN CYTOSKELETON

3.4.1 Cell Spreading

When a mammalian cell is plated onto glass in serum-containing medium, it attaches quickly and spreads out. With time, cells form focal adhesions, F-actin stress fibres and lamellipodia for movement (Khalili and Ahmad, 2015). A current hypothesis is that, the greater the metastatic potential of a cancer cell, the faster it will attach and the larger the final cell area will be, due to enhanced ability to migrate (Lyons et al., 2016; Paul et al., 2017). Therefore, the first experiment to examine the functional effects of PDIA3 inhibition was to quantify effects on cell attachment and spreading on glass in response to PDIA3 inhibition. This was assessed by pre-treating cells in FGM treated with PACMA-31, 16F16 or equivalent volume of DMSO for 24h (**Table3.2**). Then, $2.5x10^5$ pre-treated cells per well were plated in FGM into a 6-well plate containing glass coverslips for 2h, 6h, 12h or 24h, during which the treatment with PACMA-31, 16F16 or equivalent volume of DMSO was continued.

After fixation and staining with Phalloidin-FITC/DAPI, cell area was measured using ImageJ and immunofluorescence images. Graphs in **Figure 3.6** show cell area measurements over three independent experiments at each timepoint under each condition for the three breast cancer cell lines (minimum number of cells measured per condition was 100). For HCC1937 cells, there was no observable difference between cell area in response to PACMA-31 or DMSO at any time point (**Figure 3.6A**). However, treatment with 16F16 produced a significant reduction in cell area compared to DMSO at 2h and this difference became more apparent at 6h, 12h and 24h (**Figure 3.6A**).

MDA-MB-231 cells showed a marginal reduction in cell area in response to treatment with PACMA-31 for 12h or 24h when compared to DMSO (**Figure 3.6B**). 16F16 treatment resulted in reduced cell area compared to DMSO only treated cells at the later timepoints, 12h and 24h (**Figure 3.6B**). There was a larger reduction in cell area relative to DMSO when MDA-MB-231 cells were treated with 16F16 as opposed to PACMA-31 at the 12h and 24h timepoints.

For MCF-7 cells, there was no clear change in cell area after treatment with PACMA-31 relative to DMSO at any timepoint (**Figure 3.6C**). Treatment with 16F16 produced a significant reduction in cell area relative to DMSO at all timepoints (**Figure 3.6C**).

This reduction in area in response to 16F16 increased with time from 2h to 24h. Across all cell lines, cell area increased by approximately 500μm^2 over 24h under the DMSO- or PACMA-31-treatment conditions. When treated with 16F16, cell area increased by a maximum of 200μm^2 over 24h (**Figure 3.6A-C**).

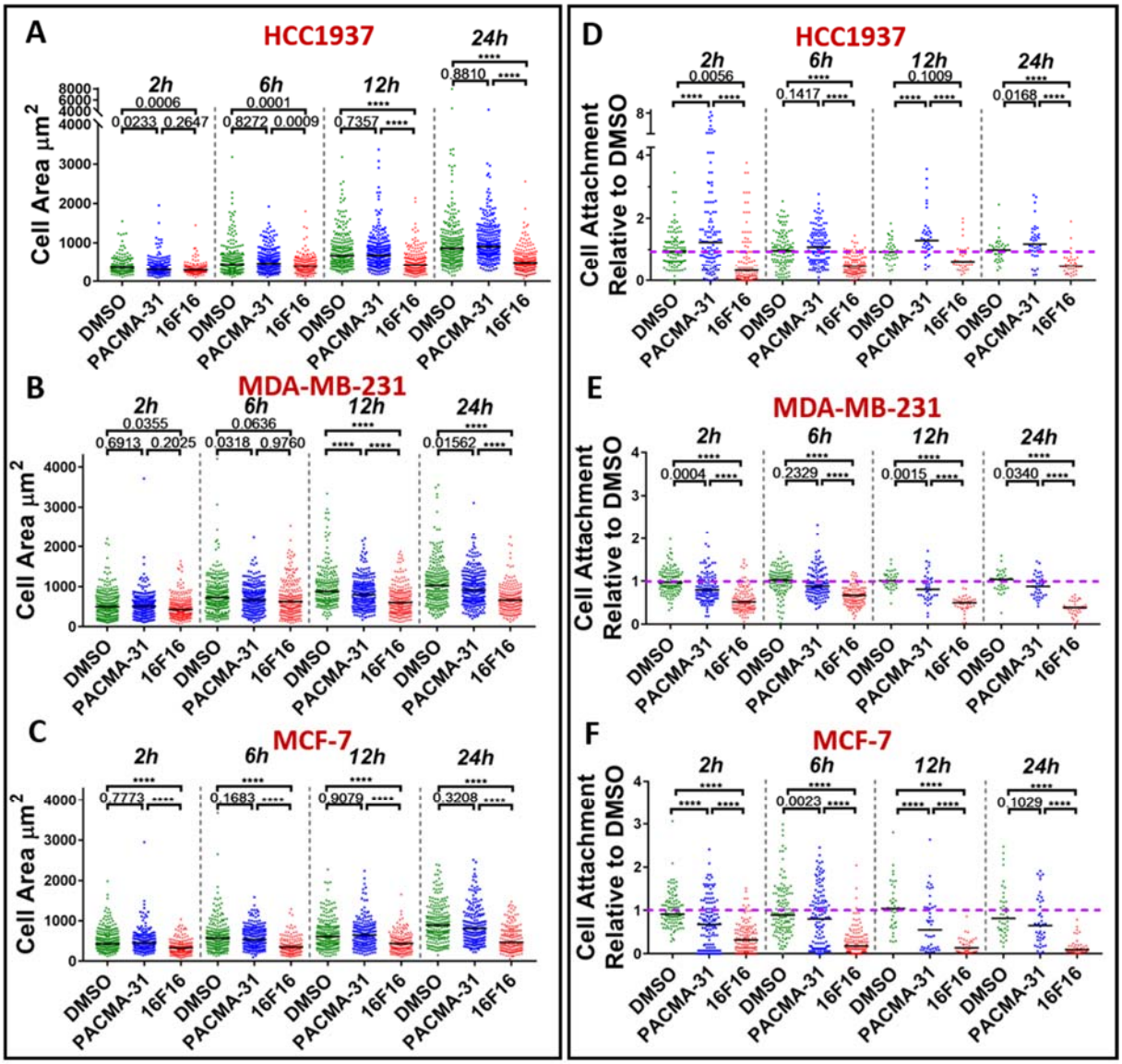

Figure 3.6 ***Change in Cell Area and Attachment After Treatment with PACMA-31 or 16F16.*** *(**A-C**) Dot plot with median value (**black bar**) of HCC1937, MDA-MB-231 and MCF-7 cell area, respectively. n=3 experiments. (**D-F**) Dot plot (where each dot represents 'Relative Attachment' of one microscope field (**See 3.4.2**)) for HCC1937, MDA-MB-231 and MCF-7, respectively. Median value (**black bar**) overlaid. **Purple dashed line** at Relative Attachment = 1 (i.e. no change). The further distributions are from this line the larger the difference in attachment. n=3 experiments. (**A-F**) Analysed using GraphPad Prism two-way ANOVA with Tukey's multiple comparisons. p-values displayed in panels, **** = <0.0001.*

3.4.2 Cell Attachment

The attachment of a cell to glass and the ability to resist the washing steps during fixing and permeabilisation is indicative of formation of sufficient cell-substratum adhesions. These adhesions are essential as they provide an anchored point to apply force through which allows cell spreading and migration (Khalili and Ahmad, 2015). Cell attachment was investigated by calculating the number of cells in FGM attached to the glass relative to the control condition:

$$Relative\ attachment\ = \frac{Number\ of\ Nuclei\ per\ Microscope\ Field\ after\ Treatment\ with\ Inhibitor\ or\ DMSO}{Mean\ Number\ of\ Nuclei\ per\ Microscope\ Field\ after\ Treatment\ with\ DMSO}$$

This gives a metric of '**relative attachment**' which accounts for any variations in the seeding density between experiments. Relative cell attachment in response to 16F16 was reduced in comparison to DMSO for all three cell lines at all timepoints except in HCC1937 cells at 12h (**Figure 3.6D-F**). HCC1937 cells treated with 16F16 showed no clear correlation of relative attachment with time, with the median relative attachment always falling between 0.4 and 0.6[2] (**Figure 3.6D**). MDA-MB-231 cells under 16F16 treatment showed a reduced median relative attachment with time, from approx. 0.5 at 2h to approx. 0.3 at 24h. This may not be a linear relationship because the relative attachment was higher at the 6h timepoint compared to 2h timepoint (**Figure 3.6E**). For MCF-7 cells, the median relative attachment after 16F16 treatment was reduced with time from approx. 0.4 at 2h to approx. 0.1 at 24h (**Figure 3.6F**).

HCC1937 cells treated with PACMA-31 had a relative attachment equal to the DMSO-only condition at 6h and greater than the DMSO-only condition at 2h, 12h and 24h (**Figure 3.6D**). MDA-MB-231 cells treated with PACMA-31 had marginally reduced relative attachment at 2h, 12h and 24h (**Figure 3.6E**). MCF-7 cells showed a significant reduction of attachment in response to PACMA-31 at every timepoint (**Figure 3.6F**). Despite this, 16F16 treatment of MCF-7 cells reduced relative attachment more strongly than PACMA-31.

In examining the dataset, it was apparent that, for all cell lines, there was reduced variance of attachment at the 12h and 24h timepoints in comparison to the 2h and 6h timepoints after inhibitor treatment (**Figure 3.6D-F**). This indicates that there was a more consistent reduction in attachment at the 12 and 24h timepoints.

The noted reductions in cell area and attachment were apparent qualitatively for both HCC1937 and MCF-7 cells in the immunofluorescence images (**Figures 3.7 and 3.9**). However, MDA-MB-231 cells were not as obviously changed in terms of cell area (**Figure 3.8**).

[2] Median value has been used due to non-parametric data with one heavy tail. This means that median will be closer to the true average of the data in this case because it is not affected by extreme values as the mean would be.

3.4.3 Cell Morphology

Next, the F-actin cytoskeleton was examined in more detail. Cancer cells are often migratory after undergoing EMT and so move in a similar manner to fibroblasts on rigid 2D surfaces (Son and Moon, 2010). Therefore, if a cancer cell is migrating it would contain F-actin stress fibres, lamellipodia, filopodia and often form a characteristic 'kite-shaped' morphology (Trepat et al., 2012).

Figure 3.7 shows images of HCC1937 cells in FGM after 12h of treatment with PACMA-31 (**middle**), 16F16 (**right**) or DMSO (**left**). The 12h timepoint was chosen for this study because there were quantifiable differences in area and attachment across all three cell lines at this timepoint (**see 3.4.1 and 3.4.2**). HCC1937 breast cancer cells formed regular shapes that were more epithelial-like in terms of morphology across all three conditions. Cells treated with DMSO (**Figure 3.7 left**) or PACMA-31 (**Figure 3.7 middle**) did not have many obvious F-actin stress fibres. However, bright staining for F-actin was visible at the cell periphery which is indicative of lamellipodia-like arrangements (**Figure 3.7**). Many cells had filopodia-like F-actin protrusions (**Figure 3.7 Insert**). Cells treated with 16F16 (**Figure 3.7 right**) had less F-actin at the cell periphery and fewer filopodia-like protrusions.

For MDA-MB-231 breast cancer cells, a more mesenchymal-like phenotype was observed (**Figure 3.8**). The cells were long and spindle-like with obvious stress fibres under DMSO (**Figure 3.8 left**) and PACMA-31 (**Figure 3.8 middle**) conditions. In general, cells treated with 16F16 either formed spindle-like cells that appear to be longer and thinner or remained as smaller, rounder cells without obvious stress fibres (**Figure 3.8 Insert**). These smaller cells were present in the other conditions but appeared most common (qualitatively) when cells were treated with 16F16 (**Figure 3.8 right**).

Under DMSO treatment, MCF-7 cells appeared as irregularly shaped cells that were not obviously epithelial or mesenchymal (**Figure 3.9 left**). Cells formed stress fibres and had many filopodia-like F-actin protrusions at the cell periphery (**Figure 3.9 left**). Cells treated with PACMA-31 were also neither consistently epithelial nor mesenchymal but some contained lamellipodia and/or stress fibres (**Figure 3.9 middle**). After PACMA-31 treatment, a minority of cells formed obvious leading-edge F-actin rich structures (**Figure 3.9 Insert**). MCF-7 cells readily adhered to one another to form chains or small colonies (**Figure 3.9 middle**). The response to treatment with 16F16 (**Figure 3.9 right**) was most dramatic in MCF-7 cells, as shown by the obvious reduction in cell area and cell attachment. Also, there were minimal F-actin structures visible within cells. Finally, cellular protrusions that were apparent seemed to of detached and folded back onto the cells (perhaps during the fixing or staining process) as exemplified in **Figure 3.8**, **16F16** - **Insert Panel**.

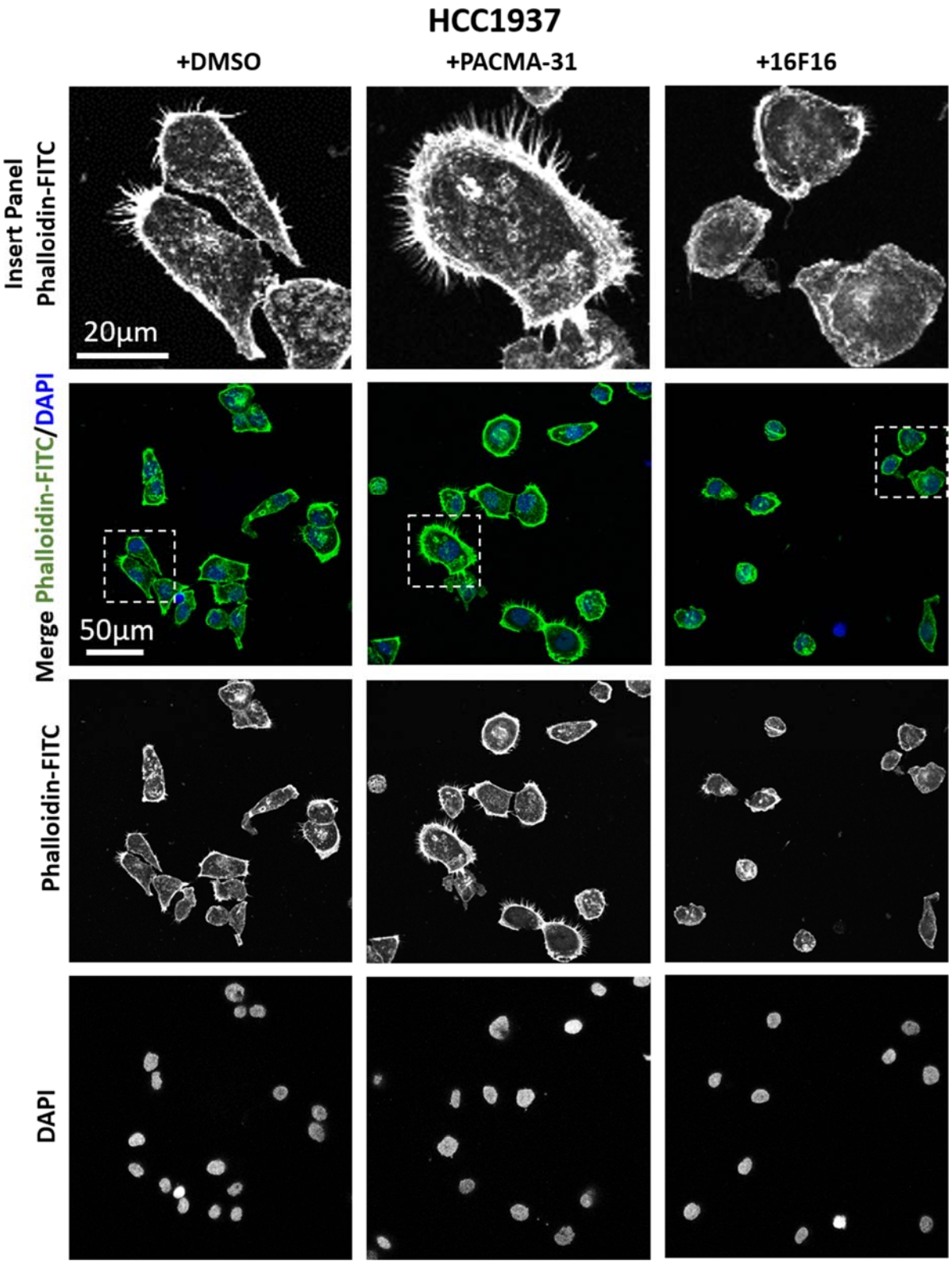

Figure 3.7 ***Fluorescence Images of HCC1937 Breast Cancer Cells Treated with PACMA-31, 16F16 or DMSO.*** *HCC1937 cells were stained with Phalloidin-FITC and DAPI after 12h treatment with PACMA-31, 16F16 or equivalent volume of DMSO. (**Top row**) Higher magnification of boxed area, FITC channel only to show F-actin organisation in more detail. Below this is the merged DAPI/FITC channel; the FITC only channel; and DAPI only channel for each condition.*

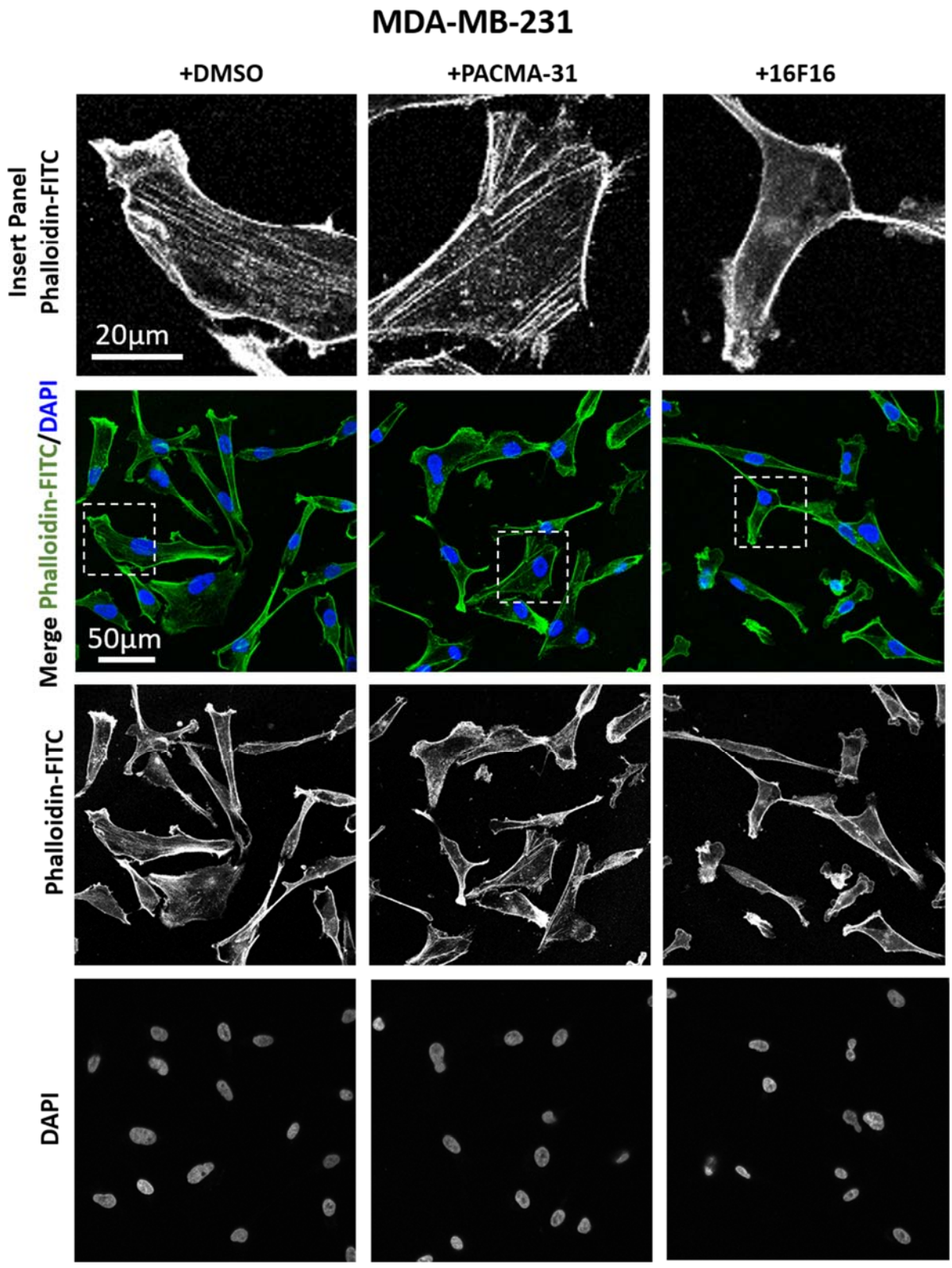

Figure 3.8 ***Fluorescence Images of MDA-MB-231 Breast Cancer Cells Treated with PACMA-31, 16F16 or DMSO.*** *MDA-MB-231 cells were stained with Phalloidin-FITC and DAPI after 12h treatment with PACMA-31, 16F16 or equivalent volume of DMSO. (**Top row**) Higher magnification of boxed area, FITC channel only to show F-actin organisation in more detail. Below this is the merged DAPI/FITC channel; the FITC only channel; and DAPI only channel for each condition.*

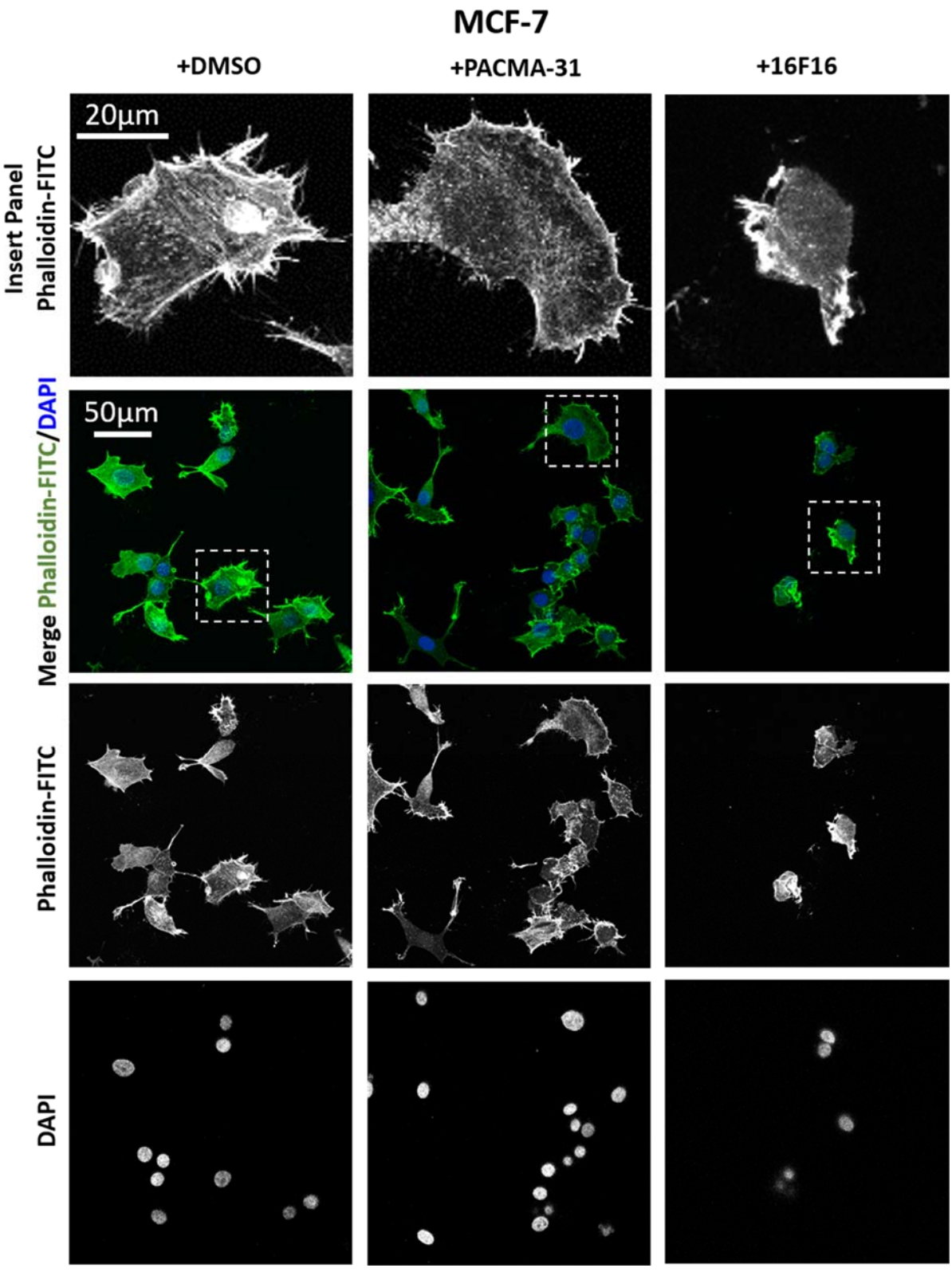

Figure 3.9 ***Fluorescence Images of MCF-7 Breast Cancer Cells Treated with PACMA-31, 16F16 or DMSO.*** *MCF-7 cells were stained with Phalloidin-FITC and DAPI after 12h treatment with PACMA-31, 16F16 or equivalent volume of DMSO. (**Top row**) Higher magnification of boxed area, FITC channel only to show F-actin organisation in more detail. Below this is the merged DAPI/FITC channel; the FITC only channel; and DAPI only channel for each condition.*

3.5 Effect of Inhibition of PDIA3 and PDIA1 on Cellular Migration

For cancer cells to metastasise, they must first migrate through tissue to reach either blood or lymphatic vessels, disseminate and then invade into a secondary site. Therefore, the heightened ability of cancer cells to migrate is essential for metastasis (Hanahan and Weinberg, 2011). The migratory capacity of cancer cells can be tested *in vitro* using a two-dimensional (2D) 'scratch-wound' assay. The ability of cancer cells to migrate in this system is considered to be indicative of a more invasive cancer (Hulkower and Herber, 2011). Also, there is increasing evidence for directional and collective migration being of importance to cancer progression (Erdogan et al., 2017; Friedl and Alexander, 2011; Paul et al., 2017).

Hence, effects of PDIA3 and PDIA1 inhibition on the ability of each breast cancer cell line to collectively migrate in 2D in comparison to the DMSO treated condition was investigated. Each cell line was tested in a high-throughput standardised 'scratch-wound assay' using the IncuCyte® automated live-cell imager. Cells were plated according to experimental design (**section 2.7.4**) into a 96-well plate and the confluent layer of cells 'scratched' at timepoint 0h. Images were taken on the hour every hour for 48h.

Figure 3.10 shows exemplary phase-contrast images of each cell line under each condition at 0h or 48h overlaid with the IncuCyte ZOOM™ Scratch Mask (yellow). These are shown to demonstrate the system for quantification of results from this experiment. In the MCF-7 panel (**right**), the wound is not as clean as the other two, due to technical issues regarding MCF-7 cells clumping together at the high cellular densities required for a scratch-wound. This effect was even more pronounced when MCF-7 cells were grown in FGM, so this assay was performed with MCF-7 cells grown in DMEM containing 10% FBS. MDA-MB-231 and HCC1937 cells were tested in FGM.

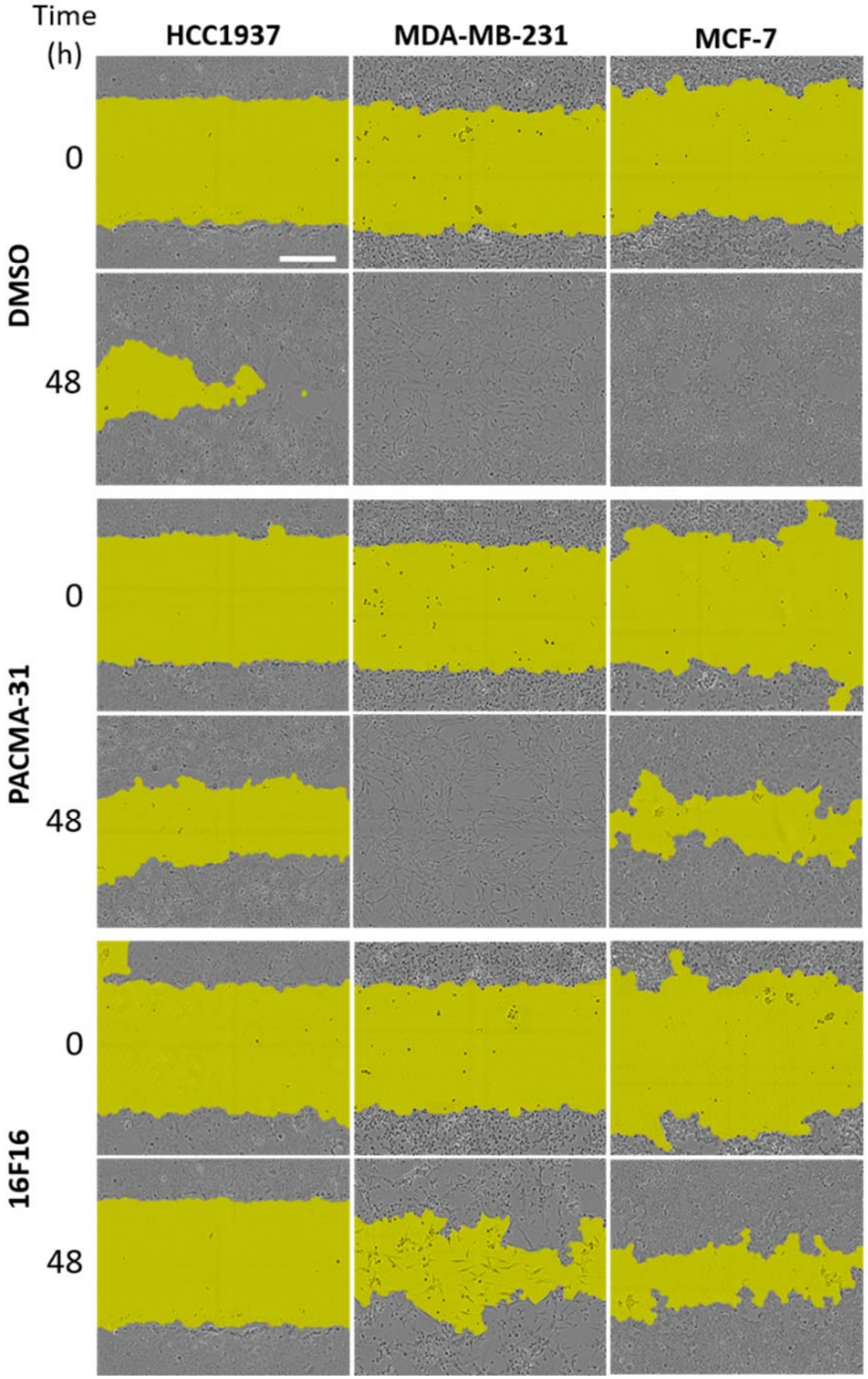

Figure 3.10 ***Incucyte ZOOM ™ 'Scratch-Wound' Mask Phase-Contrast Images Showing the Effect of PDIA3 and PDIA1 Inhibition on 'Wound Closure'.*** *Example images of 'scratch-wound' mask (yellow) automatically formed by Incucyte® system for each cell line from the start and end of each time course. Scale bar: 300µm.*

The quantitative data from these scratch-wound assays are displayed in **Figure 3.11**. The graphs show the mean % Relative Wound Density (RWD) [3] (solid line) ± 1 standard deviation (dotted line) against time. **Figure 3.11D-F** (**left**) show the area under the RWD curve of every assay. The area under the curve represents the magnitude of change over 48h. In this case it provides a metric that accounts for both the speed of closure and the overall change in RWD. This means that area under the curve is a good, all-encompassing metric to compare the ability of cells to close the wound. Also, **Figure 3.11D-F** (**right**) show the rate of initial closure calculated as the gradient of the straight line of best fit over the first 5h in change in % RWD per hour as another metric to describe the capacity of cells to migrate in 2D.

HCC1937 cells displayed a slow rate of wound closure and failed to seal the wound in all conditions (**Figure 3.11A, D**). Treatment with PACMA-31 resulted in a reduced area under the curve and lower initial rate of wound closure when compared to the DMSO condition (**Figure 3.11D**). However, cells treated with 16F16 displayed significantly reduced area under the curve and initial rate of closure compared to either the PACMA-31 or DMSO condition (**Figure 3.11D**).

MDA-MB-231 cells treated with DMSO or PACMA-31 both rapidly sealed the wound to 80% RWD with no obvious difference in area under the curve or initial rate of closure (**Figure 3.11B, E**). However, treatment with 16F16 caused a significant reduction in both area under the curve and initial rate of wound closure when compared to treatment with DMSO or PACMA-31 (**Figure 3.11E**). This was clearly visible on the overall line graph in **Figure 3.11B**.

MCF-7 cells gradually sealed the wound to 80% RWD over 48h under DMSO-treated conditions (**Figure 3.11C**). Treatment with PACMA-31 or 16F16 reduced wound-sealing, with either resulting in a partially sealed wound at 60% RWD (**Figure 3.11C**). Treatment with PACMA-31 or 16F16 also reduced both area under the curve and initial rate of wound closure with no distinction between the two treatments (**Figure 3.11F**).

The MDA-MB-231 cells had the highest initial gradient in the DMSO treated condition compared to the other two cell lines with a mean of approx. 4.8% RWD per hour (**Figure 3.11D-F**). MCF-7 cells had a mean initial gradient of approx. 2.7% RWD per hour and HCC1937 were the slowest cells, at approx. 1.7% RWD per hour (**Figure 3.11D-F**). Unsurprisingly, this pattern was replicated in the area under the curve graphs with means of 2800, 2400 and 1300 for DMSO-treated MDA-MB-231, MCF-7 and HCC1937 cells, respectively (**Figure 3.10D-F**).

[3] RWD is defined as the measurement of spatial cell density within the wound relative to the spatial cell density outside of the wound and is calculated automatically by the IncuCyte®CellPlayer™ software. As a rough guide, 80% to 100% represents a completely **sealed** wound and 0-20% is a completely **unsealed** wound.

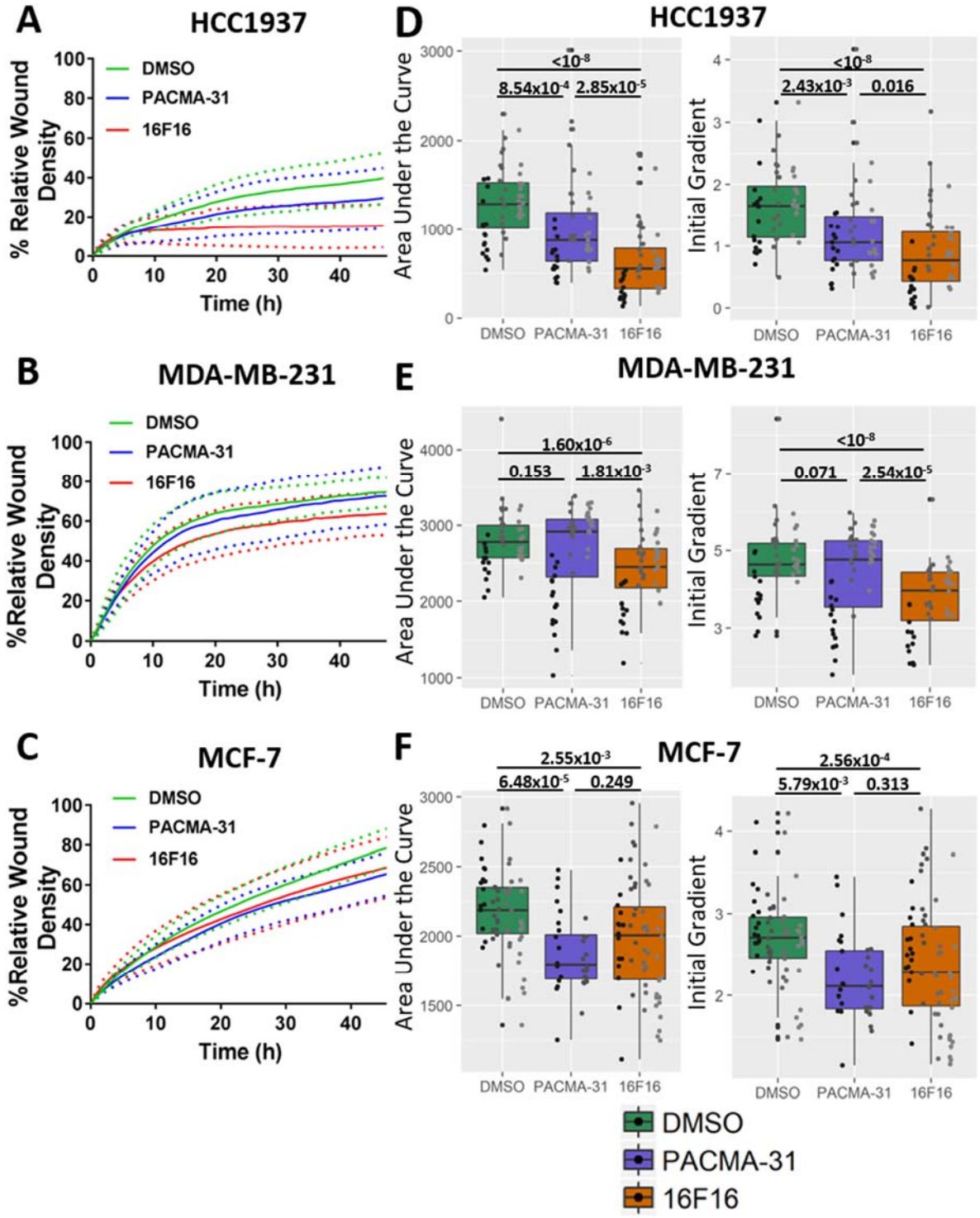

Figure 3.11 ***Graphs Describing the Rates of 'Wound Closure' as a Result of Treatment with PACMA-31.*** *(**A-C**) Change in % RWD with time in the three breast cancer cell lines treated as indicated. Plots show Mean $\pm$ SD. (solid line ± dotted line). For HCC1937 and MDA-MB-231 n=3 experiments in FGM. For MCF-7, DMSO and 16F16, n=4 experiments and PACMA-31 n=2 experiments in DMEM containing 10% FBS. (**D-F**) (**left panels**) Box-plots of 'Area under the Curve' which is a metric representing the magnitude of closure. (**D-F**) (**right panels**) 'Rate of Initial Wound Closure' which is the change in % RWD per hour over the first 5h. Each dot represents the value calculated for each metric from one well from each independent experiment and organised into columns representing each biological repeat. (**D-F**) Data were analysed using two-way ANOVA with Tukey's post hoc analysis in R and plotted using ggplot2.*

3.6 THE EFFECT OF ECM PRODUCED BY PDIA3-INHIBITED BREAST CANCER CELLS ON CELL SPREADING AND ATTACHMENT OF 'NAÏVE' CELLS

3.6.1 Cell Spreading and Attachment

Alteration to the tumour microenvironment, especially in the ECM, play significant roles on the progression of cancer (Pickup et al., 2014). It has been shown that the cancer cells themselves are in part responsible for ECM remodelling associated with cancer progression (Naba et al., 2014). Given that PDIA3 has some ECM substrates (**section 1.4.4**), the next experiments examined whether PDIA3 inhibition would alter the properties of ECM produced by HCC1937 breast cancer cells. These cells were chosen because they gave the clearest response in the previous experiments. ECM activity was measured by testing cell attachment and cell spreading of 'naïve' HCC1937 cells. HCC1937 cells were grown for 48h with 16F16, PACMA-31 or equivalent volume of DMSO in FGM. Then, ECM was isolated and naïve HCC1937 cells were seeded onto the prepared ECM in fresh FGM and allowed to attach for 1h.

Cell adhesion was quantified from cell areas and the number of attached cells. **Figure 3.12A, B** show the quantification of all measured cell areas (**A**) and nuclei per 40x frame (**B**) as dot plots with median value of all data across three biologically independent experiments. The treatment with DMSO or PACMA-31 resulted in near identical distributions of cell area (**Figure 3.12A**), whereas treatment with 16F16 led to a reduction in cell areas compared to ECM from DMSO or PACMA-31 treatment of cells. The median cell area was reduced by around 300μm^2 (**Figure 3.12A**). **Figure 3.12B** shows that treatment with 16F16 or PACMA-31 resulted in a reduced activity of ECM to support cell attachment relative to ECM from DMSO treated cells from an average of 55 nuclei per frame to 45. There was no difference in attachment of cells between 16F16 or PACMA-31 treated ECM (**Figure 3.12B**).

Examples of the fluorescence images used to measure cell attachment and cell area are displayed in **Figure 3.12C**. As these are not high-quality z-stack images as in **Figure 3.7**, **3.8** and **3.9**, the status of the actin cytoskeleton cannot be as accurately commented on. That being said, a qualitative reduction in cell area and attachment was apparent when comparing the DMSO or PACMA-31 condition to the 16F16 treatment (**Figure 3.12C**). Furthermore, there were less cells attached to ECM from 16F16-treated cells that are widely spread (**pink arrows**) and more that have barely spread, appearing as small, circular cells (**white arrows**) (**Figure 3.12C**). These data indicate that ECM properties to support HCC1937 cell adhesion were reduced after inhibition of PDIA1 or PDIA3.

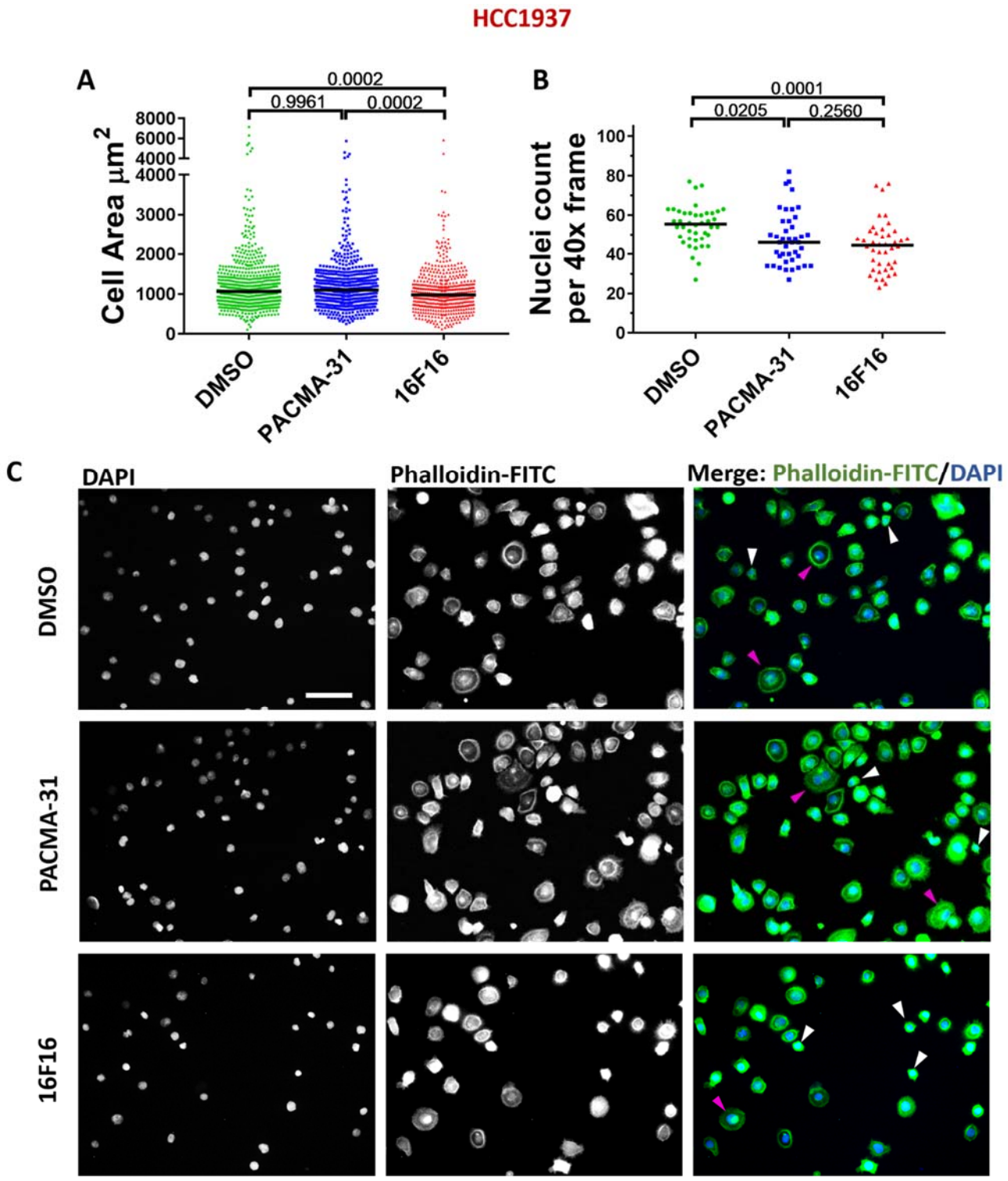

Figure 3.12 ***The Change in Cell Area and Attachment in Response to ECM Produced from PDIA1- or PDIA3-Inhibited HCC1937 cells.*** *(**A**) Dot plot with median value (**black line**) of HCC1937 cell area on ECM coated glass. n=3 experiments. (**B**) Dot plot with median value (**black line**) of HCC1937 attachment onto ECM coated glass. n=3 experiments. (**C**) HCC1937 cell morphologies, 20x objective. F-actin visualised by Phalloidin TRITC (green) and DNA by DAPI (blue) as indicated. Scale bar 100µm. (**white arrows**) Small rounded cells that have barely spread. (**pink arrows**) larger, well attached and highly spread cells.*

3.6.2 Extracellular Matrix

The effect of PDIA3 inhibition on the activity of HCC1937 ECM to support cell attachment could be due to a reduced ability of the cells to secrete ECM. For example, collagen-1 and FN upregulation, fibril formation and organisation are key markers of stiffened, pro-metastatic ECM in breast cancer progression (Kaushik et al., 2016). To investigate this question, the ECM produced by HCC1937 cells after 48h of treatment with PACMA-31, 16F16 or DMSO was isolated with ammonium hydroxide and fixed in 4% PFA (Hellewell et al., 2017). Then, collagen-I or FN were visualised using indirect immunofluorescence to observe any alterations in collagen-I or FN fibril organisation in response to PDIA3 inhibition.

Two representative images of collagen-I or FN per condition are displayed in **Figure 3.13**. All images seemed to have high background signal but, because the secondary antibody only control (**Figure 3.13C**) produced an entirely black image and this experiment was in serum-free media, the 'background' signal could be a thin layer of collagen-I and FN that has been secreted but not organised into fibrils.

The ECM from DMSO- and PACMA-31-treated cells showed very similar patterns of staining for collagen-I (**Figure 3.13A**), in which bright staining for collagen-I around apparent outer edges of cells was observed (**Figure 3.13A white arrows**). The ECM from 16F16-treated cells also had high collagen-I signal at cell outer edges but, in general, this was much less common and less clear in the samples (**Figure 3.13A**). In all cases no clearly bundled and organised collagen-I fibrils were observable.

The FN staining was much weaker than that of collagen. Shown in **Figure 3.13 B,** a 'haze' of FN staining was observed with occasional bright spots across all conditions over each coverslip (**Figure 3.13B**). The DMSO condition did contain rare (2-3 per coverslip) fibril like structures as shown in the bottom left image of **Figure 3.13B**. Also, FN of ECM from PACMA-31-treated cells formed occasional (2-4 per coverslip) structures as displayed in the top row, middle image of **Figure 3.13B**. However, these are not obvious fibrils and could be an artefact of the staining process. The ECM from 16F16-treated cells without exception displayed a haze of FN staining with occasional bright spots without exception (**Figure 3.13 B – right**). There was not time to repeat this experiment.

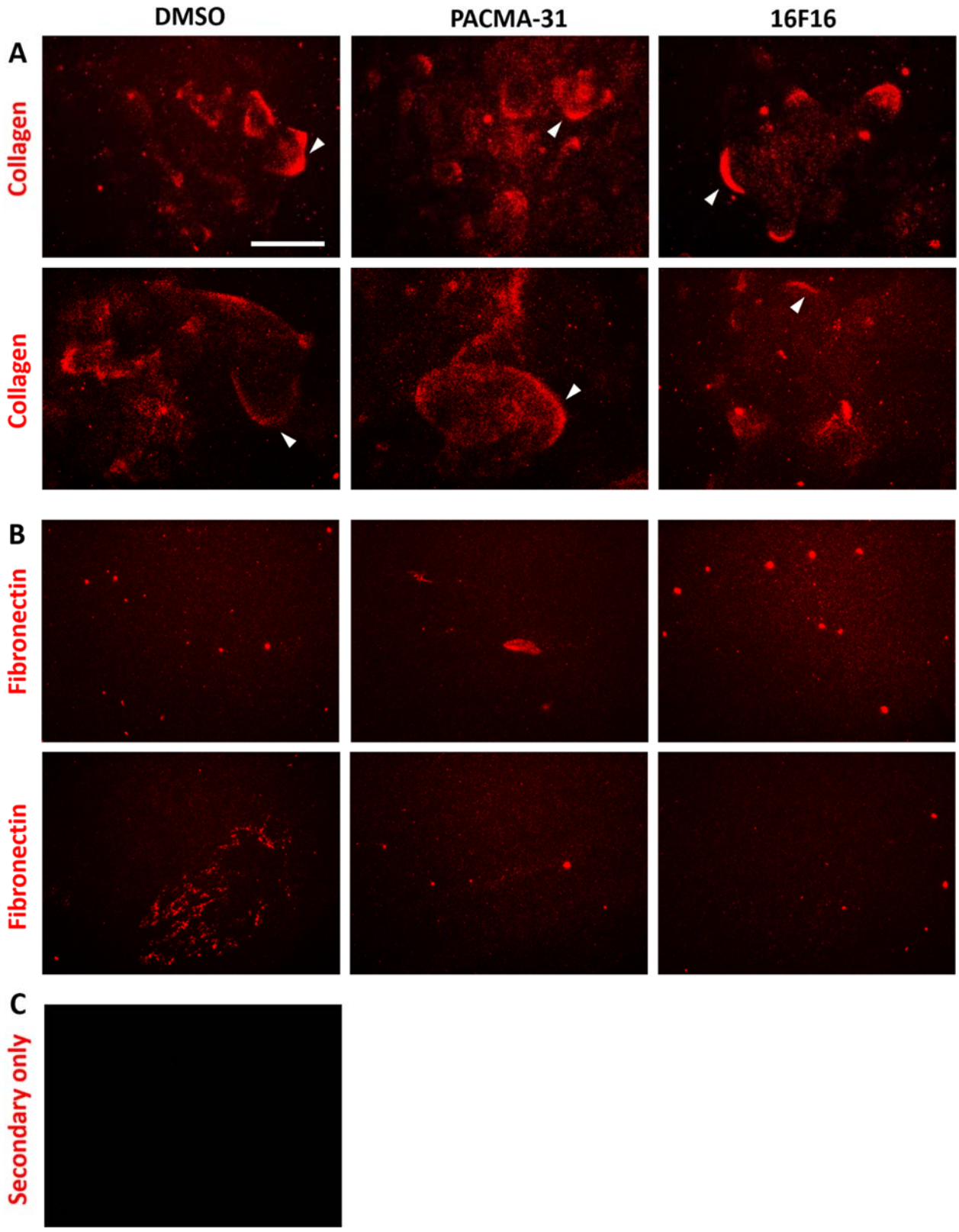

Figure 3.13 ***ECM Isolated from Control or Inhibitor-Treated HCC1937 Cells.*** *Cells were treated with indicated inhibitors at concentrations displayed in* ***Table 3.2*** *for 48h, then ECM isolated. Collagen-1 and fibronectin were detected by indirect immunofluorescence using antibodies as in* ***Table 2.7 and 2.7****. n=1 experiment. Scale bar: 50µm.*

Cells that are more mesenchymal, and migratory, secrete vastly more ECM than epithelial-like cells (Kalluri and Weinberg, 2009). Therefore, the amount of FN protein present in cell lysates and conditioned media (CM) was examined in HCC1937, MDA-MB-231 and MCF-7 cells after 24h treatment with PACMA-31, 16F16 or equivalent volume of DMSO. Protein samples were separated by SDS-PAGE and FN visualised using Western blotting (**Figure 3.14A**). HCC1937 cells produced very low amounts of FN in both cell lysate (top) and CM (bottom) under all conditions (**Figure 3.14A**). MDA-MB-231 cells also had low FN in the lysates and no detectable signal in the CM (**Figure 3.14A**). MCF-7 cells produced the most FN under all conditions (**Figure 3.14A**). FN appeared at the expected molecular weight under reducing conditions intracellularly (≈250kDa) but in CM had a lower than expected molecular weight (≈100kDa) indicating proteolysis after secretion.

Figure 3.14B shows a bar graph of the band quantification of FN (normalised against the α-tubulin loading control) from the lysate blot (**Figure 3.14A**). For HCC1937 and MCF-7 cells there was a reduction in intracellular FN content in the presence of 16F16 relative to DMSO or PACMA-31 (**Figure 3.14B**). Interestingly, both HCC1937 and MCF-7 both showed an apparent upregulation of FN in response to PDIA1 inhibition by PACMA-31 compared to the DMSO or 16F16 condition (**Figure 3.14B**). MDA-MB-231 cells showed similar FN content under all conditions (**Figure 3.14B**). However, these results are from a single experiment.

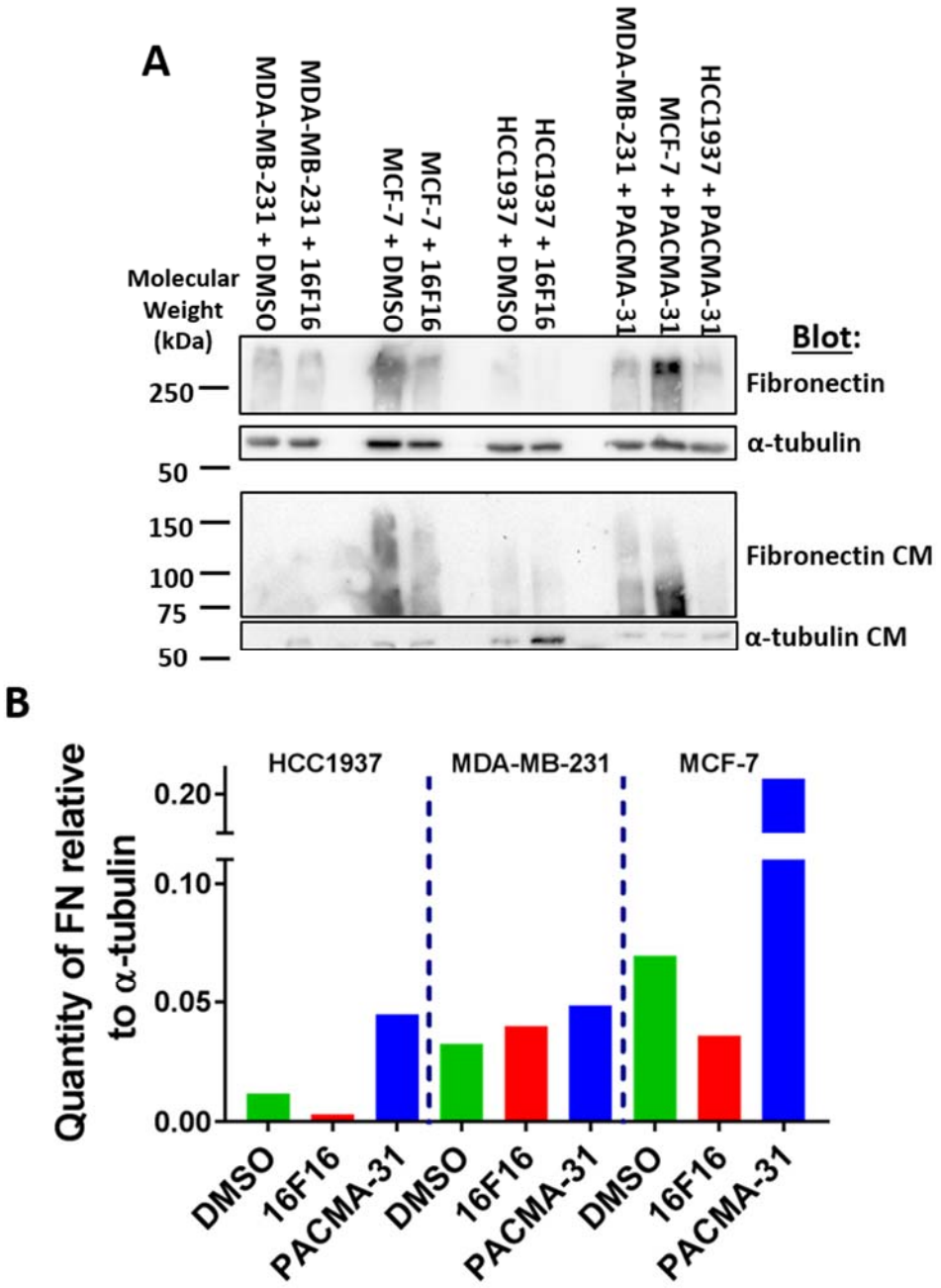

Figure 3.14 ***Western Blot of Cell Lysate and Conditioned Media from Control or Inhibitor-Treated HCC1937 Cells.*** *(**A**) Western Blots of each cell line after 24h of treatment with indicated inhibitors at concentrations detailed in **Table 3.2**. (**Top**) Cell lysates. (**Bottom**) Conditioned media (CM). (**B**) Automated quantification (Syngene GeneTools©) of the FN band intensities from each condition relative to α-tubulin loading control to give normalised amounts of protein in each cell lysate. Plotted in GraphPad Prism.*

3.7 THE EFFECTS OF CONDITIONED MEDIA FROM *PDIA3*$^{-/-}$ AND WT MOUSE EMBRYO FIBROBLASTS ON BREAST CANCER CELL AREA, ATTACHMENT AND MORPHOLOGY

3.7.1 Cell Area and Attachment

An important aspect of the TME is the contribution of the surrounding cancer-associated cells (Gascard and Tlsty, 2016; Soysal et al., 2015). CAFs in particular are of great importance to metastasis through their role as professional ECM-secreting and organising cells (Gascard and Tlsty, 2016). Given the effect of PDIA3 inhibition in breast cancer cells on cell attachment and cell spreading on glass and ECM (**sections 3.4, 3.6 and 3.7**), a logical next step was to examine whether similar results could be achieved using CM from *Pdia3*$^{-/-}$ fibroblasts. This would be indicative of a PDIA3-dependent secretome with a role in fibroblast-tumour cell communications. Professor Michalek previously isolated a stable *Pdia3*$^{-/-}$ mouse embryo fibroblast strain (Coe et al., 2010). These cells were gifted to the Adams laboratory and have been used to study a PDIA3-dependent secretome of mouse embryo fibroblasts (MEF) (**section 1.4.5.3**).

Firstly, PDIA3 was shown to be absent in *Pdia3*$^{-/-}$ MEF using SDS-PAGE and Western blotting (**Figure 3.15A**). Interestingly, there was much higher levels of PDIA1 protein within the *Pdia3*$^{-/-}$ MEF (**Figure 3.15A**). However, this graph is based on data from only one experiment and so the increase in PDIA1 needs validation.

Then, to explore possible PDIA3-dependent communication between fibroblasts and breast cancer cells, the effect of 48h serum-free FGM-based CM from WT and *Pdia3*$^{-/-}$ MEF on breast cancer cell attachment and spreading to glass coverslips was examined. The experimental design focused on initial cell adhesion and so a 2h timepoint was chosen[4]. Breast cancer cells were plated in the CM for 2h before fixation in 4% PFA and staining of F-actin using phalloidin-TRITC or -FITC. Plating into fresh FGM was used as a control.

Figure 3.15B-D show cell area and attachment data for each breast cancer cell line as dot plots of all cell areas and nuclei counts, respectively, pooled from three independent experiments. For HCC1937 cells, there was a reduction in cell area (**Figure 3.15B top**) and attachment (**Figure 3.15B bottom**) in response to CM from *Pdia3*$^{-/-}$ MEF compared to CM from WT MEF. There was no difference in these parameters when comparing incubation in CM from *Pdia3*$^{-/-}$ MEF or fresh FGM (**Figure 3.15B**). For MDA-MB-231 cells, incubation with CM from WT MEF increased in cell area relative to both CM from *Pdia3*$^{-/-}$ MEF and fresh FGM (**Figure 3.15C top**). MDA-MB-231 cells showed reduced cell attachment in response to CM from *Pdia3*$^{-/-}$ or WT MEF when compared to fresh FGM (**Figure 3.15C bottom**). In MCF-7 cells, incubation with

[4] This 2h timepoint was longer than the 1h timepoint of the previous experiment (**3.6**) as cells adhered faster to ECM coated glass and so required less time to analyse initial adhesion.

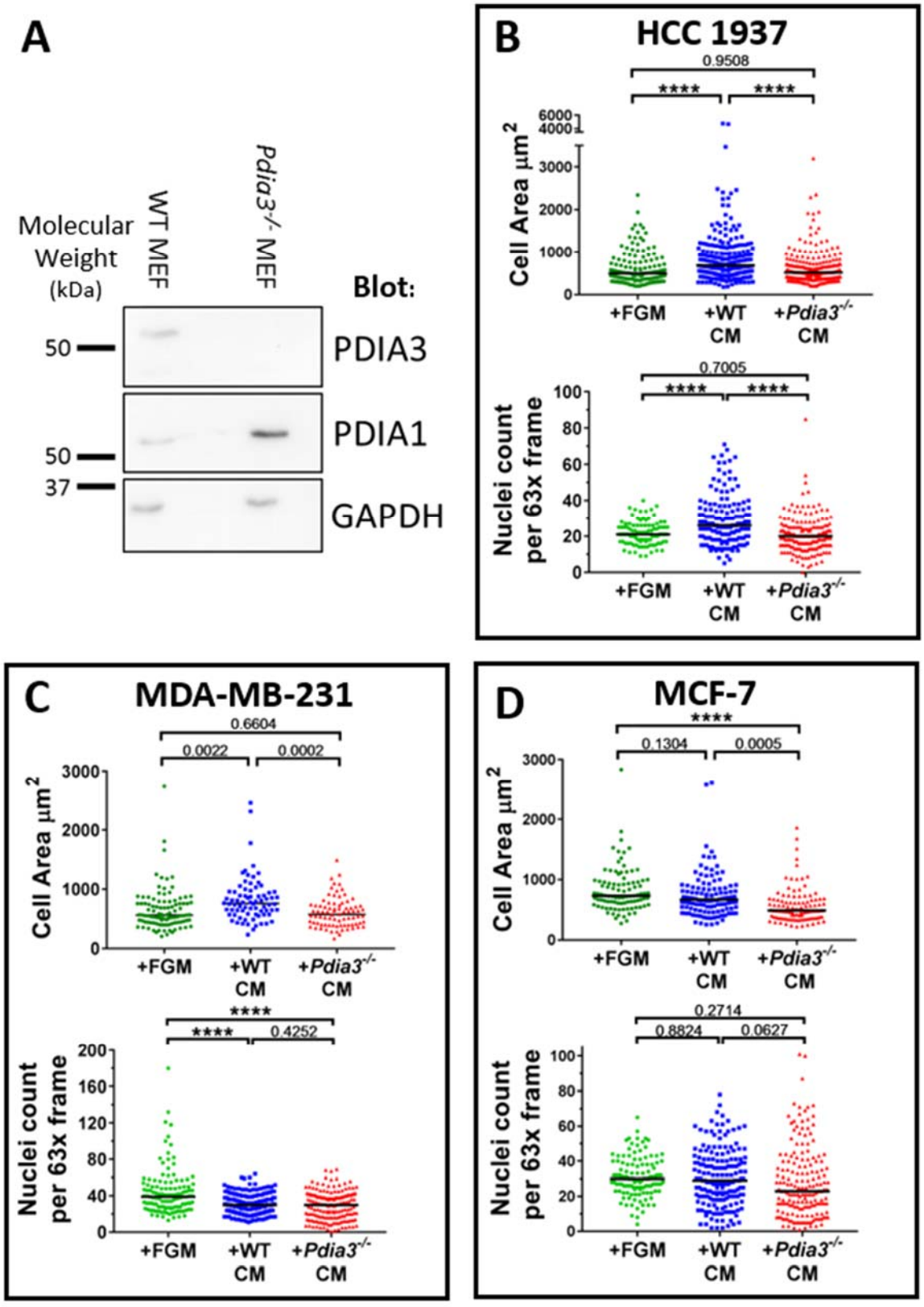

Figure 3.15 ***Quantified Comparison of Breast Cancer Cell Areas After Initial Cell Adhesion in CM from Pdia3$^{-/-}$ or WT MEF.*** *(**A**) Western Blot of WT or Pdia3$^{-/-}$ MEF cell lysates showing absences of PDIA3 in the Pdia3$^{-/-}$ MEF. (**B-D**) Upper graphs show cell area (µm^2) with median (due to non-parametric data) and each lower graph show attached nuclei count with median (due to non-parametric data) counts per 63x frame. n= 3 experiments. All data analysed by two-way ANOVA with Tukey's multiple comparisons carried out between conditions using GraphPad Prism. **** = P < 0.0001.*

CM from *Pdia3*$^{-/-}$ MEF resulted in reduced cell area compared to either CM from WT MEF or fresh FGM (**Figure 3.15D top**). There was no clear difference in cell attachment between the three conditions in MCF-7 cells probably because attachment of MCF-7 cells was more variable than the other two cell lines (**Figure 3.15D bottom**). These results imply that PDIA3 dependent proteins secreted by WT MEF have positive effects on adhesion of HCC1937, MDA-MB-231 and, to a lesser extent, MCF-7 cells.

3.7.2 Morphology and F-actin Organisation

Next, changes in F-actin structures associated with migration such as stress fibres, lamellipodia and filopodia were assessed. **Figures 3.16-3.18** shows F-actin organisation in each cell line after adhesion in fresh FGM or CM from WT or *Pdia3*$^{-/-}$ MEF.

For HCC1937 cells incubated with fresh FGM, a large proportion were small, near circular cells with limited spreading (**Figure 3.16**). In terms of F-actin organisation, HCC1937 cells grown in FGM had concentrated F-actin staining at the cell periphery (**Figure 3.16**). Intracellular F-actin structures were only observable in a minority of cells and peripheral F-actin structures only occasionally resembled classical lamellipodia (**Figure 3.16 insert**). The morphologies of HCC1937 cells incubated with CM from *Pdia3*$^{-/-}$ MEF were very similar to those incubated with fresh FGM, the only difference being that cell periphery F-actin structures, such as lamellipodia and filopodia, were qualitatively more common in HCC1937 cells incubated with CM from *Pdia3*$^{-/-}$ MEF than FGM (**Figure 3.16**). HCC1937 cells incubated in CM from WT MEF showed observably more spread cell morphologies as well as F-actin structures such as stress fibres (**pink arrows**), lamellipodia (**blue arrows**) and filopodia (**green arrows**) (**Figure 3.16 Insert**).

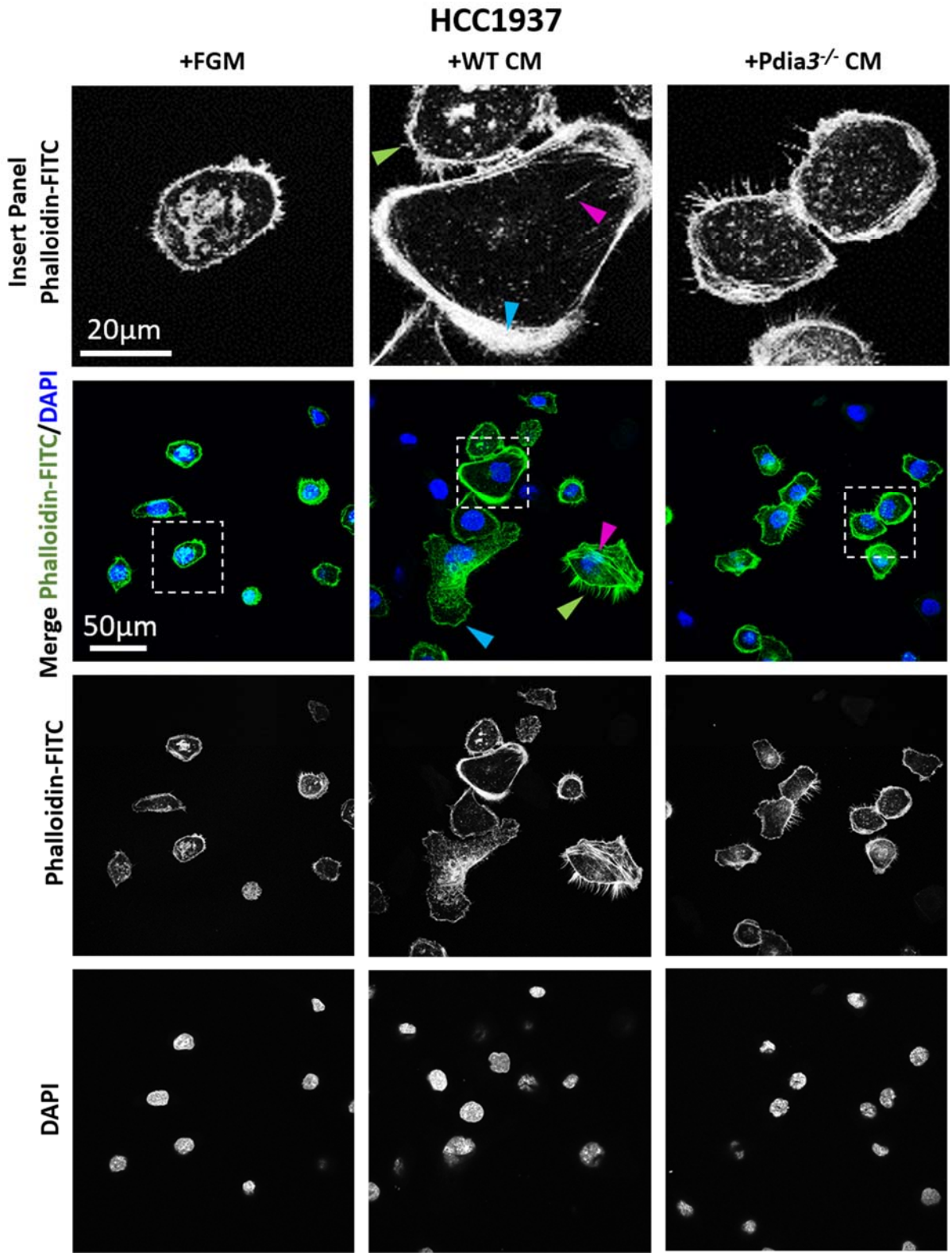

Figure 3.16 ***Fluorescence Images of HCC1937 Cells after Incubation in Different Media.*** *F-actin visualised by Phalloidin-FITC and DNA by DAPI. Boxed areas are shown enlarged on the top row. (**green arrows**) filopodia. (**blue arrows**) lamellipodia. (**pink arrows**) stress fibres.*

MDA-MB-231 cells incubated in fresh FGM attached and spread out to form classical, extended mesenchymal cell shapes (**Figure 3.17**). These cells often contained F-actin stress fibres (**pink arrows**) and filopodia (**green arrows**) (**Figure 3.17 Insert**). These morphologies were similar for cells treated with CM from WT MEF, but cells tended to be more spread and more regularly contained lamellipodia (**blue arrows**) (**Figure 3.17 Insert**). In response to CM from *Pdia3*$^{-/-}$ MEF, MDA-MB-231 cells appear less spread in comparison to the +WT CM condition (**Figure 3.17**) and most MDA-MB-231 cells had less regular cell shapes (**Figure 3.17 Insert**) with less defined lamellipodia and fewer cells with stress fibres (**Figure 3.17**).

MCF-7 cells formed the most irregular cell morphologies of the three cell lines, with random protrusions that did not resemble classical filopodia or lamellipodia under all conditions (**Figure 3.18**). For this reason, the quantified reduction in cell area in response to either CM (**Figure 3.15D**) is not obvious in these single panel images (**Figure 3.18**). Cells incubated in FGM or CM from WT MEF tended to have concentrated F-actin at the periphery and high intracellular F-actin despite only rarely being organised into stress fibres (**Figure 3.18 Insert**). Cells incubated in CM from *Pdia3*$^{-/-}$ MEF tended to spread less and had more circular bodies around the nucleus and long spindle-like protrusions (**Figure 3.18 Insert**).

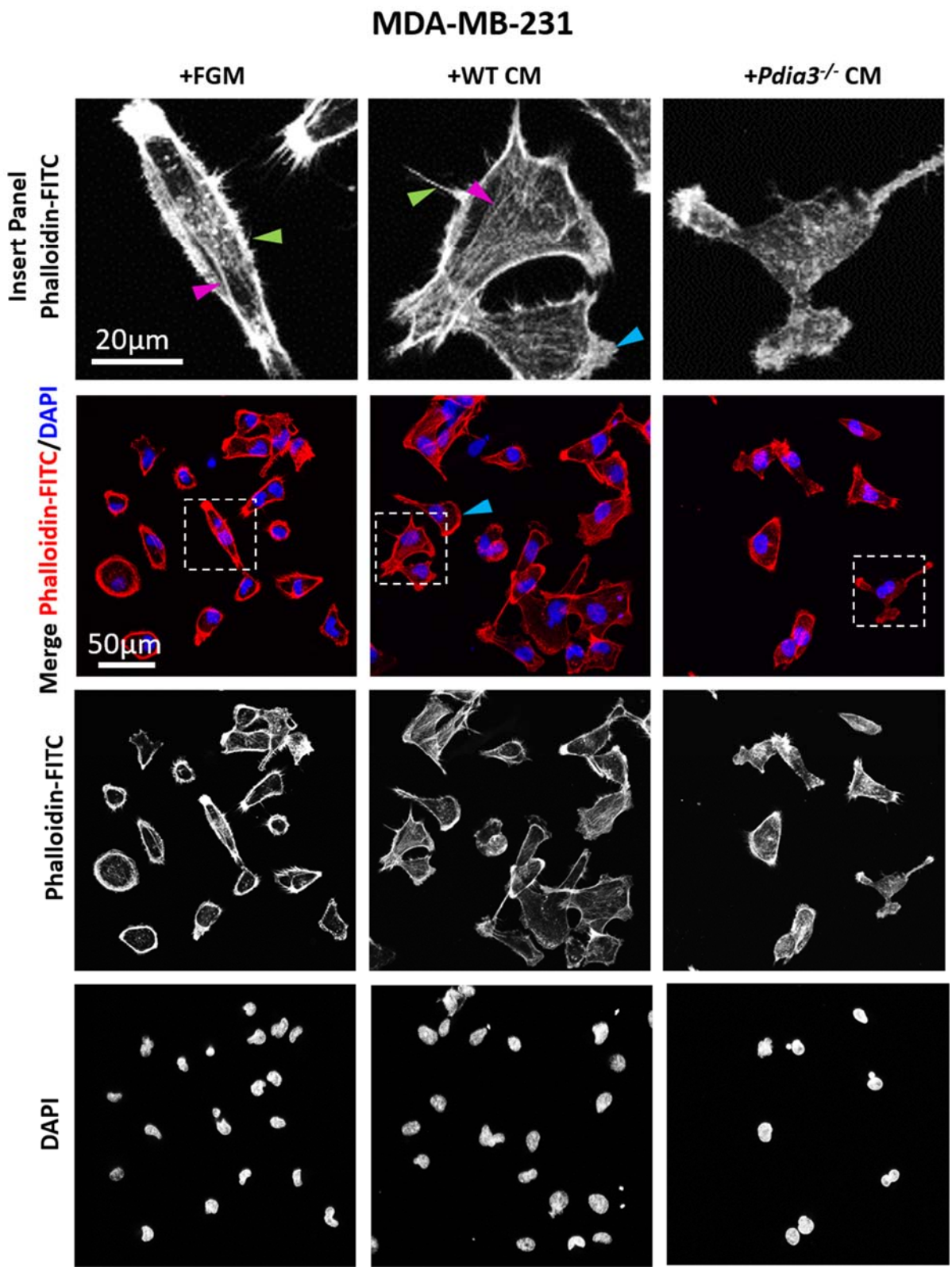

Figure 3.17 ***Fluorescence images of MDA-MB-231 Cells after Incubation in Different Media.*** *F-actin visualised by Phalloidin-TRITC and DNA by DAPI. Boxed areas are shown enlarged on the top row. (**green arrows**) filopodia. (**blue arrows**) lamellipodia. (**pink arrows**) stress fibres.*

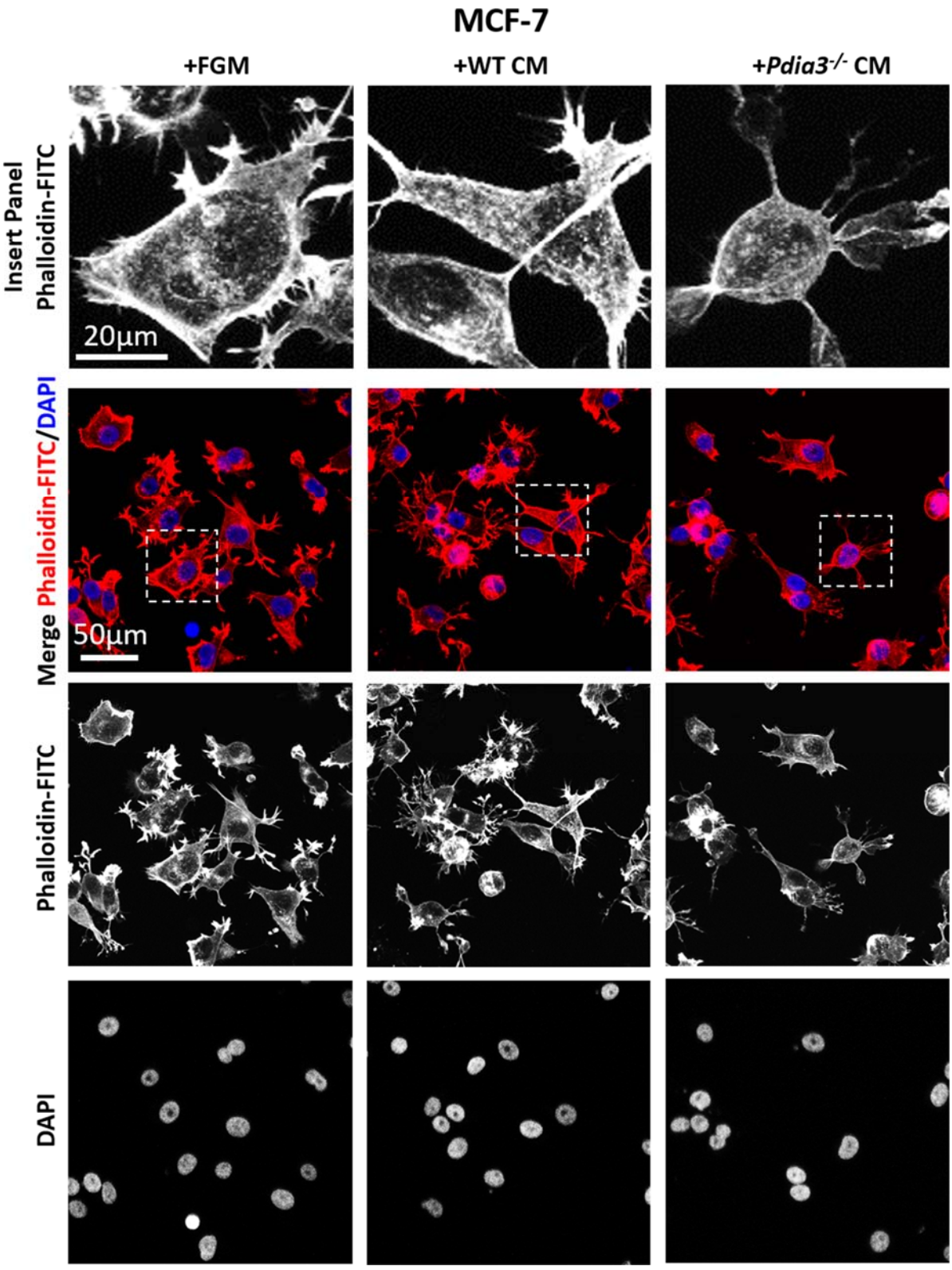

Figure 3.18 ***Fluorescence images of MCF-7 Cells after Incubation in Different Media.*** *F-actin visualised by Phalloidin-TRITC and DNA by DAPI. Boxed areas are shown enlarged on the top row.*

3.8 THE EFFECT OF PDIA3 INHIBITION ON KILLING OF BREAST CANCER CELLS BY 5-FLUOROURACIL OR CYCLOPHOSPHAMIDE

An aspect of cancer progression is the development of resistance to chemotherapeutic agents that are used clinically to kill cancer cells (Housman et al., 2014). Discovering mechanisms by which cancer cells resist chemotherapeutic killing is of paramount importance to cancer therapy. Given that PDIA3 functions as an ER quality control protein as well as a wide array of other interactions (**section 1.4.4**), it is possible that it could be involved in pathways associated with resistance against chemotherapeutic killing. For example, drug inactivation, EMT or cell death inhibition (Housman et al., 2014). Also, secreted proteins controlled by PDIA3 could promote resistance through the TME.

An initial experiment demonstrated that there was substantial killing of each cancer cell line by 16F16, at concentrations in **Table 3.2** in the absence of any chemotherapeutic agent, especially in HCC1937 cells (not shown). This would skew the results of a chemotherapeutic killing assay.

Therefore, the levels of cell killing by the PDIA3 inhibitor was assessed. 16F16 was added to cells at varying concentrations to produce a dose-response curve showing a decrease in % survival with increased concentration of 16F16 after 48h (**Figure3.19 A-C**). From each of these curves the value at which the curve starts drastically sloping (approx. IC_{80}) was chosen to be carried forward into the next experiments as a concentration that, alone, caused minimal killing, so any additional effect when combined with chemotherapeutic agents could be detected (**Table 3.4**). PACMA-31 was not assessed in these experiments as, in all experiments so far, the effect of PACMA-31 was distinct from that of 16F16, so It was considered unlikely that the off-target PDIA1 inhibition by 16F16 would affect the results. Also, the inclusion of another inhibitor would have required more large-scale experiments that were not practical in this project.

		16F16 (µM)
Cancer Cell Lines	**MDA-MB-231**	2.00
	MCF-7	0.70
	HCC1937	0.70

Table 3.4 ***Adjusted Concentrations of 16F16 for use in Assessing Chemotherapeutic Killing of Cancer Cells.***

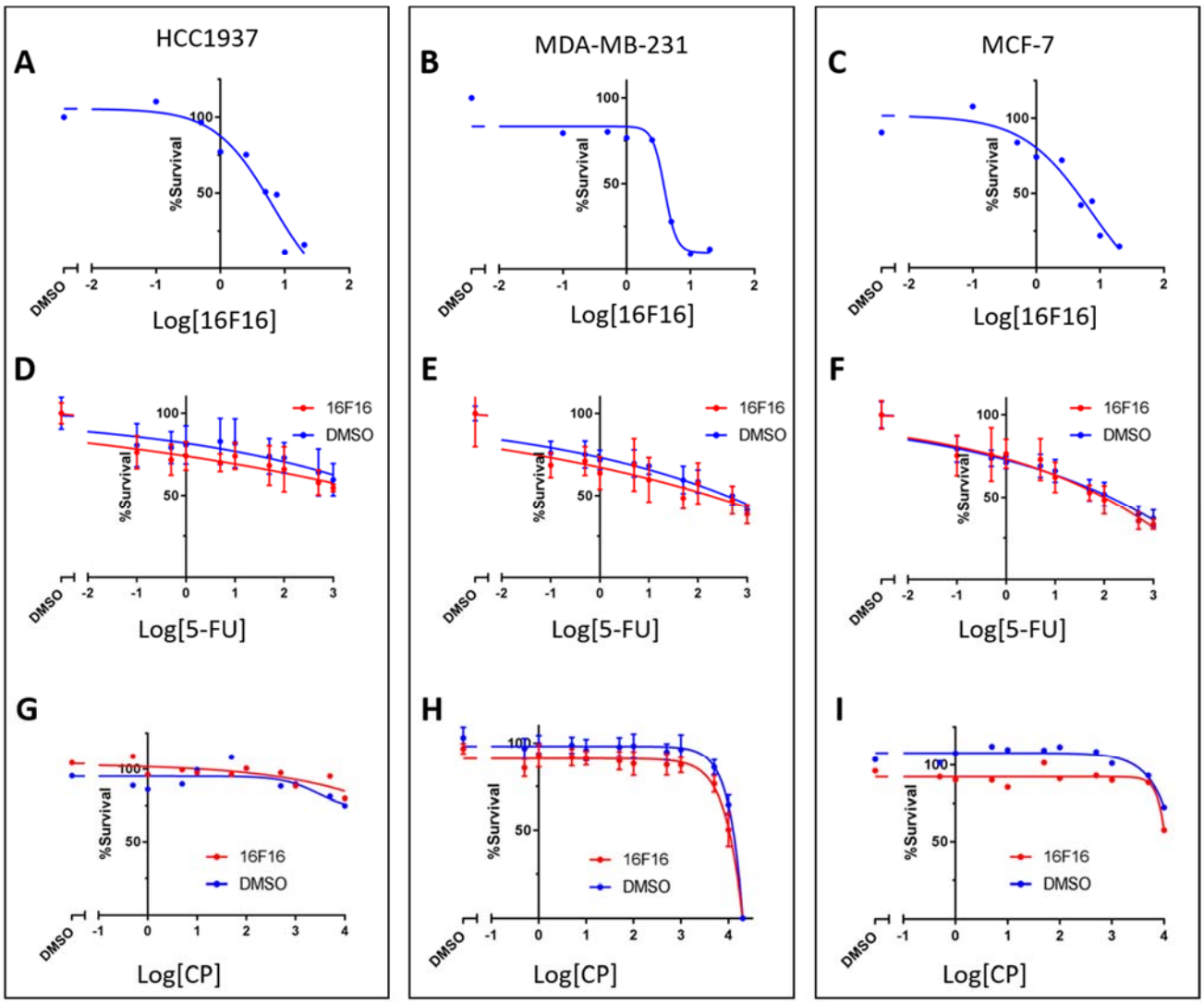

Figure 3.19 ***Killing of Cancer Cells in Response to Chemotherapeutic agents or PDIA3 Inhibition.*** *All graphs are based on Resazurin salt solution (Alamar blue) cell viability assays with % survival plotted on the y axis and log[compound] (μM) on the x axis.* ***(A-C)*** *Dose response curves for killing of cancer cells by 16F16. Each cell line was treated with 16F16 or equivalent volume of DMSO. Mean of n=1 experiment, t=48h.* ***(D-F)*** *Dose response curves for treatment with 5-FU plus 16F16 (**Table 3.4**) or equivalent volume of DMSO. Mean ± SD of n=2 experiments, t=48h.* ***(G-I)*** *Dose response curves for treatment with CP in each cell line treated with 16F16 (**Table 3.4**) or equivalent volume of DMSO. HCC1937* ***(G)*** *and MCF-7* ***(I)*** *mean of n=1 experiment, t=72h. MDA-MB-231* ***(H)*** *mean ± SD of n=3 experiments, t=72h.*

Using the concentrations of 16F16 in **Table 3.4**, the killing of each cell line by 5-FU and CP was then assessed in the presence of 16F16, or equivalent volume of DMSO (**Figure 3.19D-I**).

For all cell lines there was a negative correlation between concentration of 5-FU and % survival with no clear difference between the 16F16 and DMSO conditions (**Figure 3.19D-F**). For HCC1937 and MDA-MB-231 cell lines (**Figure 3.19D+E** respectively), treatment with 16F16 produced marginally reduced survival but, due to overlap of error bars (S.D.), it appears unlikely that this is a true enhancement of 5-FU mediated killing by 16F16. For MCF-7 cells, the 16F16 and DMSO curves are directly superimposed (**Figure 3.19F**).

To assess killing by CP, cells were incubated for 72h and at a higher range of concentrations than used for 5-FU due to no detectable cell death in preliminary, 48h experiments (not shown). **Figure 3.19G** shows that HCC1937 maintained approximately 100% survival at these concentrations of CP and the treatment with 16F16 did not change this. MDA-MB-231 cells appeared to be the most vulnerable to CP and so this experiment was carried out in three independent repeats with inclusion of 20mM CP wells (**Figure 3.19H**). Treatment with 16F16 resulted in a survival curve marginally transposed to the left, which is indicative of enhancing the sensitivity of these cells to killing by CP (**Figure 3.19H**). However, the standard deviations of the 5mM and 10mM CP points of DMSO and 16F16 conditions (which are important as these are the concentrations associated with substantial killing of cancer cells by CP) are virtually overlapping which suggests that this difference is marginal and most likely insignificant (**Figure 3.19H**). For MDA-MB-231 cells, 16F16 consistently reduced cell survival at all concentrations of CP (**Figure 3.19H**). In the case of MCF-7 cells, treatment with 16F16 seemed to have caused an initial reduction in % survival independent of CP but did not result in increased sensitivity of the cells to CP (**Figure 3.19I**). This is shown by both 16F16 and DMSO treatment resulting in horizontal lines that superimpose at the highest concentrations of CP (**Figure 3.19I**).

Overall, 16F16 at concentrations displayed in **Table 3.2** caused more cell death than 5-FU or CP at equivalent concentrations in all three breast cancer cell lines. Then, at lowered 16F16 concentrations (**Table 3.4**), 16F16 did not enhance 5-FU mediated cell killing in these three cell lines nor was CP mediated killing enhanced by 16F16 in HCC1937 or MCF-7 cells. Finally, treatment with 16F16 might have marginally enhanced CP mediated killing in MDA-MB-231 cells.

Chapter 4

Discussion

Knowledge regarding the PDIA3 in breast cancer is still in its infancy. In pilot IHC studies, PDIA3 was detected in breast IDC as has been recorded in previous proteomic studies (Da Costa et al., 2015). However, there are few data regarding the effects of PDIA3 in well-characterised breast cancer cell lines. In this research, the main findings are that inhibition of PDIA3 in three, well-known breast cancer-derived cell lines, HCC1937, MDA-MB-231 and MCF-7, resulted in significant reduction of cellular characteristics associated with migration *in vitro*. These changes were also observed when breast cancer cells were grown in CM from *Pdia3*$^{-/-}$ MEF or on ECM produced by breast cancer cells under PDIA3-inhibited conditions. The experimental findings are summarised in **Table 4.1** and strengths, limitations and implications of the data are discussed below.

4.1 THE EFFECTS OF PDIA3 INHIBITION ON BREAST CANCER CELL LINES

The role of PDIA3 in cancer cells to promote tumour progression is well documented in several cancers (Hettinghouse et al., 2018). However, the effect of pharmacological inhibition of PDIA3 on breast cancer-derived cell lines is less studied. These experiments have defined working concentrations of 16F16 and PACMA-31 in HCC1937, MDA-MB-231 and MCF-7 cells to study PDIA3 inhibition in these cell lines. The basal-like cell lines, especially HCC1937 cells, showed greater sensitivity to PDIA3 inhibition (**Table 4.1**) which might indicate that they are more reliant on PDIA3. The Western blot showing higher PDIA3 protein content than PDIA1 in HCC1937 cells supports this (**Figure 3.4**). This observation could be because basal cells are more mesenchymal and secretory due to their cell of origin being involved in maintenance of the BM (Gudjonsson et al., 2002). However, this blot is from a single experiment and so cannot be conclusive. Moreover, this hypothesis can only be applied to these three cell lines, which are unlikely to be wholly representative of their respective molecular subtypes.

Results described in **3.3-3.6** demonstrated that 16F16 causes a significantly different response to PACMA-31 (summarised in **Table 4.1**). This suggests that inhibition of PDIA1 is not solely responsible for the changes observed, so the effect of treatment with 16F16 can be attributed the inhibition of PDIA3. However, 16F16 also inhibits PDIA1 and PDIA6 and potentially interacts with other thioredoxin superfamily proteins which may have affected the results (Foster and Thorpe, 2017). To verify that the findings are specific to PDIA3, anti-PDIA3 siRNA or CRISPR-mediated *Pdia3* knock-out cells alongside use of new, more specific, pharmacological inhibitors (as they become commercially available) should be used to repeat the experiments (Giamogante et al., 2018).

PDIA3 is upregulated in invasive forms of breast cancer and in cell lines derived from metastatic breast cancer (Santana-Codina et al., 2013; Song et al., 2012). This suggests that subverting the action of PDIA3 could result in reduced tumour progression, for example, reduction in capacity to migrate, proliferate,

HCC1937 Cells (basal)		16F16	PACMA-31	DMSO
+Inhibitor on Glass (with time)	Cellular Attachment	Reduced	≈	=
	Cellular Spreading	Reduced	≈	=
	F-Actin Organisation (L/S/F)	U N U	C U C	C U C
+Inhibitor in Scratch Wound Assay	2D Migration	Reduced	Reduced	=
Naïve cells on ECM produced under inhibited conditions	Cellular Attachment	Reduced	Reduced	=
	Cellular Spreading	Reduced	≈	=
+Inhibitor with Chemotherapeutic	Change in Chemotherapeutic Killing (5-FU/CP)	≈ ≈		= =
		Pdia3$^{-/-}$*CM*	WT CM	FGM
+CM from MEF on Glass	Cellular Attachment	≈	Increased	=
	Cellular Spreading	≈	Increased	=
	F-Actin Organisation (L/S/F)	C U C	C C C	C U U

MDA-MB-231 Cells (basal)		16F16	PACMA-31	DMSO
+Inhibitor on Glass (with time)	Cellular Attachment	Reduced	Reduced	=
	Cellular Spreading	Reduced	Reduced	=
	F-Actin Organisation (L/S/F)	U LC LC	C C C	C C C
+Inhibitor in Scratch Wound Assay	2D Migration	Reduced	≈	=
+Inhibitor with Chemotherapeutic	Change in Chemotherapeutic Killing (5-FU/CP)	? ?		= =
		Pdia3$^{-/-}$*CM*	WT CM	FGM
+CM from MEF on Glass	Cellular Attachment	Reduced	Reduced	=
	Cellular Spreading	≈	Increased	=
	F-Actin Organisation (L/S/F)	U U C	C C C	C C C

MCF-7 Cells (luminal)		16F16	PACMA-31	DMSO
+Inhibitor on Glass (with time)	Cellular Attachment	Reduced	Reduced	=
	Cellular Spreading	Reduced	≈	=
	F-Actin Organisation (L/S/F)	N N U	U U C	U U C
+Inhibitor in Scratch Wound Assay	2D Migration	Reduced	Reduced	=
+Inhibitor with Chemotherapeutic	Change in Chemotherapeutic Killing (5-FU/CP)	≈ ≈		= =
		Pdia3$^{-/-}$*CM*	WT CM	FGM
+CM from MEF on Glass	Cellular Attachment	≈	≈	=
	Cellular Spreading	Reduced	≈	=
	F-Actin Organisation (L/S/F)	U N C	U U C	U U C

Table 4.1 ***Summary of Data from Results.*** *(Reduced/≈/=): each cell line compared to the control condition (**right**). Key: C – Commonly seen, F- filopodia, L- Lamellipodia, LC- less common, N- never seen, U- Uncommon, Black fill – experiment not performed, ? – unclear results, ≈ - very similar, = - identical. Colour code: Reduced/N- **red**, ≈/U- **yellow**, Increased/C- **Green**, LC- **light green**. 'Reduced' (red fill) was significantly reduced compared to 'Reduced' (white fill) and control condition.*

grow and resist apoptosis. The data presented demonstrated that inhibition of PDIA3 caused a substantial reduction in cell area and cell attachment (*in vitro* parameters associated with a migratory phenotype) compared to control or PACMA-31 treatment in all three cell lines (**Table 4.1**). This effect was increased with time of 16F16 treatment. In terms of cellular spreading, both PACMA-31- and DMSO-treated cells increased in cell area over 24h, whereas cells treated with 16F16 barely increased in area. This suggests PDIA3 activity is essential for cellular spreading. The reduction in attachment was less variable at 12h and 24h timepoints, implicating PDIA3 in long-term adhesion as well as initial adhesion in these cell lines.

As the changes in cellular morphology and F-actin cytoskeleton suggested that the migratory capacity of the cell would be decreased, the differences in cell morphology between the three cell lines were also analysed by immunofluorescence for F-actin (Yamaguchi and Condeelis, 2007). HCC1937 cells were slower to spread out than MDA-MB-231 cells, with a deeper z-volume, and were more epithelial-like in morphology. HCC1937 formed extensive filopodia but less lamellipodia and stress fibres (**Table 4.1**). The basal subtype of breast cancer is known to be genetically and phenotypically diverse between patients and this somewhat explains this discrepancy. However, this phenotypic variability could represent the difference between the primary and secondary tumour. MDA-MB-231 were isolated from a pleural effusion and so are metastasised cells, whereas HCC1937 cells were taken from a primary tumour which was known to have metastasised. In this case, cells isolated from the primary tumour appear less migratory than metastasised cells, but comparisons between more cell lines or tumour explants would be needed to establish if this is a general difference.

Fluorescence microscopy of MCF-7 cells for F-actin revealed the formation of long, irregular protrusions that detached during the staining process. This suggests weak adhesion to glass, especially given that MCF-7 cells have a much more chaotic morphology and F-actin structures than the other two cell lines.

In the interest of time, vinculin was not stained for with F-actin. However, vinculin localised at apparent focal adhesions in MDA-MB-231 cells (**Figure 3.3**). Therefore, it would be interesting to stain for vinculin in all these cell lines and observe if F-actin stress fibres, anchored by vinculin, are decreased in response to PDIA3 inhibition, growth on ECM produced by PDIA3-inhibited breast cancer cells, or growth in CM from *Pdia3*$^{-/-}$ MEF. This would be a good parameter correlating with migratory potential because focal adhesions are essential for contractile migration and implicated in tumour progression (Goldmann et al., 2013).

A direct way of testing the migratory capacity of cells is the *in vitro* 'scratch-wound' assay. It has been shown to be predictive of migratory capacity of cells *in vivo*. It is predicted that cells of a highly migratory phenotype (i.e. highly mesenchymal) will seal the wound the fastest (Justus et al., 2014). The data here

show that reduced migratory capacity was associated with PDIA3 inhibition in all three cell lines using *in vitro* 2D collective migration assays (**Table 4.1**). Moreover, both basal lines exhibited reduced rate of closure in response to 16F16 compared to PACMA-31, indicating a clear reliance on PDIA3 for 2D collective migration. MCF-7 cells did not show this difference but there were technical issues with this cell line. Due to reduced cell-substratum attachment compared to the other cell lines, the act of scratching often peeled away too many cells, resulting in uneven scratches. Performing the tests in DMEM containing 10% FBS instead of FGM only partially solved this problem and so data for MCF-7 cells are less reliable than for the other two cell lines. According to their molecular subtype, it was expected that MDA-MB-231 and HCC1937 cells would be most migratory and would rapidly seal the wound. However, the rate of initial closure was by far the slowest in HCC1937 cells (**Figure 3.11**) showing that they are less migratory even than MCF-7 luminal cells. HCC1937 rarely sealed the wound in 48h. This suggests that the molecular subtype, at least for these cell lines, are not reliable predictors of 2D migratory capacity. Although indicative of *in vivo* migratory capacity, it would be unwise to assume the results of scratch assays wholly represent *in vivo* cell behaviour. It is widely accepted that regulation of cells in a 3D context is different to how they behave in 2D culture and so this experiment should be repeated using 3D invasion assays of hydrogels/collagen matrices (Rommerswinkel et al., 2014), transwell inserts (Justus et al., 2014), or *in vivo*.

The cell viability experiments showed substantial cell death in response to 16F16 alone after 48h treatment (especially in HCC1937 cells) (**Figure 3.19**). Therefore, despite only a few cells visibly undergoing apoptosis/necrosis in the adhesion and migration experiments, it is possible that extended PDIA3 inhibition resulted in substantial cell death which may have reduced attachment, cell area, or scratch-wound closure either directly or via cell death substrates. However, this was not assessed formally, so future experiments should investigate cell death in each type of experiment. For example, incubation with resazurin salt solution to compare overall cell viability (**section 2.7.9**).

A substantial cause of mortality from cancer is the acquisition of resistance to chemotherapeutics (Coley, 2008). The experiments demonstrated that inhibition of PDIA3 has no clear effect on sensitising these three breast cancer cell lines to 5-FU or CP (**Figure 3.19**, **Table 4.1**). However, this was a limited study and, given that PDIA3 has been implicated in stress and apoptosis pathways (**section 1.4.4.2**), it seems likely that it could be involved in pathways associated with chemotherapeutic-mediated cytotoxicity. To assess this, knockdown of PDIA3 using siRNA should be used in parallel with combinations of a wider range of chemotherapeutic compounds in a high-throughput assay on these breast cancer lines. As a priority, paclitaxel should be tested because miRNA-148a-mediated reduction of PDIA3 protein content sensitised an ovarian cancer cell line to paclitaxel-mediated killing (Zhao et al., 2015b).

4.2 THE PDIA3-DEPENDENT SECRETOME AND BREAST CANCER CELL-FIBROBLAST COMMUNICATIONS

Much literature has implicated the TME as a key driver of tumour progression, with specific focus on the ECM driving transformation and migratory capacity (Kaushik et al., 2016; Pickup et al., 2014). Also, PDIA3 has been shown to be important in the secretion of ECM and ECM-associated proteins (**section 1.4.4**). Therefore, experiments assessed whether the effects on breast cancer caused by PDIA3 inhibition could relate to secreted, PDIA3-dependent products. ECM produced by HCC1937 cells under 16F16 treatment for 48h was shown to reduce cell area of naïve HCC1937 cells in comparison to DMSO or PACMA-31, and cell attachment relative to DMSO (**Figure 3.12**, **Table 4.1**). This suggests that PDIA3 is important in the production and/or secretion of ECM that is supportive of breast cancer cell attachment and spreading.

Collagen and FN represent two key components of the interstitial ECM that are upregulated and highly cross-linked in breast cancer (Kaushik et al., 2016). In this study, the collagen and FN components of ECM produced by HCC1937 cells under PDIA3-inhibited and control conditions failed to form fibrils after secretion (**Figure 3.12**). For collagen, this could be due to needing longer than 48h to develop fibrils (Rosini et al., 2018). Importantly, the breast cancer cells were shown to produce these ECM components, which implies that these cells are not fully epithelial and have undergone partial EMT (Jacobs et al., 2008). The production of ECM components by these cancer cells and the fact that their ECM is supportive of naïve breast cancer cell attachment and spreading provides further evidence for a role of breast cancer cells in regulation of the pro-tumorigenic ECM. Also, the reduction of this support when ECM was produced under 16F16 treatment implicates the PDIA3-dependent secretome of these cancer cells in the production of cancer-supporting ECM. However, this was only assessed in HCC1937 cells and so needs to be extended to the other cell lines. Ideally, this will then provide a platform to study the secretomes and organisational changes to the ECM both *in vitro* and *in vivo* in response to inhibition or knockdown of PDIA3.

Evidence that HCC1937 cells have undergone EMT, enabling interstitial ECM component production, is the presence of nuclear β-catenin in these cells (**Figure 3.3**). This is indicative of an active WNT signalling pathway that is associated with EMT and de-differentiation (Zhan et al., 2017). These findings are supported by previous reports of active, nuclear β-catenin in HCC1937 cells by various *in vitro* cellular assays and Western blotting (De et al., 2016; Xu et al., 2015). Nuclear β-catenin was also present in the other cell lines, which suggests that they too have active WNT signalling and are likely to be partial-EMT cells capable of fibroblast-like ECM secretion. However, other studies have shown that β-catenin is mainly nuclear in MDA-MB-231 cells but mainly cytoplasmic or membrane bound in MCF-7 cells (Jamieson et al., 2016; Uchino et al., 2010) which is directly opposed to data displayed in **Figure 3.3**. An interesting

extension would be to assess other EMT markers, such as E-cad/N-cad, SNAIL or TWIST, to assess their EMT status in response to PDIA3 inhibition.

These experiments also showed that cell attachment and spreading to coverslips coated in ECM was increased compared to cells plated onto plain glass. In 1 hour, HCC1937 cells attached and spread on ECM to reach cell areas comparable to 24h of attachment on glass. Even cells treated with 16F16 had a larger area on ECM after 1h than after 24h on glass. This implies that, although the ECM deposited was less supportive of adhesion because of PDIA3 inhibition, the presence of any ECM is much more supportive than plain glass. The result may point to a subtler role for PDIA3 in production of ECM that supports cancer cells. It would be interesting to perform comparative proteomic analysis on cell lysates and CM from PDIA3-inhibited versus control cancer cells (as performed on *Pdia3*$^{-/-}$ MEF by Dr. Andrew Hellewell) to assess the profile of PDIA3-dependent proteins. This would test the hypothesis that PDIA3-dependent proteins are similar between human and mouse as well as providing insight into downstream targets of PDIA3 involved in production of ECM that supports human breast cancer cell attachment and spreading.

To complement the results of the ECM-based experiment using the PDIA3 inhibitor, effects on breast cancer cells of CM from (mouse) fibroblasts was examined. MEF were used because a *Pdia3*$^{-/-}$ cell line already existed and mouse and human PDIA3 are 90% similar (UniProtKB, Swiss-Prot reviewed). Fibroblast-cancer cell communication is important to the TME (Luo et al., 2015). Evidence was detailed for PDIA3-dependent communications between fibroblasts and cancer cells which promoted breast cancer cell area, migratory F-actin structures and, potentially, cell attachment (**Figure 3.15**, **Table 4.1**). The CM from WT-MEF was supportive of cancer cell spreading and migratory F-actin structures, but not necessarily attachment. CM from *Pdia3*$^{-/-}$ MEF was less supportive of cellular attachment and spreading, producing results similar to growth in plain FGM. Together, these data implicate the PDIA3-dependent secretome of MEF in supporting breast cancer cell behaviour associated with migration. The results also demonstrate that the supportive effect of secreted products is at least partially due to factors in solution in CM as opposed to an ECM layer. An interesting extension of this experiment would be to plate naïve cancer cells onto ECM produced by *Pdia3*$^{-/-}$-MEF or WT-MEF to see if the effects produced by CM relate to ECM.

To validate these results, a *Pdia3*$^{-/-}$ human mammary fibroblast cell line would be ideal for further fibroblast-cancer cell communication experiments.

MCF-7 cells were the main exception to the above-described results with CM. This difference could have been caused by MCF-7 cells displaying mild morphological differences when grown in FGM compared to DMEM containing 10% FBS, so the effect of CM was obscured by the effect of the FGM. Also, CM was produced over 24h and so there will be waste products from the fibroblasts in the CM that may have

affected each cell line differently. Finally, as the first experiment was performed on MCF-7 cells, there may have been human error that affected the results.

4.3 CONTRIBUTION TO KNOWLEDGE

The novel research findings of this study are:

1. Pharmacological inhibition of PDIA3 in these breast cancer cells reduces *in vitro* characteristics associated with migration, including morphology and 2D migration.
2. Conditioned media from *Pdia3*$^{-/-}$ MEF also reduces the migratory phenotype of these breast cancer cells.
3. Inhibition of PDIA3 reduces the cancer-supportive nature of ECM secreted by HCC1937 cells.
4. 16F16 has distinct effects from PACMA-31 on these cell lines.

Together, these results suggest a role of PDIA3 in promoting the pro-migratory phenotype of breast cancer *in vitro* and are summarised in **Figure 4.1**.

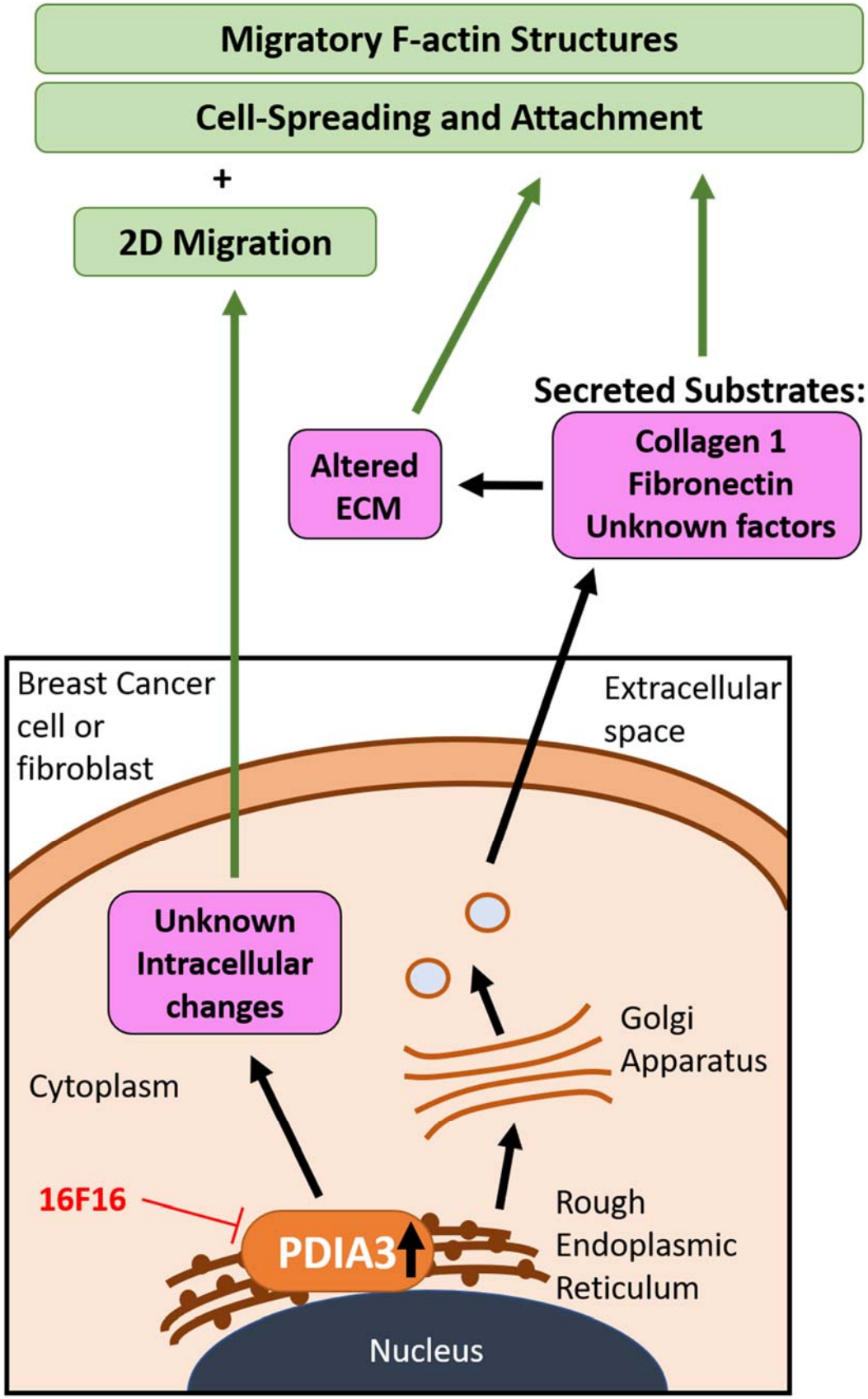

Figure 4.1 ***Summary Figure****. Figure summarising the predicted effects of PDIA3 based upon the in vitro effects of PDIA3 inhibition or loss-of-function on breast cancer cell phenotypes.*

BIBLIOGRAPHY

Abdullah, L.N., and E.K.-H. Chow. 2013. Mechanisms of chemoresistance in cancer stem cells. *Clinical and Translational Medicine*. 2:3-3.

Akrap, N., D. Andersson, E. Bom, P. Gregersson, A. Ståhlberg, and G. Landberg. 2016. Identification of Distinct Breast Cancer Stem Cell Populations Based on Single-Cell Analyses of Functionally Enriched Stem and Progenitor Pools. *Stem Cell Reports*. 6:121-136.

Al-Hajj, M., M.S. Wicha, A. Benito-Hernandez, S.J. Morrison, and M.F. Clarke. 2003. Prospective identification of tumorigenic breast cancer cells. *Proceedings of the National Academy of Sciences of the United States of America*. 100:3983-3988.

Albrechtsen, R., M. Nielsen, U. Wewer, E. Engvall, and E. Ruoslahti. 1981. Basement Membrane Changes in Breast Cancer Detected by Immunohistochemical Staining for Laminin. *Cancer Research*. 41:5076.

Arendt, L.M., J.A. Rudnick, P.J. Keller, and C. Kuperwasser. 2010. Stroma in Breast Development and Disease. *Seminars in cell & developmental biology*. 21:11-18.

Atherton, P., B. Stutchbury, D. Jethwa, and C. Ballestrem. 2016. Mechanosensitive components of integrin adhesions: Role of vinculin. *Experimental Cell Research*. 343:21-27.

Aure, M.R., V. Vitelli, S. Jernström, S. Kumar, M. Krohn, E.U. Due, T.H. Haukaas, S.-K. Leivonen, H.K.M. Vollan, T. Lüders, E. Rødland, C.J. Vaske, W. Zhao, E.K. Møller, S. Nord, G.F. Giskeødegård, T.F. Bathen, C. Caldas, T. Tramm, J. Alsner, J. Overgaard, J. Geisler, I.R.K. Bukholm, B. Naume, E. Schlichting, T. Sauer, G.B. Mills, R. Kåresen, G.M. Mælandsmo, O.C. Lingjærde, A. Frigessi, V.N. Kristensen, A.-L. Børresen-Dale, K.K. Sahlberg, E. Borgen, O. Engebråten, Ø. Fodstad, B. Fritzman, Ø. Garred, G.A. Geitvik, S. Hofvind, H.G. Russnes, H.K. Skjerven, T. Sørlie, and Osbreac. 2017. Integrative clustering reveals a novel split in the luminal A subtype of breast cancer with impact on outcome. *Breast Cancer Research*. 19:44.

Avalle, L., A. Camporeale, A. Camperi, and V. Poli. 2017. STAT3 in cancer: A double edged sword. *Cytokine*. 98:42-50.

Batlle, E., and H. Clevers. 2017. Cancer stem cells revisited. *Nature Medicine*. 23:1124.

Bertucci, F., P. Finetti, and D. Birnbaum. 2012. Basal Breast Cancer: A Complex and Deadly Molecular Subtype. *Current Molecular Medicine*. 12:96-110.

Bertucci, F., P. Finetti, J. Rougemont, E. Charafe-Jauffret, N. Cervera, C. Tarpin, C. Nguyen, L. Xerri, R. Houlgatte, J. Jacquemier, P. Viens, and D. Birnbaum. 2005. Gene Expression Profiling Identifies Molecular Subtypes of Inflammatory Breast Cancer. *Cancer Research*. 65:2170.

Bianco, P., F.D. Cancedda, M. Riminucci, and R. Cancedda. 1998. Bone formation via cartilage models: the "borderline" chondrocyte. *Matrix Biol*. 17:185-192.

Bielenberg, D.R., and B.R. Zetter. 2015. The Contribution of Angiogenesis to the Process of Metastasis. *Cancer J*. 21:267-273.

Bochaton-Piallat, M.L., G. Gabbiani, and B. Hinz. 2016. The myofibroblast in wound healing and fibrosis: answered and unanswered questions. *F1000Res*. 5.

Bochet, L., C. Lehuédé, S. Dauvillier, Y.Y. Wang, B. Dirat, V. Laurent, C. Dray, R. Guiet, I. Maridonneau-Parini, S. Le Gonidec, B. Couderc, G. Escourrou, P. Valet, and C. Muller. 2013. Adipocyte-derived fibroblasts promote tumor progression and contribute to the desmoplastic reaction in breast cancer. *Cancer Res*. 73:5657-5668.

Bodenstine, T.M., B.H. Beck, X. Cao, L.M. Cook, A. Ismail, S.J. Powers, J.K. Powers, A.M. Mastro, and D.R. Welch. 2011. Pre-osteoblastic MC3T3-E1 cells promote breast cancer growth in bone in a murine xenograft model. *Chin J Cancer*. 30:189-196.

Bombonati, A., and D.C. Sgroi. 2011. The Molecular Pathology of Breast Cancer Progression. *The Journal of pathology*. 223:307-317.

Bonde, A.K., V. Tischler, S. Kumar, A. Soltermann, and R.A. Schwendener. 2012. Intratumoral macrophages contribute to epithelial-mesenchymal transition in solid tumors. *BMC Cancer*. 12:35.

Bong, A.H.L., and G.R. Monteith. 2017. Breast cancer cells: Focus on the consequences of epithelial-to-mesenchymal transition. *Int J Biochem Cell Biol*. 87:23-26.

Boyan, B.D., J. Chen, and Z. Schwartz. 2012. Mechanism of Pdia3-dependent 1α,25-dihydroxy vitamin D3 signaling in musculoskeletal cells. *Steroids*. 77:892-896.

Broders-Bondon, F., T.H. Nguyen Ho-Bouldoires, M.-E. Fernandez-Sanchez, and E. Farge. 2018. Mechanotransduction in tumor progression: The dark side of the force. *The Journal of Cell Biology*.

Brooks, M.D., M.L. Burness, and M.S. Wicha. 2015. Therapeutic Implications of Cellular Heterogeneity and Plasticity in Breast Cancer. *Cell stem cell*. 17:260-271.

Buchsbaum, R.J., and S.Y. Oh. 2016. Breast Cancer-Associated Fibroblasts: Where We Are and Where We Need to Go. *Cancers (Basel)*. 8.

Burnier, J.V., N. Wang, R.P. Michel, M. Hassanain, S. Li, Y. Lu, P. Metrakos, E. Antecka, M.N. Burnier, A. Ponton, S. Gallinger, and P. Brodt. 2011. Type IV collagen-initiated signals provide survival and growth cues required for liver metastasis. *Oncogene*. 30:3766-3783.

Burniston, J.G., J. Kenyani, D. Gray, E. Guadagnin, I.H. Jarman, J.N. Cobley, D.J. Cuthbertson, Y.W. Chen, J.M. Wastling, P.J. Lisboa, L.G. Koch, and S.L. Britton. 2014. Conditional independence mapping of DIGE data reveals PDIA3 protein species as key nodes associated with muscle aerobic capacity. *J Proteomics*. 106:230-245.

Cailleau, R., R. Young, M. Olivé, and J.W.J. Reeves. 1974. Breast Tumor Cell Lines From Pleural Effusions2. *JNCI: Journal of the National Cancer Institute*. 53:661-674.

Caja, L., F. Dituri, S. Mancarella, D. Caballero-Diaz, A. Moustakas, G. Giannelli, and I. Fabregat. 2018. TGF-β and the Tissue Microenvironment: Relevance in Fibrosis and Cancer. *Int J Mol Sci*. 19.

CancerResearchUK. Breast Cancer statistics UK. 02-11-2017. http://www.cancerresearchuk.org/health-professional/cancer-statistics/statistics-by-cancer-type/breast-cancer?_ga=2.137919856.1973067158.1509623444-1555830032.1508337461&_gac=1.204279460.1509629691.EAIaIQobChMIkOjZ6ICg1wIVFxIbCh0JLQTBEAAYASAAEgIPMPD_BwE#heading-Three

CancerResearchUK. Comparison between different cancer's incidence. 02-11-2017. http://www.cancerresearchuk.org/health-professional/cancer-statistics/incidence/common-cancers-compared#heading-Zero.

CancerResearchUK. Types of Cancer. 06-09-2018. https://www.cancerresearchuk.org/what-is-cancer/how-cancer-starts/types-of-cancer

CancerResearchUK. 2018. Breast Cancer Treatment. 19-18-2018. https://www.cancerresearchuk.org/about-cancer/breast-cancer/treatment

Celli, C.M., and A.K. Jaiswal. 2003. Role of GRP58 in mitomycin C-induced DNA cross-linking. *Cancer Res*. 63:6016-6025.

Chaffer, C.L., B.P. San Juan, E. Lim, and R.A. Weinberg. 2016. EMT, cell plasticity and metastasis. *Cancer Metastasis Rev*. 35:645-654.

Chaffer, C.L., and R.A. Weinberg. 2011. A Perspective on Cancer Cell Metastasis. *Science*. 331:1559-1564.

Chakrabarti, A., A.W. Chen, and J.D. Varner. 2011. A review of the mammalian unfolded protein response. *Biotechnol Bioeng*. 108:2777-2793.

Chen, J., M. Doroudi, J. Cheung, A.L. Grozier, Z. Schwartz, and B.D. Boyan. 2013. Plasma membrane Pdia3 and VDR interact to elicit rapid responses to 1α,25(OH)(2)D(3). *Cell Signal*. 25:2362-2373.

Choe, M.H., J.W. Min, H.B. Jeon, D.-H. Cho, J.S. Oh, H.G. Lee, S.-G. Hwang, S. An, Y.-H. Han, and J.-S. Kim. 2015. ERp57 modulates STAT3 activity in radioresistant laryngeal cancer cells and serves as a prognostic marker for laryngeal cancer. *Oncotarget*. 6:2654-2666.

Chung, A.S., and N. Ferrara. 2011. Developmental and Pathological Angiogenesis. *Annual Review of Cell and Developmental Biology*. 27:563-584.

Cocchiola, R., D. Romaniello, C. Grillo, F. Altieri, M. Liberti, F.M. Magliocca, S. Chichiarelli, I. Marrocco, G. Borgoni, G. Perugia, and M. Eufemi. 2017. Analysis of STAT3 post-translational modifications (PTMs) in human prostate cancer with different Gleason Score. *Oncotarget*. 8:42560-42570.

Coe, H., J. Jung, J. Groenendyk, D. Prins, and M. Michalak. 2010. ERp57 Modulates STAT3 Signaling from the Lumen of the Endoplasmic Reticulum. *The Journal of Biological Chemistry*. 285:6725-6738.

Coffelt, S.B., M.D. Wellenstein, and K.E. de Visser. 2016. Neutrophils in cancer: neutral no more. *Nature Reviews Cancer*. 16:431.

Coley, H.M. 2008. Mechanisms and strategies to overcome chemotherapy resistance in metastatic breast cancer. *Cancer Treatment Reviews*. 34:378-390.

Coller, H.A. 2014. Is Cancer a Metabolic Disease? *The American Journal of Pathology*. 184:4-17.

Coppari, S., F. Altieri, A. Ferraro, S. Chichiarelli, M. Eufemi, and C. Turano. 2002. Nuclear localization and DNA interaction of protein disulfide isomerase ERp57 in mammalian cells. *Journal of Cellular Biochemistry*. 85:325-333.

Cox, T.R., and J.T. Erler. 2011. Remodeling and homeostasis of the extracellular matrix: implications for fibrotic diseases and cancer. *Dis Model Mech*. 4:165-178.

Crabtree, J.S., and L. Miele. 2018. Breast Cancer Stem Cells. *Biomedicines*. 6:77.

Cunningham, T.J., and G. Duester. 2015. Mechanisms of retinoic acid signalling and its roles in organ and limb development. *Nat Rev Mol Cell Biol*. 16:110-123.

Czerwinska, P., and B. Kaminska. 2015. Regulation of breast cancer stem cell features. *Contemp Oncol (Pozn)*. 19:A7-A15.

Da Costa, G.G., T.H. Gomig, R. Kaviski, K. Santos Sousa, C. Kukolj, R.S. De Lima, C. De Andrade Urban, I.J. Cavalli, and E.M. Ribeiro. 2015. Comparative Proteomics of Tumor and Paired Normal Breast Tissue Highlights Potential Biomarkers in Breast Cancer. *Cancer Genomics Proteomics*. 12:251-261.

Dai, X., T. Li, Z. Bai, Y. Yang, X. Liu, J. Zhan, and B. Shi. 2015. Breast cancer intrinsic subtype classification, clinical use and future trends. *Am J Cancer Res*. 5:2929-2943.

Davies, A.E., and J.G. Albeck. 2018. Microenvironmental Signals and Biochemical Information Processing: Cooperative Determinants of Intratumoral Plasticity and Heterogeneity. *Front Cell Dev Biol*. 6:44.

De, P., J.H. Carlson, H. Wu, A. Marcus, B. Leyland-Jones, and N. Dey. 2016. Wnt-beta-catenin pathway signals metastasis-associated tumor cell phenotypes in triple negative breast cancers. *Oncotarget*. 7:43124-43149.

Dihazi, H., G.H. Dihazi, A. Bibi, M. Eltoweissy, C.A. Mueller, A.R. Asif, D. Rubel, R. Vasko, and G.A. Mueller. 2013. Secretion of ERP57 is important for extracellular matrix accumulation and progression of renal fibrosis, and is an early sign of disease onset. *J Cell Sci*. 126:3649-3663.

Dirat, B., L. Bochet, M. Dabek, D. Daviaud, S. Dauvillier, B. Majed, Y.Y. Wang, A. Meulle, B. Salles, S. Le Gonidec, I. Garrido, G. Escourrou, P. Valet, and C. Muller. 2011. Cancer-associated adipocytes exhibit an activated phenotype and contribute to breast cancer invasion. *Cancer Res*. 71:2455-2465.

Dong, G., P.A. Wearsch, D.R. Peaper, P. Cresswell, and K.M. Reinisch. 2009. Insights into MHC class I peptide loading from the structure of the tapasin-ERp57 thiol oxidoreductase heterodimer. *Immunity*. 30:21-32.

Doroudi, M., Z. Schwartz, and B.D. Boyan. 2012. Phospholipase A2 activating protein is required for 1α,25-dihydroxyvitamin D3 dependent rapid activation of protein kinase C via Pdia3. *The Journal of Steroid Biochemistry and Molecular Biology*. 132:48-56.

Draoui, N., P. de Zeeuw, and P. Carmeliet. 2017. Angiogenesis revisited from a metabolic perspective: role and therapeutic implications of endothelial cell metabolism. *Open Biol*. 7(12), 170219.

Drebin, J.A., V.C. Link, D.F. Stern, R.A. Weinberg, and M.I. Greene. 1985. Down-modulation of an oncogene protein product and reversion of the transformed phenotype by monoclonal antibodies. *Cell*. 41:697-706.

Duong, M.N., A. Geneste, F. Fallone, X. Li, C. Dumontet, and C. Muller. 2017. The fat and the bad: Mature adipocytes, key actors in tumor progression and resistance. *Oncotarget*. 8:57622-57641.

Dvorak, H.F. 2015. Tumors: Wounds that do not heal--Redux. *Cancer immunology research*. 3:1-11.

Ehrbar, M., A. Sala, P. Lienemann, A. Ranga, K. Mosiewicz, A. Bittermann, S.C. Rizzi, F.E. Weber, and M.P. Lutolf. 2011. Elucidating the Role of Matrix Stiffness in 3D Cell Migration and Remodeling. *Biophysical Journal*. 100:284-293.

Emery, L.A., A. Tripathi, C. King, M. Kavanah, J. Mendez, M.D. Stone, A. de las Morenas, P. Sebastiani, and C.L. Rosenberg. 2009. Early dysregulation of cell adhesion and extracellular matrix pathways in breast cancer progression. *Am J Pathol*. 175:1292-1302.

Engler, A.J., S. Sen, H.L. Sweeney, and D.E. Discher. 2006. Matrix Elasticity Directs Stem Cell Lineage Specification. *Cell*. 126:677-689.

Erdogan, B., M. Ao, L.M. White, A.L. Means, B.M. Brewer, L. Yang, M.K. Washington, C. Shi, O.E. Franco, A.M. Weaver, S.W. Hayward, D. Li, and D.J. Webb. 2017. Cancer-associated fibroblasts promote directional cancer cell migration by aligning fibronectin. *The Journal of Cell Biology*. 216(11):3799-3816

Erler, J.T., K.L. Bennewith, T.R. Cox, G. Lang, D. Bird, A. Koong, Q.T. Le, and A.J. Giaccia. 2009. Hypoxia-induced lysyl oxidase is a critical mediator of bone marrow cell recruitment to form the premetastatic niche. *Cancer Cell*. 15:35-44.

Erler, J.T., and V.M. Weaver. 2009. Three-dimensional context regulation of metastasis. *Clin Exp Metastasis*. 26:35-49.

Eufemi, M., S. Coppari, F. Altieri, C. Grillo, A. Ferraro, and C. Turano. 2004. ERp57 is present in STAT3-DNA complexes. *Biochem Biophys Res Commun*. 323:1306-1312.

Fan, W., J. Chang, and P. Fu. 2015. Endocrine therapy resistance in breast cancer: current status, possible mechanisms and overcoming strategies. *Future Med Chem*. 7:1511-1519.

Fang, M., J. Yuan, C. Peng, and Y. Li. 2014. Collagen as a double-edged sword in tumor progression. *Tumour Biol*. 35:2871-2882.

Foster, C.K., and C. Thorpe. 2017. Challenges in the evaluation of thiol-reactive inhibitors of human protein disulfide Isomerase. *Free Radic Biol Med*. 108:741-749.

Frantz, C., K.M. Stewart, and V.M. Weaver. 2010. The extracellular matrix at a glance. *J Cell Sci*. 123:4195-4200.

Friedl, P., and S. Alexander. 2011. Cancer Invasion and the Microenvironment: Plasticity and Reciprocity. *Cell*. 147:992-1009.

Fu, N., G.J. Lindeman, and J.E. Visvader. 2014. Chapter Five - The Mammary Stem Cell Hierarchy. *In* Current Topics in Developmental Biology. Vol. 107. M. Rendl, editor. Academic Press. 133-160.

Furqan, M., A. Akinleye, N. Mukhi, V. Mittal, Y. Chen, and D. Liu. 2013. STAT inhibitors for cancer therapy. *Journal of Hematology & Oncology*. 6:90.

Gabrilovich, D.I., and S. Nagaraj. 2009. Myeloid-derived suppressor cells as regulators of the immune system. *Nat Rev Immunol*. 9:162-174.

Gaggioli, C., S. Hooper, C. Hidalgo-Carcedo, R. Grosse, J.F. Marshall, K. Harrington, and E. Sahai. 2007. Fibroblast-led collective invasion of carcinoma cells with differing roles for RhoGTPases in leading and following cells. *Nature Cell Biology*. 9:1392.

Gao, D., N. Joshi, H. Choi, S. Ryu, M. Hahn, R. Catena, H. Sadik, P. Argani, P. Wagner, L.T. Vahdat, J.L. Port, B. Stiles, S. Sukumar, N.K. Altorki, S. Rafii, and V. Mittal. 2012. Myeloid progenitor cells

in the premetastatic lung promote metastases by inducing mesenchymal to epithelial transition. *Cancer Res*. 72:1384-1394.

Gascard, P., and T.D. Tlsty. 2016. Carcinoma-associated fibroblasts: orchestrating the composition of malignancy. *Genes & Development*. 30:1002-1019.

Gaucci, E., F. Altieri, C. Turano, and S. Chichiarelli. 2013. The protein ERp57 contributes to EGF receptor signaling and internalization in MDA-MB-468 breast cancer cells. *J Cell Biochem*. 114:2461-2470.

Ge, J., C.J. Zhang, L. Li, L.M. Chong, X. Wu, P. Hao, S.K. Sze, and S.Q. Yao. 2013. Small molecule probe suitable for in situ profiling and inhibition of protein disulfide isomerase. *ACS Chem Biol*. 8:2577-2585.

Gehler, S., S.M. Ponik, K.M. Riching, and P.J. Keely. 2013. Bi-directional signaling: extracellular matrix and integrin regulation of breast tumor progression. *Crit Rev Eukaryot Gene Expr*. 23:139-157.

Genard, G., S. Lucas, and C. Michiels. 2017. Reprogramming of Tumor-Associated Macrophages with Anticancer Therapies: Radiotherapy versus Chemo- and Immunotherapies. *Front Immunol*. 8:828.

Geng, S.-Q., A.T. Alexandrou, and J.J. Li. 2014. Breast Cancer Stem Cells: Multiple Capacities in Tumor Metastasis. *Cancer letters*. 349:1-7.

Gialeli, C., A.D. Theocharis, and N.K. Karamanos. 2011. Roles of matrix metalloproteinases in cancer progression and their pharmacological targeting. *FEBS J*. 278:16-27.

Giamogante, F., I. Marrocco, L. Cervoni, M. Eufemi, S. Chichiarelli, and F. Altieri. 2018. Punicalagin, an active pomegranate component, is a new inhibitor of PDIA3 reductase activity. *Biochimie*. 147:122-129.

Ginestier, C., M.H. Hur, E. Charafe-Jauffret, F. Monville, J. Dutcher, M. Brown, J. Jacquemier, P. Viens, C. Kleer, S. Liu, A. Schott, D. Hayes, D. Birnbaum, M.S. Wicha, and G. Dontu. 2007. ALDH1 is a marker of normal and malignant human mammary stem cells and a predictor of poor clinical outcome. *Cell stem cell*. 1:555-567.

Goldhirsch, A., E.P. Winer, A.S. Coates, R.D. Gelber, M. Piccart-Gebhart, B. Thürlimann, H.J. Senn, K.S. Albain, F. André, J. Bergh, H. Bonnefoi, D. Bretel-Morales, H. Burstein, F. Cardoso, M. Castiglione-Gertsch, A.S. Coates, M. Colleoni, A. Costa, G. Curigliano, N.E. Davidson, A. Di Leo, B. Ejlertsen, J.F. Forbes, R.D. Gelber, M. Gnant, A. Goldhirsch, P. Goodwin, P.E. Goss, J.R. Harris, D.F. Hayes, C.A. Hudis, J.N. Ingle, J. Jassem, Z. Jiang, P. Karlsson, S. Loibl, M. Morrow, M. Namer, C. Kent Osborne, A.H. Partridge, F. Penault-Llorca, C.M. Perou, M.J. Piccart-Gebhart, K.I. Pritchard, E.J.T. Rutgers, F. Sedlmayer, V. Semiglazov, Z.-M. Shao, I. Smith, B. Thürlimann, M. Toi, A. Tutt, M. Untch, G. Viale, T. Watanabe, N. Wilcken, E.P. Winer, and W.C. Wood. 2013. Personalizing the treatment of women with early breast cancer: highlights of the St Gallen International Expert Consensus on the Primary Therapy of Early Breast Cancer 2013. *Annals of Oncology*. 24:2206-2223.

Goldmann, W.H., V. Auernheimer, I. Thievessen, and B. Fabry. 2013. Vinculin, cell mechanics and tumour cell invasion. *Cell Biol Int*. 37:397-405.

Gordon, R.R., and P.S. Nelson. 2012. Cellular senescence and cancer chemotherapy resistance. *Drug Resist Updat*. 15:123-131.

Gough, D.J., I.J. Marié, C. Lobry, I. Aifantis, and D.E. Levy. 2014. STAT3 supports experimental K-RasG12D-induced murine myeloproliferative neoplasms dependent on serine phosphorylation. *Blood*. 124:2252-2261.

Grindel, B.J., B. Rohe, S.E. Safford, J.J. Bennett, and M.C. Farach-Carson. 2011. Tumor necrosis factor-α treatment of HepG2 cells mobilizes a cytoplasmic pool of ERp57/1,25D_3-MARRS to the nucleus. *J Cell Biochem*. 112:2606-2615.

Gudjonsson, T., M.C. Adriance, M.D. Sternlicht, O.W. Petersen, and M.J. Bissell. 2005. Myoepithelial cells: their origin and function in breast morphogenesis and neoplasia. *J Mammary Gland Biol Neoplasia*. 10:261-272.

Gudjonsson, T., L. Rønnov-Jessen, R. Villadsen, F. Rank, M.J. Bissell, and O.W. Petersen. 2002. Normal and tumor-derived myoepithelial cells differ in their ability to interact with luminal breast epithelial cells for polarity and basement membrane deposition. *Journal of cell science*. 115:39-50.

Guo, G.G., K. Patel, V. Kumar, M. Shah, V.A. Fried, J.D. Etlinger, and P.B. Sehgal. 2002. Association of the chaperone glucose-regulated protein 58 (GRP58/ER-60/ERp57) with Stat3 in cytosol and plasma membrane complexes. *J Interferon Cytokine Res*. 22:555-563.

Hale, T.W., and Hartmann. 2007. Hale & Hartmann's Textbook of Human Lactation.

Halperin, L., J. Jung, and M. Michalak. 2014. The many functions of the endoplasmic reticulum chaperones and folding enzymes. *IUBMB Life*. 66:318-326.

Hanahan, D., and R.A. Weinberg. 2011. Hallmarks of cancer: the next generation. *Cell*. 144:646-674.

Hassiotou, F., and D. Geddes. 2012. Anatomy of the human mammary gland: Current status of knowledge. *Clinical Anatomy*. 26:29-48.

He, Y., F. Shao, W. Pi, C. Shi, Y. Chen, D. Gong, B. Wang, Z. Cao, and K. Tang. 2016. Largescale Transcriptomics Analysis Suggests Over-Expression of BGH3, MMP9 and PDIA3 in Oral Squamous Cell Carcinoma. *PLoS ONE*. 11:e0146530.

Hebert, D.N., and M. Molinari. 2007. In and Out of the ER: Protein Folding, Quality Control, Degradation, and Related Human Diseases. *Physiological Reviews*. 87:1377-1408.

Hellewell, A.L., S. Rosini, and J.C. Adams. 2017. A Rapid, Scalable Method for the Isolation, Functional Study, and Analysis of Cell-derived Extracellular Matrix. *Journal of Visualized Experiments : JoVE*:55051.

Hennigs, A., F. Riedel, A. Gondos, P. Sinn, P. Schirmacher, F. Marmé, D. Jäger, H.-U. Kauczor, A. Stieber, K. Lindel, J. Debus, M. Golatta, F. Schütz, C. Sohn, J. Heil, and A. Schneeweiss. 2016. Prognosis of breast cancer molecular subtypes in routine clinical care: A large prospective cohort study. *BMC Cancer*. 16:734.

Hettinghouse, A., R. Liu, and C.-j. Liu. 2018. Multifunctional molecule ERp57: From cancer to neurodegenerative diseases. *Pharmacology & Therapeutics*. 181:34-48.

High, S., F.J.L. Lecomte, S.J. Russell, B.M. Abell, and J.D. Oliver. 2000. Glycoprotein folding in the endoplasmic reticulum: a tale of three chaperones? *FEBS Letters*. 476:38-41.

Hii, C.S., and A. Ferrante. 2016. The Non-Genomic Actions of Vitamin D. *Nutrients*. 8:135.

Hoffstrom, B.G., A. Kaplan, R. Letso, R. Schmid, G.J. Turmel, D.C. Lo, and B.R. Stockwell. 2010. Inhibitors of protein disulfide isomerase suppress apoptosis induced by misfolded proteins. *Nature chemical biology*. 6:900-906.

Hogan, P.G., R.S. Lewis, and A. Rao. 2010. Molecular basis of calcium signaling in lymphocytes: STIM and ORAI. *Annu Rev Immunol*. 28:491-533.

Housman, G., S. Byler, S. Heerboth, K. Lapinska, M. Longacre, N. Snyder, and S. Sarkar. 2014. Drug resistance in cancer: an overview. *Cancers (Basel)*. 6:1769-1792.

Hu, G., L. Li, and W. Xu. 2017. Extracellular matrix in mammary gland development and breast cancer progression. *Frontiers in Laboratory Medicine*. 1:36-39.

Huang, G., H. Yan, S. Ye, C. Tong, and Q.L. Ying. 2014. STAT3 phosphorylation at tyrosine 705 and serine 727 differentially regulates mouse ESC fates. *Stem Cells*. 32:1149-1160.

Hui, M., A. Cazet, R. Nair, D.N. Watkins, S.A. O'Toole, and A. Swarbrick. 2013. The Hedgehog signalling pathway in breast development, carcinogenesis and cancer therapy. *Breast Cancer Res*. 15:203.

Hulkower, K.I., and R.L. Herber. 2011. Cell migration and invasion assays as tools for drug discovery. *Pharmaceutics*. 3:107-124.

Hussmann, M., K. Janke, P. Kranz, F. Neumann, E. Mersch, M. Baumann, K. Goepelt, U. Brockmeier, and E. Metzen. 2015. Depletion of the thiol oxidoreductase ERp57 in tumor cells inhibits proliferation and increases sensitivity to ionizing radiation and chemotherapeutics. *Oncotarget*. 6:39247-39261.

Idelevich, A., M. Kerschnitzki, R. Shahar, and E. Monsonego-Ornan. 2011. 1,25(OH)2D3 Alters Growth Plate Maturation and Bone Architecture in Young Rats with Normal Renal Function. *PLOS ONE*. 6:e20772.

Ilina, O., and P. Friedl. 2009. Mechanisms of collective cell migration at a glance. *Journal of Cell Science*. 122:3203.

Inman, J.L., C. Robertson, J.D. Mott, and M.J. Bissell. 2015. Mammary gland development: cell fate specification, stem cells and the microenvironment. *Development*. 142:1028.

Insua-Rodríguez, J., and T. Oskarsson. 2016. The extracellular matrix in breast cancer. *Advanced Drug Delivery Reviews*. 97:41-55.

Izrailit, J., and M. Reedijk. 2012. Developmental pathways in breast cancer and breast tumor-initiating cells: Therapeutic implications. *Cancer Letters*. 317:115-126.

Jacobs, J.M., K.M. Waters, L.E. Kathmann, D.G. Camp, H.S. Wiley, R.D. Smith, and B.D. Thrall. 2008. The mammary epithelial cell secretome and its regulation by signal transduction pathways. *J Proteome Res*. 7:558-569.

Jamieson, C., K.M. Mills, C. Lui, C. Semaan, M.P. Molloy, M. Sharma, J.K. Forwood, and B.R. Henderson. 2016. Characterization of a beta-catenin nuclear localization defect in MCF-7 breast cancer cells. *Exp Cell Res*. 341:196-206.

Janssen, L.M.E., E.E. Ramsay, C.D. Logsdon, and W.W. Overwijk. 2017. The immune system in cancer metastasis: friend or foe? *J Immunother Cancer*. 5:79.

Jessop, C.E., S. Chakravarthi, N. Garbi, G.J. Hämmerling, S. Lovell, and N.J. Bulleid. 2007. ERp57 is essential for efficient folding of glycoproteins sharing common structural domains. *EMBO J*. 26:28-40.

Johnson, S.C., P.S. Rabinovitch, and M. Kaeberlein. 2013. mTOR is a key modulator of ageing and age-related disease. *Nature*. 493:338-345.

Justus, C.R., N. Leffler, M. Ruiz-Echevarria, and L.V. Yang. 2014. In vitro cell migration and invasion assays. *J Vis Exp*.

Kalluri, R. 2003. Basement membranes: structure, assembly and role in tumour angiogenesis. *Nature Reviews Cancer*. 3:422.

Kalluri, R., and R.A. Weinberg. 2009. The basics of epithelial-mesenchymal transition. *The Journal of Clinical Investigation*. 119:1420-1428.

Kanchanawong, P., G. Shtengel, A.M. Pasapera, E.B. Ramko, M.W. Davidson, H.F. Hess, and C.M. Waterman. 2010. Nanoscale architecture of integrin-based cell adhesions. *Nature*. 468:580-584.

Kaushik, S., M.W. Pickup, and V.M. Weaver. 2016. From transformation to metastasis: deconstructing the extracellular matrix in breast cancer. *Cancer metastasis reviews*. 35:655-667.

Kehlet, S.N., R. Sanz-Pamplona, S. Brix, D.J. Leeming, M.A. Karsdal, and V. Moreno. 2016. Excessive collagen turnover products are released during colorectal cancer progression and elevated in serum from metastatic colorectal cancer patients. *Scientific Reports*. 6:30599.

Khalili, A.A., and M.R. Ahmad. 2015. A Review of Cell Adhesion Studies for Biomedical and Biological Applications. *Int J Mol Sci*. 16:18149-18184.

Kozlov, G., P. Maattanen, J.D. Schrag, S. Pollock, M. Cygler, B. Nagar, D.Y. Thomas, and K. Gehring. 2006. Crystal Structure of the bb' Domains of the Protein Disulfide Isomerase ERp57. *Structure*. 14:1331-1339.

Kozlov, G., P. Määttänen, D.Y. Thomas, and K. Gehring. 2010. A structural overview of the PDI family of proteins. *FEBS Journal*. 277:3924-3936.

Kranz, P., F. Neumann, A. Wolf, F. Classen, M. Pompsch, T. Ocklenburg, J. Baumann, K. Janke, M. Baumann, K. Goepelt, H. Riffkin, E. Metzen, and U. Brockmeier. 2017. PDI is an essential redox-sensitive activator of PERK during the unfolded protein response (UPR). *Cell Death & Disease*. 8:e2986.

Lambert, A.W., D.R. Pattabiraman, and R.A. Weinberg. 2017. Emerging Biological Principles of Metastasis. *Cell*. 168:670-691.
Lamouille, S., J. Xu, and R. Derynck. 2014. Molecular mechanisms of epithelial-mesenchymal transition. *Nat Rev Mol Cell Biol*. 15:178-196.
Larson, E.M., D.J. Doughman, D.S. Gregerson, and W.F. Obritsch. 1997. A new, simple, nonradioactive, nontoxic in vitro assay to monitor corneal endothelial cell viability. *Investigative Ophthalmology & Visual Science*. 38:1929-1933.
Larsson, B., and I. Nemere. 2003. Effect of growth and maturation on membrane-initiated actions of 1,25-dihydroxyvitamin D3-II: calcium transport, receptor kinetics, and signal transduction in intestine of female chickens. *J Cell Biochem*. 90:901-913.
Lee, A.S. 1981. The accumulation of three specific proteins related to glucose-regulated proteins in a temperature-sensitive hamster mutant cell line K12. *Journal of Cellular Physiology*. 106:119-125.
Leone, P., E.-C. Shin, F. Perosa, A. Vacca, F. Dammacco, and V. Racanelli. 2013. MHC Class I Antigen Processing and Presenting Machinery: Organization, Function, and Defects in Tumor Cells. *JNCI: Journal of the National Cancer Institute*. 105:1172-1187.
Levental, K.R., H. Yu, L. Kass, J.N. Lakins, M. Egeblad, J.T. Erler, S.F.T. Fong, K. Csiszar, A. Giaccia, W. Weninger, M. Yamauchi, D.L. Gasser, and V.M. Weaver. 2009. Matrix Crosslinking Forces Tumor Progression by Enhancing Integrin Signaling. *Cell*. 139:891-906.
Linde, N., M. Casanova-Acebes, M.S. Sosa, A. Mortha, A. Rahman, E. Farias, K. Harper, E. Tardio, I. Reyes Torres, J. Jones, J. Condeelis, M. Merad, and J.A. Aguirre-Ghiso. 2018. Macrophages orchestrate breast cancer early dissemination and metastasis. *Nature Communications*. 9:21.
Linz, A., Y. Knieper, T. Gronau, U. Hansen, A. Aszodi, N. Garbi, G.J. Hämmerling, T. Pap, P. Bruckner, and R. Dreier. 2015. ER Stress During the Pubertal Growth Spurt Results in Impaired Long-Bone Growth in Chondrocyte-Specific ERp57 Knockout Mice. *J Bone Miner Res*. 30:1481-1493.
Liou, J., M.L. Kim, W.D. Heo, J.T. Jones, J.W. Myers, J.E. Ferrell, and T. Meyer. 2005. STIM is a Ca2+ sensor essential for Ca2+-store-depletion-triggered Ca2+ influx. *Curr Biol*. 15:1235-1241.
Lloyd-Lewis, B., O.B. Harris, C.J. Watson, and F.M. Davis. 2017. Mammary Stem Cells: Premise, Properties, and Perspectives. *Trends in Cell Biology*. 27:556-567.
Lobb, R.J., L.G. Lima, and A. Möller. 2017. Exosomes: Key mediators of metastasis and pre-metastatic niche formation. *Seminars in Cell & Developmental Biology*. 67:3-10.
Lu, P., V.M. Weaver, and Z. Werb. 2012. The extracellular matrix: A dynamic niche in cancer progression. *The Journal of Cell Biology*. 196:395-406.
Luo, H., G. Tu, Z. Liu, and M. Liu. 2015. Cancer-associated fibroblasts: A multifaceted driver of breast cancer progression. *Cancer Letters*. 361:155-163.
Lyons, S.M., E. Alizadeh, J. Mannheimer, K. Schuamberg, J. Castle, B. Schroder, P. Turk, D. Thamm, and A. Prasad. 2016. Changes in cell shape are correlated with metastatic potential in murine and human osteosarcomas. *Biol Open*. 5:289-299.
Markowitz, J., R. Wesolowski, T. Papenfuss, T.R. Brooks, and W.E. Carson. 2013. Myeloid-derived suppressor cells in breast cancer. *Breast Cancer Res Treat*. 140:13-21.
Martinez, F.O., and S. Gordon. 2014. The M1 and M2 paradigm of macrophage activation: time for reassessment. *F1000Prime Rep*. 6:13.
Mitrus, I., E. Bryndza, A. Sochanik, and S. Szala. 2012. Evolving models of tumor origin and progression. *Tumour Biology*. 33:911-917.
Mongiat, M., E. Andreuzzi, G. Tarticchio, and A. Paulitti. 2016. Extracellular Matrix, a Hard Player in Angiogenesis. *Int J Mol Sci*. 17.
Morrissey, M.A., E.J. Hagedorn, and D.R. Sherwood. 2013. Cell invasion through basement membrane: The netrin receptor DCC guides the way. *Worm*. 2:e26169.

Morrissey, M.A., R. Jayadev, G.R. Miley, C.A. Blebea, Q. Chi, S. Ihara, and D.R. Sherwood. 2016. SPARC Promotes Cell Invasion In Vivo by Decreasing Type IV Collagen Levels in the Basement Membrane. *PLOS Genetics*. 12:e1005905.

Moses, H., and M.H. Barcellos-Hoff. 2011. TGF-beta biology in mammary development and breast cancer. *Cold Spring Harb Perspect Biol*. 3:a003277.

Mutze, K., S. Vierkotten, J. Milosevic, O. Eickelberg, and M. Königshoff. 2015. Enolase 1 (ENO1) and protein disulfide-isomerase associated 3 (PDIA3) regulate Wnt/β-catenin-driven trans-differentiation of murine alveolar epithelial cells. *Dis Model Mech*. 8:877-890.

Naba, A., K.R. Clauser, J.M. Lamar, S.A. Carr, and R.O. Hynes. 2014. Extracellular matrix signatures of human mammary carcinoma identify novel metastasis promoters. *Elife*. 3:e01308.

Nagy, J.A., S.H. Chang, A.M. Dvorak, and H.F. Dvorak. 2009. Why are tumour blood vessels abnormal and why is it important to know? *Br J Cancer*. 100:865-869.

Nemere, I. 1996. Apparent nonnuclear regulation of intestinal phosphate transport: effects of 1,25-dihydroxyvitamin D3,24,25-dihydroxyvitamin D3, and 25-hydroxyvitamin D3. *Endocrinology*. 137:2254-2261.

Nemere, I., M.C. Farach-Carson, B. Rohe, T.M. Sterling, A.W. Norman, B.D. Boyan, and S.E. Safford. 2004. Ribozyme knockdown functionally links a $1,25(OH)_2D_3$ membrane binding protein ($1,25D_3$-MARRS) and phosphate uptake in intestinal cells. *Proceedings of the National Academy of Sciences of the United States of America*. 101:7392.

Neve, R.M., K. Chin, J. Fridlyand, J. Yeh, F.L. Baehner, T. Fevr, L. Clark, N. Bayani, J.-P. Coppe, F. Tong, T. Speed, P.T. Spellman, S. DeVries, A. Lapuk, N.J. Wang, W.-L. Kuo, J.L. Stilwell, D. Pinkel, D.G. Albertson, F.M. Waldman, F. McCormick, R.B. Dickson, M.D. Johnson, M. Lippman, S. Ethier, A. Gazdar, and J.W. Gray. 2006. A collection of breast cancer cell lines for the study of functionally distinct cancer subtypes. *Cancer Cell*. 10:515-527.

Nicholson, R.I., K.J. Walker, A. Turkes, J. Dyas, P.N. Plowman, M. Williams, and R.W. Blamey. 1985. Endocrinological and clinical aspects of LHRH action (ICI 118630) in hormone dependent breast cancer. *J Steroid Biochem*. 23:843-847.

Noy, R., and J.W. Pollard. 2014. Tumor-associated macrophages: from mechanisms to therapy. *Immunity*. 41:49-61.

Nundlall, S., M.H. Rajpar, P.A. Bell, C. Clowes, L.A. Zeeff, B. Gardner, D.J. Thornton, R.P. Boot-Handford, and M.D. Briggs. 2010. An unfolded protein response is the initial cellular response to the expression of mutant matrilin-3 in a mouse model of multiple epiphyseal dysplasia. *Cell Stress Chaperones*. 15:835-849.

Nwabo Kamdje, A.H., P.F. Seke Etet, L. Vecchio, J.M. Muller, M. Krampera, and K.E. Lukong. 2014. Signaling pathways in breast cancer: Therapeutic targeting of the microenvironment. *Cellular Signalling*. 26:2843-2856.

Nwabo Kamdje, A.H., P. Takam Kamga, R. Tagne Simo, L. Vecchio, P.F. Seke Etet, J.M. Muller, G. Bassi, E. Lukong, R. Kumar Goel, J. Mbo Amvene, and M. Krampera. 2017. Developmental pathways associated with cancer metastasis: Notch, Wnt, and Hedgehog. *Cancer Biology & Medicine*. 14:109-120.

Ocana, A., C. Nieto-Jiménez, A. Pandiella, and A.J. Templeton. 2017. Neutrophils in cancer: prognostic role and therapeutic strategies. *Mol Cancer*. 16:137.

Ojha, R., and R.K. Amaravadi. 2017. Targeting the unfolded protein response in cancer. *Pharmacol Res*. 120:258-266.

Ojo, D., F. Wei, Y. Liu, E. Wang, H. Zhang, X. Lin, N. Wong, A. Bane, and D. Tang. 2015. Factors Promoting Tamoxifen Resistance in Breast Cancer via Stimulating Breast Cancer Stem Cell Expansion. *Curr Med Chem*. 22:2360-2374.

Oliveira, N.C., T.H. Gomig, H.H. Milioli, F. Cordeiro, G.G. Costa, C.A. Urban, R.S. Lima, I.J. Cavalli, and E.M. Ribeiro. 2016. Comparative proteomic analysis of ductal and lobular invasive breast carcinoma. *Genet Mol Res*. 15(2): gmr.15027701.

Oliver, J.D., H.L. Roderick, D.H. Llewellyn, and S. High. 1999. ERp57 functions as a subunit of specific complexes formed with the ER lectins calreticulin and calnexin. *Mol Biol Cell*. 10:2573-2582.
Osborne, C.K. 1998. Tamoxifen in the treatment of breast cancer. *N Engl J Med*. 339:1609-1618.
Oskarsson, T. 2013. Extracellular matrix components in breast cancer progression and metastasis. *The Breast*. 22:S66-S72.
Pang, M.F., M.J. Siedlik, S. Han, M. Stallings-Mann, D.C. Radisky, and C.M. Nelson. 2016. Tissue Stiffness and Hypoxia Modulate the Integrin-Linked Kinase ILK to Control Breast Cancer Stem-like Cells. *Cancer Res*. 76:5277-5287.
Paul, C.D., P. Mistriotis, and K. Konstantopoulos. 2017. Cancer cell motility: lessons from migration in confined spaces. *Nat Rev Cancer*. 17:131-140.
Perou, C.M., T. Sørlie, M.B. Eisen, M. van de Rijn, S.S. Jeffrey, C.A. Rees, J.R. Pollack, D.T. Ross, H. Johnsen, L.A. Akslen, Ø. Fluge, A. Pergamenschikov, C. Williams, S.X. Zhu, P.E. Lønning, A.-L. Børresen-Dale, P.O. Brown, and D. Botstein. 2000. Molecular portraits of human breast tumours. *Nature*. 406:747.
Petersen, O.H., M. Michalak, and A. Verkhratsky. 2005. Calcium signalling: Past, present and future. *Cell Calcium*. 38:161-169.
Pickup, M.W., J.K. Mouw, and V.M. Weaver. 2014. The extracellular matrix modulates the hallmarks of cancer. *EMBO Reports*. 15:1243-1253.
Plaks, V., N. Kong, and Z. Werb. 2015. The Cancer Stem Cell Niche: How Essential is the Niche in Regulating Stemness of Tumor Cells? *Cell stem cell*. 16:225-238.
Polyak, K., and R. Kalluri. 2010. The Role of the Microenvironment in Mammary Gland Development and Cancer. *Cold Spring Harbor Perspectives in Biology*. 2:a003244.
Poole, R., and R. Paridaens. 2007. The use of third-generation aromatase inhibitors and tamoxifen in the adjuvant treatment of postmenopausal patients with hormone-dependent breast cancer: evidence based review. *Curr Opin Oncol*. 19:564-572.
Porta, C., C. Paglino, and A. Mosca. 2014. Targeting PI3K/Akt/mTOR Signaling in Cancer. *Front Oncol*. 4:64.
Prat, A., E. Pineda, B. Adamo, P. Galván, A. Fernández, L. Gaba, M. Díez, M. Viladot, A. Arance, and M. Muñoz. 2015. Clinical implications of the intrinsic molecular subtypes of breast cancer. *Breast*. 24 Suppl 2:S26-35.
Prins, D., J. Groenendyk, N. Touret, and M. Michalak. 2011. Modulation of STIM1 and capacitative Ca2+ entry by the endoplasmic reticulum luminal oxidoreductase ERp57. *EMBO reports*. 12:1182-1188.
Raafat, A., A.S. Goldhar, M. Klauzinska, K. Xu, I. Amirjazil, D. McCurdy, K. Lashin, D. Salomon, B.K. Vonderhaar, S. Egan, and R. Callahan. 2011. Expression of Notch receptors, ligands, and target genes during development of the mouse mammary gland. *J Cell Physiol*. 226:1940-1952.
Radisky, D.C., and L.C. Hartmann. 2009. Mammary Involution and Breast Cancer Risk: Transgenic Models and Clinical Studies. *Journal of Mammary Gland Biology and Neoplasia*. 14:181-191.
Ramos, F.S., L.T. Serino, C.M. Carvalho, R.S. Lima, C.A. Urban, I.J. Cavalli, and E.M. Ribeiro. 2015. PDIA3 and PDIA6 gene expression as an aggressiveness marker in primary ductal breast cancer. *Genet Mol Res*. 14:6960-6967.
Ramírez-Rangel, I., I. Bracho-Valdés, A. Vázquez-Macías, J. Carretero-Ortega, G. Reyes-Cruz, and J. Vázquez-Prado. 2011. Regulation of mTORC1 complex assembly and signaling by GRp58/ERp57. *Mol Cell Biol*. 31:1657-1671.
Redig, A.J., and S.S. McAllister. 2013. Breast cancer as a systemic disease: a view of metastasis. *J Intern Med*. 274:113-126.
Ren, B., K.O. Yee, J. Lawler, and R. Khosravi-Far. 2006. Regulation of tumor angiogenesis by thrombospondin-1. *Biochimica et Biophysica Acta (BBA) - Reviews on Cancer*. 1765:178-188.
Rommerswinkel, N., B. Niggemann, S. Keil, K.S. Zänker, and T. Dittmar. 2014. Analysis of cell migration within a three-dimensional collagen matrix. *J Vis Exp*:e51963.

Roos, J., P.J. DiGregorio, A.V. Yeromin, K. Ohlsen, M. Lioudyno, S. Zhang, O. Safrina, J.A. Kozak, S.L. Wagner, M.D. Cahalan, G. Veliçelebi, and K.A. Stauderman. 2005. STIM1, an essential and conserved component of store-operated Ca2+ channel function. *J Cell Biol*. 169:435-445.

Rose, A.S., A.R. Bradley, Y. Valasatava, J.M. Duarte, A. Prlić, and P.W. Rose. 2018. NGL viewer: web-based molecular graphics for large complexes. *Bioinformatics*:bty419-bty419.

Rosini, S., N. Pugh, A.M. Bonna, D.J.S. Hulmes, R.W. Farndale, and J.C. Adams. 2018. Thrombospondin-1 promotes matrix homeostasis by interacting with collagen and lysyl oxidase precursors and collagen cross-linking sites. *Science Signaling*. 11.

Ruggiano, A., O. Foresti, and P. Carvalho. 2014. ER-associated degradation: Protein quality control and beyond. *The Journal of Cell Biology*. 204:869.

Russell, S.J., L.W. Ruddock, K.E. Salo, J.D. Oliver, Q.P. Roebuck, D.H. Llewellyn, H.L. Roderick, P. Koivunen, J. Myllyharju, and S. High. 2004. The primary substrate binding site in the b' domain of ERp57 is adapted for endoplasmic reticulum lectin association. *J Biol Chem*. 279:18861-18869.

Santana-Codina, N., R. Carretero, R. Sanz-Pamplona, T. Cabrera, E. Guney, B. Oliva, P. Clezardin, O.E. Olarte, P. Loza-Alvarez, A. Méndez-Lucas, J.C. Perales, and A. Sierra. 2013. A transcriptome-proteome integrated network identifies endoplasmic reticulum thiol oxidoreductase (ERp57) as a hub that mediates bone metastasis. *Mol Cell Proteomics*. 12:2111-2125.

Santos, S.G., E.C. Campbell, S. Lynch, V. Wong, A.N. Antoniou, and S.J. Powis. 2007. Major histocompatibility complex class I-ERp57-tapasin interactions within the peptide-loading complex. *J Biol Chem*. 282:17587-17593.

Satelli, A., and S. Li. 2011. Vimentin in cancer and its potential as a molecular target for cancer therapy. *Cell Mol Life Sci*. 68:3033-3046.

Schedin, P., and P.J. Keely. 2011. Mammary Gland ECM Remodeling, Stiffness, and Mechanosignaling in Normal Development and Tumor Progression. *Cold Spring Harbor Perspectives in Biology*. 3:a003228.

Schultz, G.S., and A. Wysocki. 2009. Interactions between extracellular matrix and growth factors in wound healing. *Wound Repair and Regeneration*. 17:153-162.

Sheen, M.R., J.D. Marotti, M.J. Allegrezza, M. Rutkowski, J.R. Conejo-Garcia, and S. Fiering. 2016. Constitutively activated PI3K accelerates tumor initiation and modifies histopathology of breast cancer. *Oncogenesis*. 5:e267.

Slamon, D.J., B. Leyland-Jones, S. Shak, H. Fuchs, V. Paton, A. Bajamonde, T. Fleming, W. Eiermann, J. Wolter, M. Pegram, J. Baselga, and L. Norton. 2001. Use of chemotherapy plus a monoclonal antibody against HER2 for metastatic breast cancer that overexpresses HER2. *N Engl J Med*. 344:783-792.

Son, H., and A. Moon. 2010. Epithelial-mesenchymal Transition and Cell Invasion. *Toxicol Res*. 26:245-252.

Song, M.N., P.G. Moon, J.E. Lee, M. Na, W. Kang, Y.S. Chae, J.Y. Park, H. Park, and M.C. Baek. 2012. Proteomic analysis of breast cancer tissues to identify biomarker candidates by gel-assisted digestion and label-free quantification methods using LC-MS/MS. *Arch Pharm Res*. 35:1839-1847.

Sottile, J., D.C. Hocking, and M. Schwartz. 2002. Fibronectin Polymerization Regulates the Composition and Stability of Extracellular Matrix Fibrils and Cell-Matrix Adhesions. *Molecular Biology of the Cell*. 13:3546-3559.

Soule, H.D., J. Vazquez, A. Long, S. Albert, and M. Brennan. 1973. A Human Cell Line From a Pleural Effusion Derived From a Breast Carcinoma2. *JNCI: Journal of the National Cancer Institute*. 51:1409-1416.

Soysal, S.D., A. Tzankov, and S.E. Muenst. 2015. Role of the Tumor Microenvironment in Breast Cancer. *Pathobiology*. 82:142-152.

Takata, H., M. Kudo, T. Yamamoto, J. Ueda, K. Ishino, W.X. Peng, R. Wada, N. Taniai, H. Yoshida, E. Uchida, and Z. Naito. 2016. Increased expression of PDIA3 and its association with cancer cell proliferation and poor prognosis in hepatocellular carcinoma. *Oncol Lett*. 12:4896-4904.
Tanjore, H., and R. Kalluri. 2006. The role of type IV collagen and basement membranes in cancer progression and metastasis. *Am J Pathol*. 168:715-717.
Tannous, A., G.B. Pisoni, D.N. Hebert, and M. Molinari. 2015. N-linked sugar-regulated protein folding and quality control in the ER. *Semin Cell Dev Biol*. 41:79-89.
Tomlinson, G.E., T.T.L. Chen, V.A. Stastny, A.K. Virmani, M.A. Spillman, V. Tonk, J.L. Blum, N.R. Schneider, I.I. Wistuba, J.W. Shay, J.D. Minna, and A.F. Gazdar. 1998. Characterization of a Breast Cancer Cell Line Derived from a Germ-Line BRCA1 Mutation Carrier. *Cancer Research*. 58:3237.
Trepat, X., Z. Chen, and K. Jacobson. 2012. Cell migration. *Compr Physiol*. 2:2369-2392.
Tripathi, C., B.N. Tewari, R.K. Kanchan, K.S. Baghel, N. Nautiyal, R. Shrivastava, H. Kaur, M.L. Bhatt, and S. Bhadauria. 2014. Macrophages are recruited to hypoxic tumor areas and acquire a pro-angiogenic M2-polarized phenotype via hypoxic cancer cell derived cytokines Oncostatin M and Eotaxin. *Oncotarget*. 5:5350-5368.
Turano, C., E. Gaucci, C. Grillo, and S. Chichiarelli. 2011. ERp57/GRP58: A protein with multiple functions. *Cellular & Molecular Biology Letters*. 16:539.
Uchino, M., H. Kojima, K. Wada, M. Imada, F. Onoda, H. Satofuka, T. Utsugi, and Y. Murakami. 2010. Nuclear β-catenin and CD44 upregulation characterize invasive cell populations in non-aggressive MCF-7 breast cancer cells. *BMC Cancer*. 10:414.
van der Wal, F.J., J.D. Oliver, and S. High. 1998. The transient association of ERp57 with N-glycosylated proteins is regulated by glucose trimming. *European Journal of Biochemistry*. 256:51-59.
Vandewynckel, Y.P., D. Laukens, A. Geerts, E. Bogaerts, A. Paridaens, X. Verhelst, S. Janssens, F. Heindryckx, and H. Van Vlierberghe. 2013. The paradox of the unfolded protein response in cancer. *Anticancer Res*. 33:4683-4694.
Vempati, P., A.S. Popel, and F. Mac Gabhann. 2014. Extracellular regulation of VEGF: isoforms, proteolysis, and vascular patterning. *Cytokine Growth Factor Rev*. 25:1-19.
Visvader, J.E., and J. Stingl. 2014. Mammary stem cells and the differentiation hierarchy: current status and perspectives. *Genes Dev*. 28:1143-1158.
Vuong, D., P.T. Simpson, B. Green, M.C. Cummings, and S.R. Lakhani. 2014. Molecular classification of breast cancer. *Virchows Arch*. 465:1-14.
Wang, H., P.K. Chan, S.Y. Pan, K.H. Kwon, Y. Ye, J.H. Chu, W.F. Fong, W.M. Tsui, and Z.L. Yu. 2010. ERp57 is up-regulated in free fatty acids-induced steatotic L-02 cells and human nonalcoholic fatty livers. *J Cell Biochem*. 110:1447-1456.
Wang, J., A.M. Betancourt, J.A. Mobley, and C.A. Lamartiniere. 2011. Proteomic discovery of genistein action in the rat mammary gland. *J Proteome Res*. 10:1621-1631.
Wei, S.C., L. Fattet, J.H. Tsai, Y. Guo, V.H. Pai, H.E. Majeski, A.C. Chen, R.L. Sah, S.S. Taylor, A.J. Engler, and J. Yang. 2015. Matrix stiffness drives epithelial-mesenchymal transition and tumour metastasis through a TWIST1-G3BP2 mechanotransduction pathway. *Nat Cell Biol*. 17:678-688.
White, D.E., N.A. Kurpios, D. Zuo, J.A. Hassell, S. Blaess, U. Mueller, and W.J. Muller. 2004. Targeted disruption of β1-integrin in a transgenic mouse model of human breast cancer reveals an essential role in mammary tumor induction. *Cancer Cell*. 6:159-170.
Wise, R., S. Duhachek-Muggy, Y. Qi, M. Zolkiewski, and A. Zolkiewska. 2016. Protein disulfide isomerases in the endoplasmic reticulum promote anchorage-independent growth of breast cancer cells. *Breast Cancer Res Treat*. 157:241-252.
Wishart, D.S. 2015. Is Cancer a Genetic Disease or a Metabolic Disease? *EBioMedicine*. 2:478-479.
Wu, W., G. Beilhartz, Y. Roy, C.L. Richard, M. Curtin, L. Brown, D. Cadieux, M. Coppolino, M.C. Farach-Carson, I. Nemere, and K.A. Meckling. 2010. Nuclear translocation of the 1,25D3-

MARRS (membrane associated rapid response to steroids) receptor protein and NFkappaB in differentiating NB4 leukemia cells. *Exp Cell Res*. 316:1101-1108.
Wyckoff, J., W. Wang, E.Y. Lin, Y. Wang, F. Pixley, E.R. Stanley, T. Graf, J.W. Pollard, J. Segall, and J. Condeelis. 2004. A paracrine loop between tumor cells and macrophages is required for tumor cell migration in mammary tumors. *Cancer Res*. 64:7022-7029.
Wynn, T.A. 2008. Cellular and molecular mechanisms of fibrosis. *J Pathol*. 214:199-210.
Xiong, G., L. Deng, J. Zhu, P.G. Rychahou, and R. Xu. 2014. Prolyl-4-hydroxylase α subunit 2 promotes breast cancer progression and metastasis by regulating collagen deposition. *BMC Cancer*. 14:1.
Xu, D., R.E. Perez, M.H. Rezaiekhaligh, M. Bourdi, and W.E. Truog. 2009. Knockdown of ERp57 increases BiP/GRP78 induction and protects against hyperoxia and tunicamycin-induced apoptosis. *Am J Physiol Lung Cell Mol Physiol*. 297:L44-51.
Xu, J., J.R. Prosperi, N. Choudhury, O.I. Olopade, and K.H. Goss. 2015. β-Catenin is required for the tumorigenic behavior of triple-negative breast cancer cells. *PLoS One*. 10:e0117097.
Xu, S., A.N. Butkevich, R. Yamada, Y. Zhou, B. Debnath, R. Duncan, E. Zandi, N.A. Petasis, and N. Neamati. 2012. Discovery of an orally active small-molecule irreversible inhibitor of protein disulfide isomerase for ovarian cancer treatment. *Proceedings of the National Academy of Sciences of the United States of America*. 109:16348-16353.
Yamaguchi, H., and J. Condeelis. 2007. Regulation of the actin cytoskeleton in cancer cell migration and invasion. *Biochim Biophys Acta*. 1773:642-652.
Yamashita, M., T. Ogawa, X. Zhang, N. Hanamura, Y. Kashikura, M. Takamura, M. Yoneda, and T. Shiraishi. 2012. Role of stromal myofibroblasts in invasive breast cancer: stromal expression of alpha-smooth muscle actin correlates with worse clinical outcome. *Breast Cancer*. 19:170-176.
Ye, J., D. Wu, P. Wu, Z. Chen, and J. Huang. 2014. The cancer stem cell niche: cross talk between cancer stem cells and their microenvironment. *Tumor Biology*. 35:3945-3951.
Yu, H., H. Lee, A. Herrmann, R. Buettner, and R. Jove. 2014. Revisiting STAT3 signalling in cancer: new and unexpected biological functions. *Nature Reviews Cancer*. 14:736.
Yu, Q.C., E.M. Verheyen, and Y.A. Zeng. 2016. Mammary Development and Breast Cancer: A Wnt Perspective. *Cancers (Basel)*. 8.
Zhan, T., N. Rindtorff, and M. Boutros. 2017. Wnt signaling in cancer. *Oncogene*. 36:1461-1473.
Zhang, S.L., Y. Yu, J. Roos, J.A. Kozak, T.J. Deerinck, M.H. Ellisman, K.A. Stauderman, and M.D. Cahalan. 2005. STIM1 is a Ca2+ sensor that activates CRAC channels and migrates from the Ca2+ store to the plasma membrane. *Nature*. 437:902-905.
Zhang, X.Q., Y. Pan, C.H. Yu, C.F. Xu, L. Xu, Y.M. Li, and W.X. Chen. 2015. PDIA3 Knockdown Exacerbates Free Fatty Acid-Induced Hepatocyte Steatosis and Apoptosis. *PLoS One*. 10:e0133882.
Zhang, Y., E. Baig, and D.B. Williams. 2006. Functions of ERp57 in the Folding and Assembly of Major Histocompatibility Complex Class I Molecules. *Journal of Biological Chemistry*. 281:14622-14631.
Zhao, G., H. Lu, and C. Li. 2015a. Proapoptotic activities of protein disulfide isomerase (PDI) and PDIA3 protein, a role of the Bcl-2 protein Bak. *J Biol Chem*. 290:8949-8963.
Zhao, J. 2016. Cancer Stem Cells and Chemoresistance: The Smartest Survives the Raid. *Pharmacology & therapeutics*. 160:145-158.
Zhao, J., and J.L. Guan. 2009. Signal transduction by focal adhesion kinase in cancer. *Cancer Metastasis Rev*. 28:35-49.
Zhao, S., Z. Wen, S. Liu, Y. Liu, X. Li, Y. Ge, and S. Li. 2015b. MicroRNA-148a inhibits the proliferation and promotes the paclitaxel-induced apoptosis of ovarian cancer cells by targeting PDIA3. *Mol Med Rep*. 12:3923-3929.

Zhou, Q.M., H. Zhang, Y.Y. Lu, X.F. Wang, and S.B. Su. 2009. Curcumin reduced the side effects of mitomycin C by inhibiting GRP58-mediated DNA cross-linking in MCF-7 breast cancer xenografts. *Cancer Sci*. 100:2040-2045.

Zhu, L., N.C. Santos, and K.H. Kim. 2010. Disulfide isomerase glucose-regulated protein 58 is required for the nuclear localization and degradation of retinoic acid receptor α. *Reproduction*. 139:717-731.

Zhuang, Z., L. Zhang, X. Wang, L. Tao, and B. Lv. 2016. PDIA3 gene induces visceral hypersensitivity in rats with irritable bowel syndrome through the dendritic cell-mediated activation of T cells. *PeerJ*. 4:e2644.

Ziani, L., S. Chouaib, and J. Thiery. 2018. Alteration of the Antitumor Immune Response by Cancer-Associated Fibroblasts. *Front Immunol*. 9:414.

Zitvogel, L., L. Apetoh, F. Ghiringhelli, F. André, A. Tesniere, and G. Kroemer. 2008. The anticancer immune response: indispensable for therapeutic success? *J Clin Invest*. 118:1991-2001.

Zou, H., C. Wen, Z. Peng, Y.-Y. Shao, L. Hu, S. Li, C. Li, and H.-H. Zhou. 2018. P4HB and PDIA3 are associated with tumor progression and therapeutic outcome of diffuse gliomas. *Oncology Reports*. 39:501-510.